# Inflicted Head Injury by Shaking Trauma in Infants

Part I
The potential effect of spatiotemporal variation of the rotation center on injury mechanisms

Part II
The importance of spatiotemporal variation of the rotation center when modeling external head-dynamics

L.A.H. Schiks

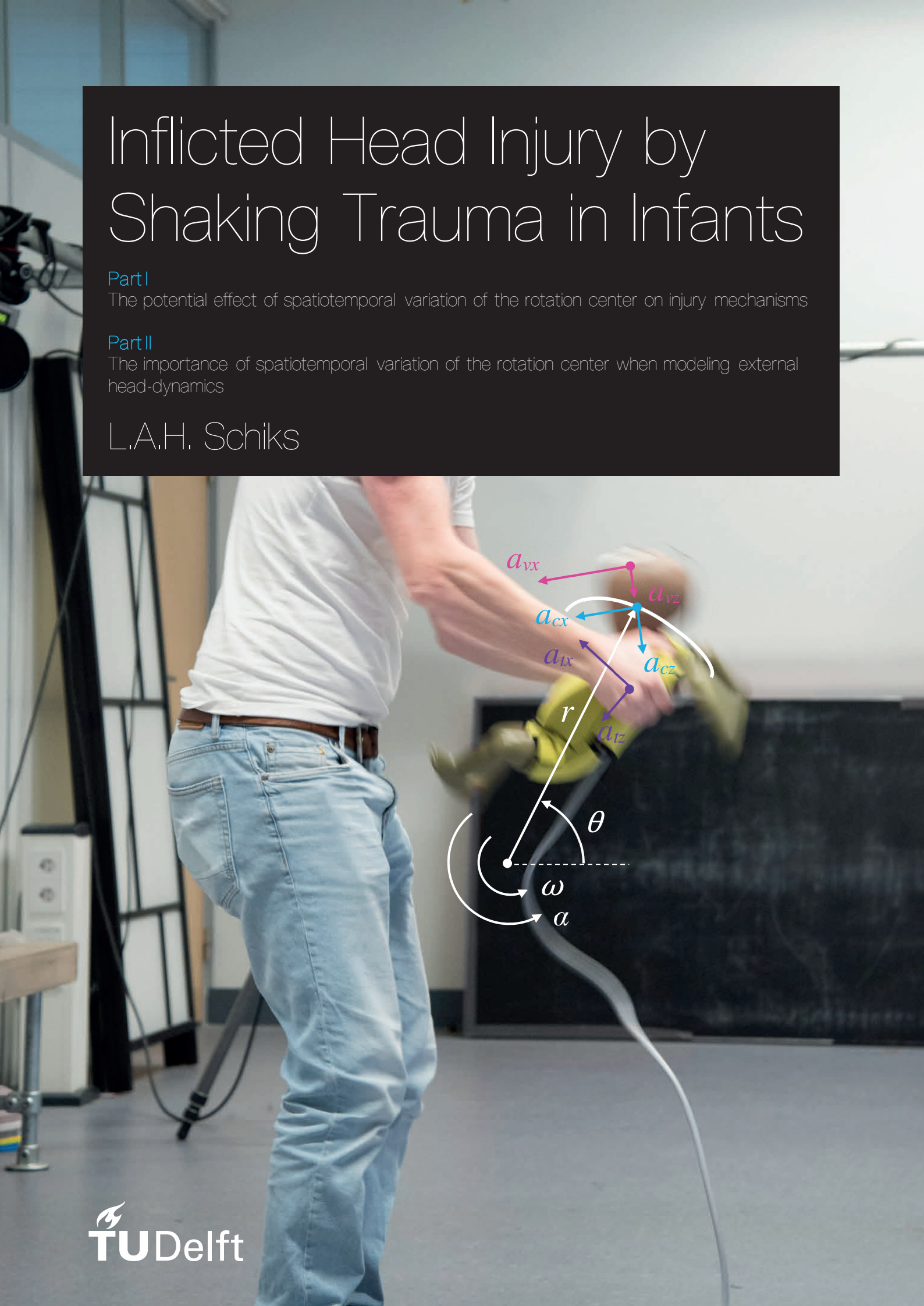


TU Delft

# Inflicted Head Injury by Shaking Trauma in Infants

Part I

The potential effect of spatiotemporal variation of the rotation center on injury mechanisms

Part II

The importance of spatiotemporal variation of the rotation center when modeling external head-dynamics

by

L.A.H. Schiks

to obtain the degree of

**Master of Science**
in Biomedical Engineering

at the Delft University of Technology,
to be defended publicly on Thursday July 18, 2019 at 11:00 AM.

| | | |
|---|---|---|
| Thesis committee: | Prof. Dr. J. Dankelman, | TU Delft, chair |
| | Dr. Ir. A.J. Loeve, | TU Delft, supervisor |
| | Prof. Dr. Ir. H. Vallery, | TU Delft |



TU Delft

# Preface

*I never lose. I either win or learn.*

Nelson Mandela
(1918-2013)

This thesis is the final result of my graduation project, the last step in completing the master Biomedical Engineering at the TU Delft. The incredible journey of the past few years finds its origin in the conversations with my physiotherapist, Willem Jan Becker. At that time I was finishing my bachelor in Mechanical Engineering when we discussed my study and future planning during our sessions. Here, I (or actually; we) came to the conclusion that my study was not going that great, I lacked motivation and had no plans. Willem Jan noticed how the technical nature of my spine issues got my interest, and suggested to take a look at the study Biomedical Engineering. From this point on, it all went on the fast track. To try out, a Biomedical topic became my bachelor graduation project; development of a CNC manufacturing process for allografts. After that, I was hooked.

With my motivation at sky-high levels, I completed the master courses. And it was here, at one of these courses that I met my supervisor, Arjo Loeve. His sharp feedback, great eye for detail, passion for the field, and relaxed manner of guidance are a much valued addition to the work presented in this thesis. During my internship, literature study, and graduation project I learned a lot from him, for which I would like to express my gratitude. Also, I would like to thank professor Jenny Dankelman for her time, advice, and quick responses despite her busy schedule.

Together with Anne, Edo, Else, Emilie, Hashim, Govert, Kim, Max, Suzanne, Sven and Yvonne I completed this master's course. I enjoyed the great time together, the joint study sessions, the drinks, the dinner nights, the karaoke nights, and the infinite amount of coffee breaks. To Bob and Rees, two of my closest friends from Delft; thank you for the support from the first year on. You guys were always available for help, motivation, and relaxation. That really made a difference.

Jim, thanks for the in depth discussions and advice throughout. It is great to share my interest for science with you. Manouk, thank you for being there for me, for your incredible support, and for putting up with me. Finally, I would like to thank my dear parents for their unconditional help and support throughout my entire studies.

*L.A.H. Schiks*
*Delft, July 2019*

# Contents

## Part I
The potential effect of spatiotemporal variation of the rotation center on injury mechanisms

## Part II

### The importance of spatiotemporal variation of the rotation center when modeling external head-dynamics



## Appendices

# Inflicted Head Injury by Shaking Trauma in Infants

## Part I: the potential effect of spatiotemporal variation of the rotation center on injury mechanisms

L.A.H. Schiks, J. Dankelman, A.J. Loeve
Department of BioMedical Engineering, Delft University of Technology, The Netherlands

**Abstract**

Inflicted head injury by shaking trauma (IHI-ST) is often simulated to better understand the injury mechanisms and to analyze whether violent shaking can cause head injury in infants. Computational models are usually subjected to linear and rotational inputs to simulate shaking scenarios. In existing studies, the head's rotation center is kept fixed over time during shaking. However, the infant's head is unlikely to rotate around a fixed pivoting point in real life due to the flexibility of the infant's neck and the external imposed shaking motion by the perpetrator. It is currently unknown how the location of the rotation center changes over time and how this manifests itself in the expression of the injury mechanisms associated with IHI-ST.

In this study, the variation of the rotation center of an infant's head during shaking and its potential effect on injury mechanisms were analyzed. First, dynamics of the infant's head were obtained in shaking experiments with an infant surrogate. Next, the variation of the rotation center was calculated and relations between characteristics of the participants and shaking variables were analyzed.

Key findings: during shaking the location of the head's rotation center varied in both anterior-posterior and vertical direction with respect to the head, causing the head's radius of curvature to vary six orders of magnitude. Therefore, head-dynamics and injury mechanisms underlying IHI-ST are possibly simulated incorrectly when using a fixed rotation center. It remains unclear how this affects the validity of IHI-ST injury risk assessments and the injury thresholds on which these assessments are based. Future research should therefore evaluate the performance of head-dynamic simulations regarding IHI-ST.

**Keywords**

Closed head injuries—child abuse—biomechanics—forensic pathology.

### Introduction

Each year 14-41 per 100.000 infants up to 1 year of age are diagnosed with inflicted head injuries [1–3]. Retinal hemorrhage, subdural hemorrhage, diffuse axonal injury, and neck injury are symptoms often associated with violent shaking of an infant. The diagnosis of inflicted head injury by shaking trauma (IHI-ST) based on the presence of such symptoms is often debated because these symptoms can also be caused by events other than abusive shaking [4–7]. However, no consensus has been reached yet regarding the question if shaking alone can actually result in loading anatomy beyond its failure thresholds [8–11].

Dynamic parameters such as angular acceleration or angular velocity, and biomechanical tissue properties such as ultimate strength, are examples of thresholds that are currently used to estimate injury risk [12,13]. Injury thresholds and head dynamics are hard to obtain directly from infants due to ethical considerations and hence are based on experiments with surrogates [14–16], mathematical models [15,17,18] or on extrapolated or scaled adult- or animal data [10,11,19]. Such studies investigate the effects of head dynamics during shaking on loading—and subsequent deformation—of anatomical structures, which is essential knowledge to determine whether or not violent shaking may cause damage to an infant's anatomy. However, the literature study preceding this thesis (submitted) showed that many infant shaking trauma assessment studies use inappropriate injury thresholds which did not match shaking loading conditions [12] (Appendix I). Furthermore, the center of rotation of an infant's head in IHI-ST computational models is usually defined as a fixed point somewhere at the cervical spine [20–25], although the infant's head is unlikely to rotate around a fixed pivoting point in real life due to the flexibility of the human neck and the external imposed shaking motion by the perpetrator.

Compressive and shear forces in the brain, strain rate, and relative displacement of the brain with respect to the skull, are all injury mechanisms that may result from linear and/or angular acceleration of the head [26–28]. However, whether rotation of the head will result in either predominantly compression forces in the brain, or shear

forces in- and rotation of the brain with respect to the skull, depends on the distance between the rotation center and the center of gravity of the head (COG); the radius of curvature (ROC) [20]. This can be illustrated best by two examples of the head in pure rotation; if the brain accelerates—with a certain magnitude X—around the center of gravity of the head, this will cause predominantly shear forces and rotation of the brain with respect to the skull[1]. In another case, if the brain accelerates—with the same magnitude X—around a point far away—in the order of meters—from the head's center of gravity, this results in a predominantly linear displacement of the brain within the skull. Although the angular acceleration magnitude is the same in both cases, they may result in distinctive tissue responses because the inertial acceleration experienced by each particle within the head is related to the ROC [20,29]. The former case is associated with ruptured bridging veins and diffuse injuries, while the latter is associated with contusions and focal injuries [26,30,31]. (See Appendix I for an extensive description of injuries and injury mechanisms in IHI-ST). Considering the above, model-based injury thresholds for IHI-ST may be over- or underestimated when using a fixed center of rotation over time.

It is currently unknown how the location of the instantaneous center of rotation (ICOR) changes over time and how this manifests itself in the expression of the injury mechanisms associated with IHI-ST. Therefore, it is also unknown to what extent IHI-ST computational studies accurately replicate the tissue-loading that results from violent shaking.

The aim of the present study is to obtain the spatiotemporal variation of the instantaneous center of rotation of an infant's head during shaking and to discuss its potential effect on injury mechanisms. Additionally, participant characteristics (gender, age, height, and weight) and shaking variables (e.g. accelerations of the head) were analyzed to identify which factors increase shaking intensity.

## Methods

### Experimental protocol and study population

An infant surrogate shaking experiment was performed at the BioMechaMotion lab of the Delft University of Technology (Delft, The Netherlands). Participants were instructed to shake an infant surrogate back and forth in the sagittal plane as violently and as long as possible, in order to investigate the maximum accelerations occurring during violent shaking. Approval for this experiment was granted by the university's Human Research Ethics Committee under study number 698 (Appendix II). A total of 33 volunteers participated in the experiment, data of 29 volunteers were included in the analysis. Mean age of the included 29 participants was 33 years (range 21 to 64, 8 female and 21 male).

### Data acquisition

#### Instrumented infant surrogate

Motion of the dummy's head and bulk dynamics during shaking were measured simultaneously by means of sensors attached to the infant surrogate and a motion capture system; both calibrated prior to the experiments. An instrumented Q0 crash-test dummy (First Technology Safety Systems, Delft, The Netherlands) was used as an infant surrogate (mimicking a 6 week-old, 3.4 kg infant, based on [32]) to capture kinematic and dynamic data during the shaking experiments; i.e. angular velocity of the head, and linear accelerations in three directions at the torso, at the COG and at the vertex of the dummy's head.

A custom-made sensor bracket replaced the dummy's original load cell and contained the necessary sensors for additional measuring at the head's vertex (Figure 1). The bracket was designed to match the dimensions and inertial properties of the original load cell to not compromise the biofidelity of the dummy. (See Appendix III for a detailed description and technical drawings of the custom made sensor bracket and modified dummy). The sensor bracket was equipped with a uniaxial vibration rejecting gyroscope—ADXRS649, measurement range ±20,000 °/sec, Analog Devices, Inc., Norwood Massachusetts, USA—and two tri-axial accelerometers—ADXL377, measurement range ±200 *g*, Analog Devices, Inc., Norwood Massachusetts, USA. An identical accelerometer was placed in the torso.

A power spectral density analysis of the acceleration data of similar experiments [33] (under submission) with the Q0 dummy revealed that the accelerometer signal power beyond 250 Hz was less than -25 dB. Therefore it was decided to set the bandwidth of the accelerometers to 500 Hz, providing a safe margin. Unfortunately, no such data were available on the angular velocity, hence it was decided to use the gyroscope's maximum bandwidth of 2 KHz.

[1] Due to mass inertia of the brain and the surrounding cerebrospinal fluid layer.

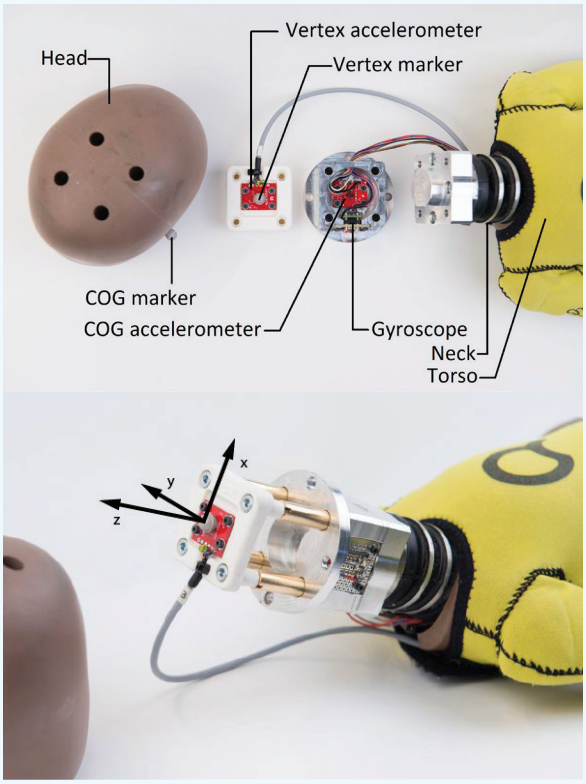


**Figure 1.** Bracket for the two head-accelerometers and gyroscope. (Top) Component overview. COG: Center of gravity. (Bottom) Sensing axes according to a right-hand coordinate system with respect to human body axes: x-direction, longitudinal axis, anterior positive; y-direction, transverse axis, left positive; z-direction, vertical axis, superior positive. Flexion of the neck represents a positive rotation around the y-axis.

### Motion capture system

An Oqus 700 motion capture system (Qualysis, Göteborg, Sweden) was used to record the three-dimensional trajectory of the dummy's head during shaking. This system consists of 12 motion-tracking infrared cameras, tracking passive 7 mm spherical reflective markers that were attached to the vertex and to the left side of the dummy's head, coinciding with the z- and y-axis of the dummy's head respectively. (See Appendix IV for the applied camera settings of the motion capture system).

### Data logging

Data of the dummy sensors were recorded with a Data Acquisition system (DAQ)—NI USB-6211, National Instruments, Austin, Texas, U.S.A. The trigger signal of the motion capture system was recorded to synchronize the sensor data with the motion capture data later in the data analysis. (See Appendix V for the connection diagram of the setup). Sensor data was sampled at a frequency of 5 KHz in order to capture the steep peaks in the linear accelerations accurately. The maximum sampling frequency of the motion capture system was only 1 KHz, but this proved sufficient. Motion data were up-sampled by interpolation to match the sensor data.

## Data analysis

### Calculations

The shaking motion occurred mainly in the sagittal plane (x-z-plane), making accelerations in y-direction negligible with respect to accelerations in the x- and z-direction (Figure 2). Therefore, the analysis was reduced from three to two dimensions to simplify the calculations.

The angle $\theta$ (rad) between z-axis of the dummy's head and the z-axis of the inertial reference frame was calculated using the positions of the reflective markers. The angular velocity $\omega$ (rad/s) was then calculated by differentiation of the angle $\theta$. Likewise, the angular acceleration $\alpha$ (rad/s$^2$) was calculated by differentiation of the angular velocity $\omega$. The maximum angular velocity $\omega_{max}$ and maximum angular acceleration $\alpha_{max}$ were obtained from these calculated values of ω and $\alpha$.

Maximum values of the resultant vertex-, COG- and torso accelerations, $a_{tor\text{-}max}$ (m/s$^2$), $a_{cog\text{-}max}$ (m/s$^2$), $a_{ver\text{-}max}$ (m/s$^2$) respectively, were extracted from the sensor data. The vertex motion x-direction data were differentiated to determine the maximum tangential velocity of the dummy head vertex $v_{vx\text{-}max}$ (m/s).

The rotation center location was calculated for the entire shake cycle (Figure 3) with the highest vertex tangential acceleration peak. For each time step the following calculations were performed: 1) a line tangential to each of the trajectories of the vertex and COG was calculated, 2) for both the vertex and COG, a line perpendicular to the tangent line and coinciding the trajectory was calculated, 3) finally the location of the instantaneous center of rotation (ICOR) was defined as the intersection point of the two lines perpendicular to the trajectories. The ROC was

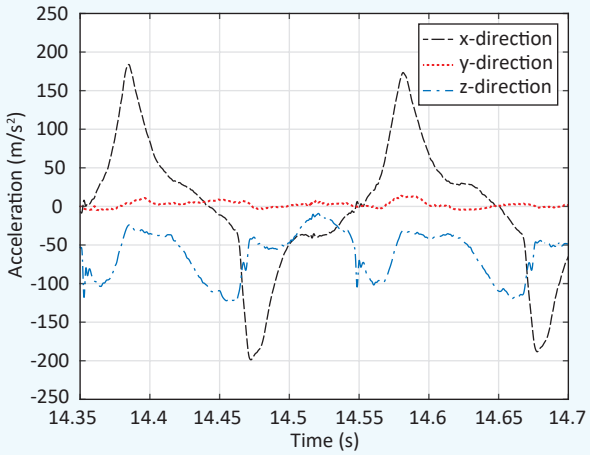


**Figure 2.** Typical vertex accelerations of the dummy's head during violent shaking.

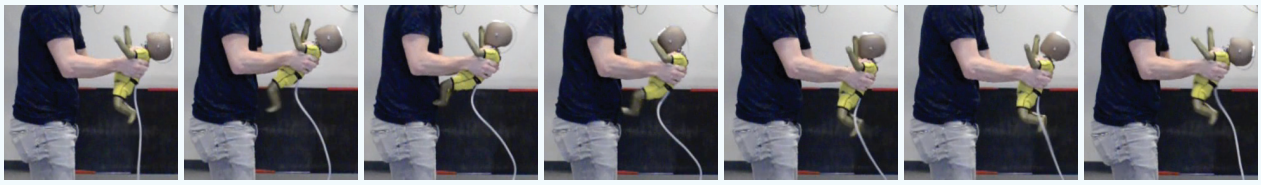


**Figure 3.** Subsequent stages in the full shake cycle of the dummy (a-g). The shake cycle starts (a) when the dummy neck is fully extended, half way the cycle (d) the dummy neck is fully flexed and at the end of the cycle (g) the situation is equal to (a) again.

defined as the absolute distance between the ICOR and COG of the dummy's head. Figure 4 provides a visual representation of the steps above. MathWorks MATLAB was used to perform the calculations and to filter the data. (See Appendix VI for the full algorithm).

### Data filtering

Initial visualization of the data indicated the presence of high-frequent noise in the unfiltered signals of the accelerometers, gyroscope and motion data. A power spectral density analysis of the accelerometer signals showed that low power noise peaks were present at frequencies above the frequency bandwidth—up to 500 Hz—of the accelerometers (Figure 5).

A Butterworth 12th-order low-pass zero-phase-lag digital IIR filter with a cutoff frequency of 500 Hz was applied to smooth the accelerometer signals and thereby enabling the algorithm to calculate the actual acceleration peaks instead of detecting the noise peaks.

The recorded marker trajectories were smoothed to enable fitting tangential lines to these curves. Noise in the motion data would result in errors in the tangent lines and consequently in the calculated location of the rotation center. Therefore, the motion data was smoothed using the same Butterworth filter as for the accelerometer data, but with a cutoff frequency of 10 Hz.

### Statistics

IBM SPSS Statistics 25 was used for the statistical analysis. Linear regression analysis was used to find correlations between shaking variables (i.e. torso acceleration, head COG acceleration, head vertex

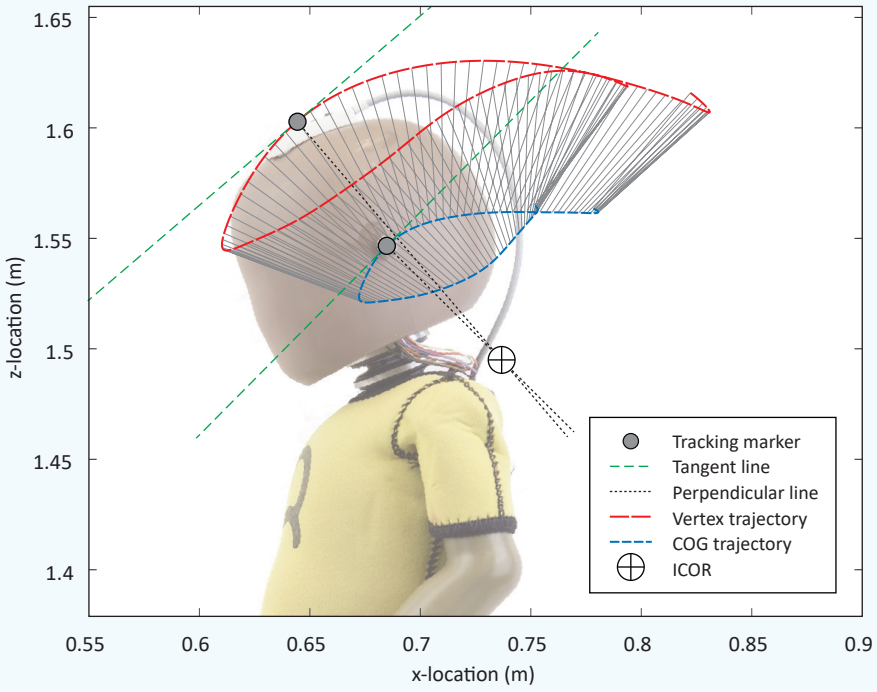


**Figure 4.** Visual representation of the 3-step calculation of the instantaneous center of rotation (ICOR). Each tangent line is tangential to the marker's trajectory. The intersection point of the lines perpendicular to the tangent lines is the ICOR; corresponding to a *single* calculation-step in a single typical shake cycle. The depicted trajectories show a *full* single typical shake cycle. The solid lines between the vertex and COG trajectories indicate corresponding datapoints from the same time-step.

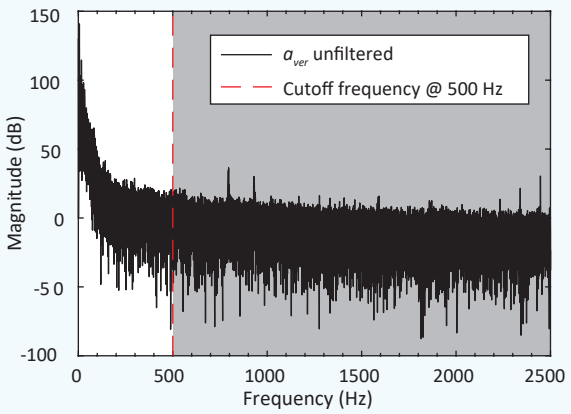


**Figure 5.** The power spectral density analysis indicated dominant noise peaks around 850 Hz. The unshaded area represents the signal of interest. Low power, high-frequent noise was filtered out, indicated by the shaded area.

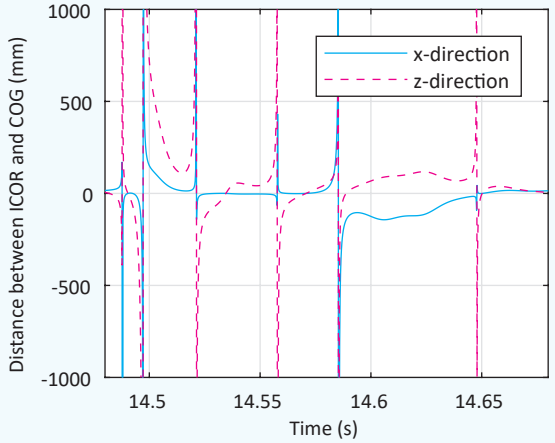


**Figure 6.** Typical example of the location of the instantaneous center of rotation (ICOR) over time with respect to the center of gravity (COG) of the dummy's head.

acceleration, head angular velocity, head angular acceleration, head vertex velocity and shake frequency) and anthropometric characteristics of the participants (i.e. age, height, weight).

A multivariate analysis of variance (MANOVA) was conducted to test whether differences were present in the shaking variables (i.e. torso acceleration, head COG acceleration, head vertex acceleration, head angular velocity, head angular acceleration, head vertex velocity and shake frequency) between men and women. (See Appendix VII for the complete analysis).

## Results

### Spatiotemporal variation of the rotation center

The location of the ICOR of the dummy's head varied over time within a shaking cycle, in both x- and z-direction with respect to the COG (Figures 6 and 7). The ROC—which is the absolute distance between the ICOR and the COG—also varied greatly over time during a shaking cycle (Figure 8: top).

The minimum and maximum ROC that were attained were $2.9 \cdot 10^{-3}$ m and $2.1 \cdot 10^{3}$ m respectively; a difference of six orders of magnitude. The mean value of the median ROC during the shake cycle with the highest vertex acceleration was 97 mm, SD = 39 mm, across all participants.

The ROC fluctuated largely in the proximity of angular acceleration peaks (Figure 8: bottom). The ROC at the instance of the absolute maximum $\omega$ and $\alpha$ had a median over all participants of 26 mm (min. 2 mm, max. 244 mm) and 38 mm (min. 3 mm, max. 155 mm) respectively.

### Shaking variable statistics

No significant correlations were found between the anthropometric variables age, height and weight and any of the shaking variables (Table 1). However, large differences were found between the maximum values of shaking variables obtained by male and female participants (Figure 9). The mean values of all shaking variables were significantly higher for men than for women (Table 2).

Descriptive statistics of the peak values of shaking variables during the shaking experiment and the average shaking frequency across all participants are provided in Table 3. Peak linear accelerations of the torso, the head's COG, and the head's vertex represent the highest acceleration peaks that were encountered in the entire trial of each participant. The same holds for the peak tangential vertex velocity $v_{vx\text{-}max}$, peak angular velocity $\omega_{max}$ and angular acceleration $\alpha_{max}$. The shaking frequency $f_{shake}$ was averaged over the entire trial of each participant. (See Appendix VIII for a full overview of the shaking variables for each participant).

### Shaking pattern

Among the participants, considerable variations were present in the trajectories of the dummy's head during shaking. Some notable differences in the trajectories were; small vs. large amplitude, weakly curved vs. strongly curved, circular vs. eight-shaped, little vs. much vertical displacement of the COG, and horizontal vs. gravity assisted[2] shaking (Figure 10).

[2] i.e. shaking the infant in a more downward direction to make use of the gravity acceleration

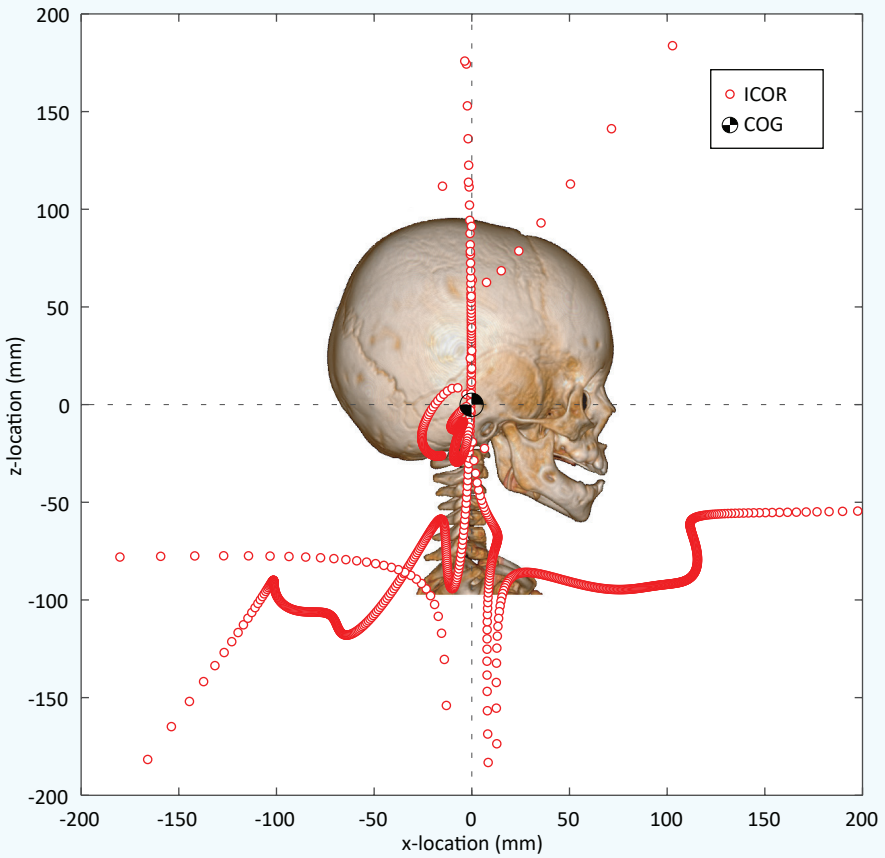


**Figure 7.** Graphical representation of spatiotemporal variation of the instantaneous center of rotation (ICOR) with respect to the center of gravity (COG) of the head, during a single typical shake cycle. 3D CT-scan of a 6-week old infant.

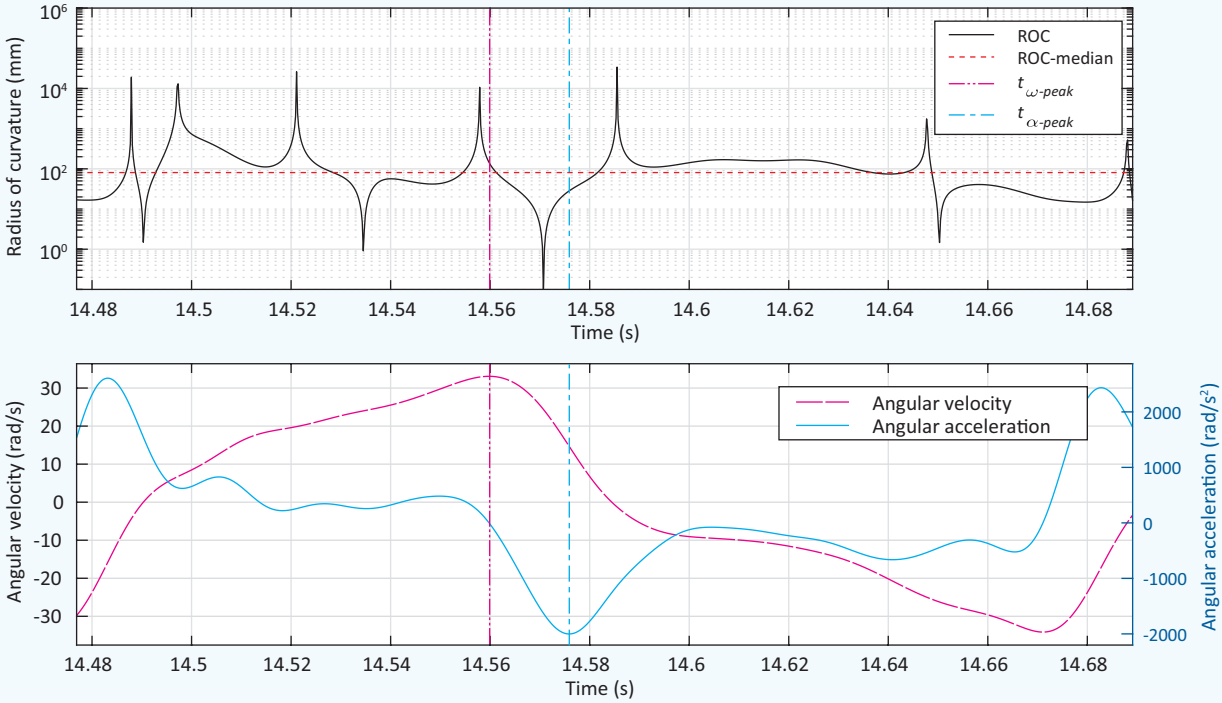


**Figure 8.** (Top) radius of curvature (ROC) of the head's center of gravity during a single typical shake cycle. (Bottom) angular velocity of the head and angular acceleration of the head during a single typical shake cycle. The ROC was highly variable at some points in the shake cycle, also in the proximity of angular acceleration peaks.

**Table 1.** Correlation coefficient matrix of the study variables (Pearson's r (sig.)). None of the correlations were significant (p>0.05).

| | $a_{tor\text{-}max}$ | $a_{cog\text{-}max}$ | $a_{ver\text{-}max}$ | $\omega_{max}$ | $\alpha_{max}$ | $v_{vx\text{-}max}$ | $f_{shake}$ |
|---|---|---|---|---|---|---|---|
| **Age** | -.154 (.427) | -.271 (.156) | -.241 (.209) | -.206 (.283) | -.272 (.154) | -.190 (.323) | .068 (.726) |
| **Height** | .205 (.285) | .116 (.549) | .149 (.439) | .205 (.287) | .200 (.297) | .177 (.357) | .293 (.123) |
| **Weight** | .220 (.250) | .046 (.812) | .126 (.516) | .265 (.165) | .165 (.393) | .173 (.369) | .151 (.434) |

**Table 2.** Differences between men and woman in peak magnitudes of all shaking variables. All differences were significant (p≤0.05).

| | Mean [SD] men | Mean [SD] women | Difference in mean | F-value | Sig. |
|---|---|---|---|---|---|
| $a_{tor\text{-}max}$ $(m/s^2)$ | 137 [49] | 87 [23] | 50 | F(1,27) = 7.45 | .011 |
| $a_{cog\text{-}max}$ $(m/s^2)$ | 163 [46] | 113 [31] | 50 | F(1,27) = 8.02 | .009 |
| $a_{ver\text{-}max}$ $(m/s^2)$ | 333 [110] | 214 [73] | 119 | F(1,27) = 7.99 | .009 |
| $\omega_{max}$ $(rad/s)$ | 47 [10] | 33 [6] | 14 | F(1,27) = 13.93 | .001 |
| $\alpha_{max}$ $(rad/s^2)$ | 3,362 [933] | 2,058 [591] | 1,304 | F(1,27) = 13.40 | .001 |
| $v_{vx\text{-}max}$ $(m/s)$ | 4.7 [1.2] | 3.4 [1.0] | 1.3 | F(1,27) = 7.05 | .013 |
| $f_{shake}$ $(Hz)$ | 4.7 [0.8] | 4.0 [0.5] | 0.7 | F(1,27) = 4.76 | .038 |

**Table 3.** Peak magnitudes of the shaking variables across all participants.

| | $a_{tor\text{-}max}$ $(m/s^2)$ | $a_{cog\text{-}max}$ $(m/s^2)$ | $a_{ver\text{-}max}$ $(m/s^2)$ | $\omega_{max}$ $(rad/s)$ | $\alpha_{max}$ $(rad/s^2)$ | $v_{vx\text{-}max}$ $(m/s)$ | $f_{shake}$ $(Hz)$ |
|---|---|---|---|---|---|---|---|
| **Maximum** | 257 | 276 | 606 | -66 | 6,010 | 7.0 | 6.2 |
| **Mean** | 130 | 155 | 302 | 43 | 3,033 | 4.5 | 4.5 |
| **SD** | 51 | 51 | 108 | 10 | 995 | 1.3 | 0.8 |

## Discussion

### Injury mechanisms

The location of the instantaneous center of rotation (ICOR) of the dummy's head varied over time during shaking, this could affect current understandings regarding the injury mechanisms of IHI-ST. Differences between linear accelerations of the head's vertex and center of gravity (COG) were large; peak vertex accelerations were often over twice the corresponding COG accelerations.

The difference in acceleration magnitude between the head's vertex and the COG is determined by three factors: 1) the magnitude of the angular acceleration; causing a difference in the tangential acceleration components of the vertex and the COG independent of the ICOR location, 2) the magnitude of the angular velocity; causing a difference in the normal acceleration components of the vertex and the COG independent of ICOR location and 3) the location of the ICOR; causing a difference in both the tangential and normal acceleration components. Hence, to some extent, the location of the ICOR may attribute to the nature of tissue deformations. Theoretically, when the skull and brain are considered as a rigid body, those differences in acceleration magnitude between the vertex and the COG create the optimal conditions for shear forces in the brain. In practice, however, the brain is surrounded by a layer of cerebrospinal fluid, which allows the brain to rotate with respect to the skull. This lessens the effect of head rotation on shear forces in the brain somewhat, although it is precisely that displacement of the brain with respect to the skull which causes stretching of bridging veins.

### Validity of injury thresholds

At the moments of peak angular velocity and peak angular acceleration—the parameters on which several existing injury thresholds are based [10,11,34–38]—the median ROCs were found to be 26 mm and 38 mm, respectively.

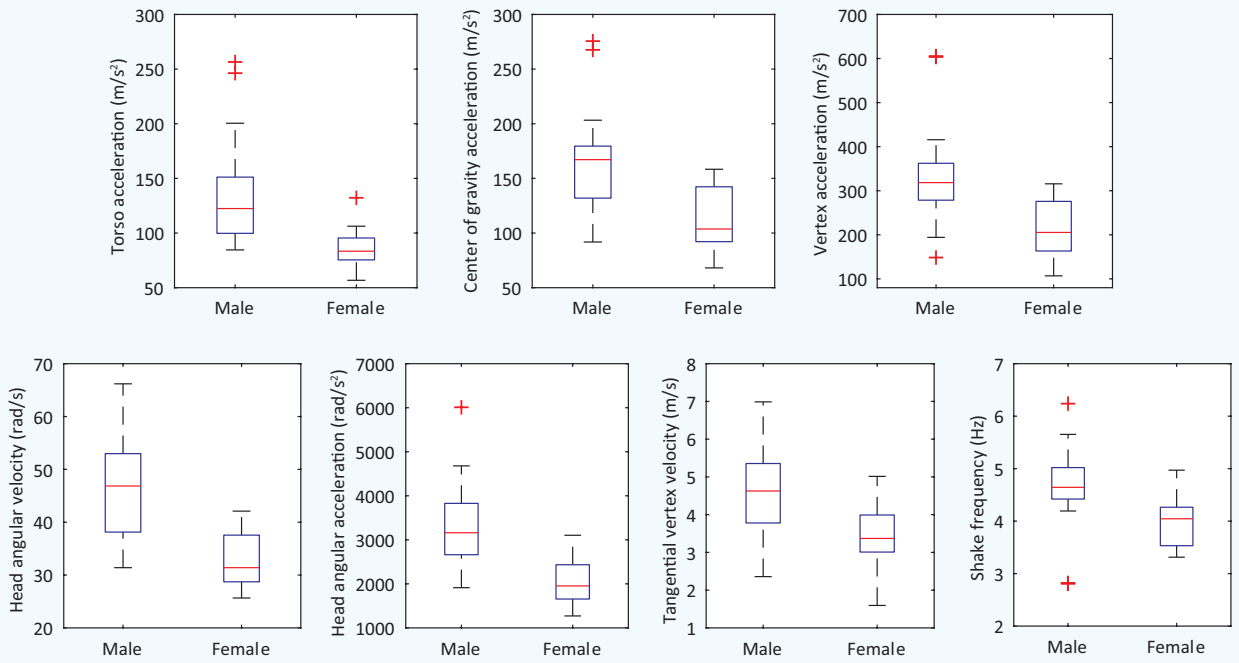


**Figure 9.** Boxplot of the maximum values of shaking variables. Large differences were present between the values obtained by male and female participants and within these two groups. Multiple outliers were found for some of the variables.

Computational models in the literature, however, usually define the base of the skull, the C5-C6 junction or the base of the neck as the ICOR [20–25]; corresponding with ROCs of around 25 mm, 65 mm and 80 mm, respectively.

A small ROC might cause completely different deformations of anatomical structures and displacement of the brain with respect to the skull, compared to a larger ROC, because the acceleration experienced by each particle in the head is depending on its distance to the rotation center [20]. Evidently, tissue deformations are related to accelerations experienced by each particle, their connections with surrounding particles, and to interactions with other anatomical structures, which are all directly or indirectly related to the location of the ICOR. Hence stating all the above, it could be that injury thresholds based on peak magnitudes [10,11,34–38] are overestimated, and tissue deformations simulated by computational models with the ICOR at the base of the skull, the C5-C6 junction or the base of the neck [20–25], are underestimated.

In the proximity of the maxima of the angular velocity and angular acceleration, the ICOR showed to be very near the COG of the dummy's head while at the same moment angular accelerations close to the maximum were present. Since it is the combination of the angular velocity, angular acceleration and the location of the ICOR that determines how the anatomy in the head is loaded and deformed, it might be the case that tissue is loaded at its maximum on a moment that is not necessarily the point of maximum angular acceleration/velocity. Furthermore, the participant obtaining the highest angular acceleration/velocity (among all participants) did not obtain the highest linear head acceleration, and moreover, maximum values of the head's angular acceleration and angular velocity did not occur at the same time. Therefore, it is questionable whether currently used injury thresholds based on kinematic parameters [10,11,34–38] (e.g. maximum angular acceleration, maximum angular velocity, maximum linear head accelerations) are valid.

## Shaking variables

Results of the present study show that outliers can be around twice the mean value across all participants for peak accelerations and velocities. However, studies in the literature in which a physical model was used to obtain shaking dynamics [10,15,16,37,39–41], had a relatively small sample size (varying from 1-11 participants) compared to the present study. When examining the worst case shaking dynamics that a human is physically able to produce, it is important to take a sufficiently large sample size and include subjects that largely deviate from the average.

Furthermore, the results indicate that maximum values of some shaking variables (torso-, head COG-, and vertex linear accelerations; head angular velocity and acceleration; shaking frequency) were outside the range of mean+2SD. This implies that during violent shaking, 95% of the people

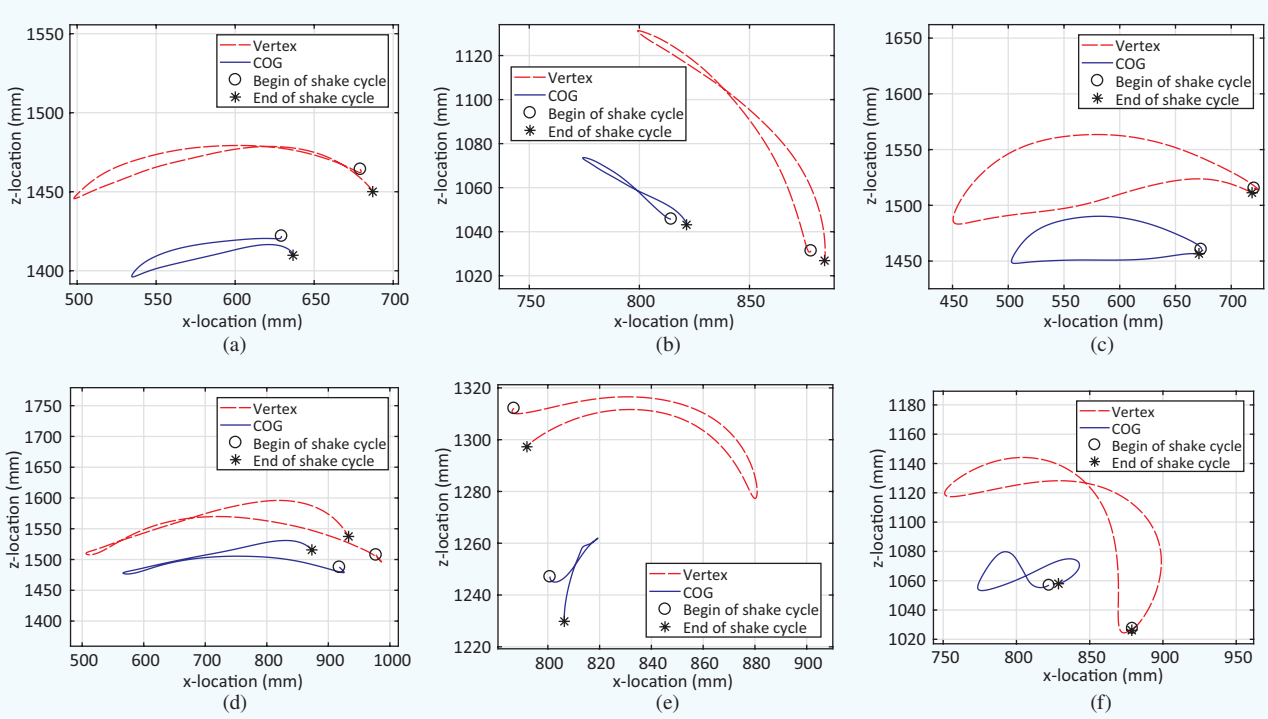


**Figure 10.** Typical examples of the various shaking pattern variations encountered during the study: (a,d) small vs. large amplitude; (d,f) weakly curved vs. strongly curved; (c,f) circular vs. eight-shaped; (a,e) little vs. much vertical displacement of the COG; (a,b) horizontal vs. gravity assisted shaking. Coordinates are expressed in the inertial reference frame.

will not reach those maximum values, it also demonstrates the importance of taking into account that there is a difference between 'what an *average human* is physically capable of' and 'what *the suspect* is physically capable of'.

The experimental results demonstrate that men cause more vigorous shakes than women, though the participant's age, height, and weight did not correlate with shaking variables. Presumably, other factors such as shaking pattern, muscle force, condition, sports habits, or the ratio of body weight to muscle mass, are determinants for the intensity of shaking.

## Limitations

### Infant surrogate

Exposure of the dummy to the violent shaking during the present- and previous experiments, caused the 4 mm steel cable in the dummy's neck to break. After 29 trials one end of the neck cable was broken, and several strands on the other end of the cable were damaged as well. Therefore, data from 4 volunteers were excluded from the analysis. (See Appendix IX for excluded experimental data).

### Instrumentation

The frequency bandwidth of the gyroscope chip itself (2 KHz) was more than sufficient, yet a (retrospectively noticed) low-pass filter in the third party sensor-evaluation-board limited the frequency bandwidth to only 10 Hz. Comparison of the gyroscope data with the analyzed motion data demonstrated insufficient frequency bandwidth of the gyroscope setup for analyzing violent shaking motions. For this reason, gyroscope data were not used in the analysis.

### Shaking scenario

Participants were instructed only once, during the briefing, to shake an infant surrogate as violently and as long as possible. However, it is expected that the limits—regarding the shaking variables—of what a human is physically capable of, are not reached yet. Feelings of anger and despair experienced by a perpetrator might result in more vigorous shaking.

## Recommendations for future research

### Computational studies

Future research should investigate the effect of the time-varying nature of the ICOR on the temporal accuracy of external skull-dynamics in IHI-ST computational models (see Part II). In order to investigate the effect of the time-varying nature of the center of rotation on internal skull-dynamics (e.g. tissue deformation or intracranial pressure), the calculated values of the ICOR and its acceleration may be used as model-input in future IHI-ST simulation studies. The full dataset is available for download through the repository of the 4TU Centre for Research Data. doi:10.4121/uuid:29853e7a-4074-46cf-802b-6ba63a9a791b.

The present findings can have important implications for comparable scenarios of head injury. The approach presented in this study can therefore be useful in other scientific areas, such as forensic science and vehicle safety studies.

### Instrumentation for physical model studies

Further tests with physical models using gyroscopes and accelerometers must take into account a minimum frequency bandwidth. This is vital to prevent underestimation of peak magnitudes of angular velocity and linear accelerations of the infant's head in violent shaking scenarios. Based on the power spectral density analyses, minimum bandwidths of 100 Hz and 500 Hz are advised for gyroscopes and accelerometers respectively.

### Shaking scenario

Future studies should focus on the identification of shaking-intensity determinants to aid simulating worst-case shaking scenarios. Also, induced anger feelings and encouragement of the participants during shaking may result in more intense shaking. When giving participants a free choice of shaking method, new, even more damaging shaking methods may be discovered. Recruiting specifically young participants may better reflect the group of common offenders, who are typically younger than 18 years old [42].

## Conclusion

The results showed that the location of the instantaneous center of rotation (ICOR) of the dummy's head varied greatly over time during violent shaking. Currently existing IHI-ST computational studies usually define the ICOR as a fixed point in the cervical spine, while the location of the ICOR with respect to the dummy's head differed six orders of magnitude during shaking. Therefore, it is questionable whether simulation results of currently existing computational studies, including injury thresholds following from such studies, are valid.

## Acknowledgments

The authors would like to thank Dr. Arne Stray-Pedersen and the Department of Forensic Medicine (University of Oslo, Oslo, Norway) for providing the Q0 infant surrogate, and Prof.Dr.Ir. Jaap Harlaar (Delft University of Technology, Delft, The Netherlands), who provided the opportunity to work in the BioMechaMotion lab and made all equipment available to us.

## Abbreviations

| | |
|---|---|
| **IHI-ST** | Inflicted head injuries by shaking trauma in infants |
| **COG** | Center of gravity |
| **ROC** | Radius of curvature |
| **ICOR** | Instantaneous center of rotation |
| **DAQ** | Data acquisition system |
| **MANOVA** | Multivariate analysis of variances |

## References

[1] M. Fanconi, U. Lips, Shaken baby syndrome in Switzerland: results of a prospective follow-up study, 2002-2007, Eur. J. Pediatr. 169 (2010) 1023–28. doi:10.1007/s00431-010-1175-x.

[2] K.D. Ellingson, J.M. Leventhal, H.B. Weiss, Using Hospital Discharge Data to Track Inflicted Traumatic Brain Injury, Am. J. Prev. Med. 34 (2008) S157–S162. doi:10.1016/j.amepre.2007.12.021.

[3] I. Talvik, T. Metsvaht, K. Leito, H. Põder, P. Kool, M. Väli, M. Lintrop, A. Kolk, T. Talvik, Inflicted traumatic brain injury (ITBI) or shaken baby syndrome (SBS) in Estonia, Acta Paediatr. 95 (2006) 799–804. doi:10.1111/j.1651-2227.2006.tb02343.x.

[4] M. Mian, J. Shah, A. Dalpiaz, R. Schwamb, Y. Miao, K. Warren, S. Khan, Shaken baby syndrome: A review, Fetal Pediatr. Pathol. 34 (2015) 169–75. doi:10.3109/15513815.2014.999394.

[5] M. Vinchon, O. Noizet, S. Defoort-Dhellemmes, G. Soto-Ares, P. Dhellemmes, Infantile subdural hematomas due to traffic accidents, Pediatr. Neurosurg. 37 (2002) 245–53. doi:10.1159/000066216.

[6] G. Elinder, A. Eriksson, B. Hallberg, N. Lynøe, P.M. Sundgren, M. Rosén, I. Engström, B.E. Erlandsson, Traumatic shaking: The role of the triad in medical investigations of suspected traumatic shaking, Acta Paediatr. Int. J. Paediatr. 107 (2018) 3–23. doi:10.1111/apa.14473.

[7] M. Laghmari, H. Skiker, H. Handor, B. Mansouri, K. Ouazzani Chahdi, R. Lachkar, Y. Salhi, O. Cherkaoui, B. Ouazzani Tnacheri, W. Ibrahimy, H. Alami, R. Bezad, S. Ahid, R. Abouqal, R. Daoudi, [Birth-related retinal hemorrhages in the newborn: incidence and relationship with maternal, obstetric and neonatal factors. Prospective study of 2,031 cases], J. Fr. d Opthalmologie. 37 (2014) 313–9. doi:http://dx.doi.org/10.1016/j.jfo.2013.06.005.

[8] S.C. Gabaeff, Challenging the Pathophysiologic Connection between Subdural Hematoma, Retinal Hemorrhage and Shaken Baby Syndrome, West. J. Emerg. Med. 12 (2011) 144–58.

[9] W. Squier, Shaken baby syndrome: The quest for evidence, Dev. Med. Child Neurol. 50 (2008) 10–4. doi:10.1111/j.1469-8749.2007.02004.x.

[10] C.Z. Cory, M.D. Jones, Can shaking alone cause fatal brain injury? A biomechanical assessment of the Duhaime shaken baby syndrome model, Med. Sci. Law. 43 (2003) 317–33. doi:10.1258/rsmmsl.43.4.317.

[11] T.O. Lintern, M.P. Nash, P. Kelly, F.H. Bloomfield, A.J. Taberner, P.M.F. Nielsen, Probabilistic description of infant head kinematics in abusive head trauma, Comput. Methods Biomech. Biomed. Engin. 20 (2017) 1633–42. doi:10.1080/10255842.2017.1403593.

[12] L.A.H. Schiks, J. Dankelman, A.J. Loeve, Thresholds for the assessment of inflicted head injury by shaking trauma in infants: a systematic review, Forensic Sci. Int. (2019) Submitted.

[13] J.P. van Zandwijk, M.E.M. Vester, R.A. Bilo, R.R. van Rijn, A.J. Loeve, Modeling of inflicted head injury by shaking trauma in children: what can we learn? Part II: A systematic review of mathematical and physical models, Forensic Sci. Med. Pathol. (2019). doi:10.1007/s12024-019-00093-7.

[14] T. Koizumi, N. Tsujiuchi, K. Hara, Y. Miyazaki, Dynamic response and damage estimation of infant brain for vibration, in: Proc. Soc. Exp. Mech. Ser., 2013: pp. 11–8. doi:10.1007/978-1-4614-6546-1_2.

[15] J. Lloyd, E.N. Willey, J.G. Galaznik, W.E. Lee, S.E. Luttner, Biomechanical Evaluation of Head Kinematics During Infant Shaking Versus Pediatric Activities of Daily Living, J. Forensic Biomech. 2 (2011) 1–9. doi:10.4303/jfb/f110601.

[16] S. Cirovic, M. Freddolini, R. Goodwin, D. Zimarev, Shaken Mannequin Experiments: Head Motion Pattern and Its Potential Effect on Blood Pressure, J. Forensic Biomech. 3 (2012). doi:10.4303/jfb/235476.

[17] L. Ren, D. Baumgartner, J. Yang, J. Davidsson, R. Willinger, Investigation of diffuse axonal injury induced by rotational acceleration via numerical reconstructions of in vivo rat head impact experiments, Int. J. Crashworthiness. 20 (2015) 602–12. doi:10.1080/13588265.2015.1073132.

[18] B. Coats, S.A. Eucker, S. Sullivan, S.S. Margulies, Finite element model predictions of intracranial hemorrhage from non-impact, rapid head rotations in the piglet, Int. J. Dev. Neurosci. 30 (2012) 191–200. doi:10.1016/j.ijdevneu.2011.12.009.

[19] S.A. Pasquesi, S.S. Margulies, Failure and fatigue properties of immature human and porcine parasagittal bridging veins, Ann. Biomed. Eng. 45 (2017) 1877–1889. doi:10.1007/s10439-017-1833-5.

[20] C.N. Morison, The dynamics of shaken baby syndrome, University of Birmingham, 2002.

[21] S. Roth, J.S. Raul, B. Ludes, R. Willinger, Finite element analysis of impact and shaking inflicted to a child, Int. J. Legal Med. 121 (2007) 223–8. doi:10.1007/s00414-006-0129-3.

[22] J.S. Raul, S. Roth, B. Ludes, R. Willinger, Influence of the benign enlargement of the subarachnoid space on the bridging veins strain during a shaking event: A finite element study, Int. J. Legal Med. 122 (2008) 337–40. doi:10.1007/s00414-008-0242-6.

[23] S.A. Hans, S.Y. Bawab, M.L. Woodhouse, A finite element infant eye model to investigate retinal forces in shaken baby syndrome, Graefe's Arch. Clin. Exp. Ophthalmol. 247 (2009) 561–71. doi:10.1007/s00417-008-0994-1.

[24] Z. Couper, F. Albermani, Mechanical response of infant brain to manually inflicted shaking, Proc. Inst. Mech. Eng. Part H J. Eng. Med. 224 (2010) 1–15. doi:10.1243/09544119JEIM587.

[25] D.C. Batterbee, N.D. Sims, W. Becker, K. Worden, J. Rowson, Computational model of an infant brain subjected to periodic motion simplified modelling and bayesian sensitivity analysis, in: Proc. Inst. Mech. Eng. Part H J. Eng. Med., 2011: pp. 1136–49. doi:10.1177/0954411911420002.

[26] A.I. King, K.H. Yang, L. Zhang, W. Hardy, D.C. Viano, Is head injury caused by linear or angular acceleration, in: IRCOBI Conf., 2003.

[27] S.J. Strich, Shearing of nerve fibres as a cause of brain damage due to head injury. A pathological study of twenty cases, Lancet. 278 (1961) 443–48. doi:10.1016/S0140-6736(61)92426-6.

[28] A.H.S. Holbourn, Mechanics of head injuries, Lancet. 242 (1943) 438–41. doi:10.1016/S0140-6736(00)87453-X.

[29] F.J. Unterharnscheidt, Translational versus rotational acceleration: animal experiments with measured input., in: Proc. 15th Stapp Car Crash Conf., 1971: pp. 767–70. doi:10.4271/710880.

[30] T.A. Gennarelli, L.E. Thibault, A.K. Ommaya, Pathophysiologic responses to rotational and translational accelerations of the head, in: Proc. 16th Stapp Car Crash Conf., 1972: pp. 296–307. doi:10.4271/720970.

[31] T.A. Gennarelli, A.K. Ommaya, L.E. Thibault, Comparison of translational and rotational head motions in experimental cerebral concussion, in: Proc. 15th Stapp Car Crash Conf., 1971. doi:10.1017/S000748530002229X.

[32] D. Twisk, Anthropometric data of children for the development of dummies, 1994.

[33] A. Stray-Pedersen, A.J. Loeve, L.A.H. Schiks, Violent infant surrogate shaking: Continuous high magnitude centripetal force and abrupt shift in tangential acceleration may explain high risk for subdural haemorrhage (under submission), (2019).

[34] J. Davidsson, M. Angeria, M.G. Risling, Injury threshold for sagittal plane rotational induced diffuse axonal injuries, in: Proc. Int. Res. Conf. Biomech. Impact, 2009.

[35] H.M. Huang, M.C. Lee, W.T. Chiu, C.T. Chen, S.Y. Lee, Three-dimensional finite element analysis of subdural hematoma, J. Trauma - Inj. Infect. Crit. Care. 47 (1999) 538–44. doi:10.1097/00005373-199909000-00019.

[36] D.F. Meaney, Biomechanics of acute subdural hematoma in the subhuman primate and man, University of Pennsylvania, 1991.

[37] A.C. Duhaime, T.A. Gennarelli, L.E. Thibault, D.A. Bruce, S.S. Margulies, R. Wiser, The shaken baby syndrome. A clinical, pathological, and biomechanical study, J. Neurosurg. 66 (1987) 409–15. doi:10.3171/jns.1987.66.3.0409.

[38] M.C. Lee, J.W. Melvin, K. Ueno, Finite Element Analysis of Traumatic Subdural Hematoma, in: Proc. 31st Stapp Car Crash Conf., 1987: pp. 67–77. doi:10.4271/872201.

[39] C.A. Jenny, T. Shams, N. Rangarajan, T. Fukuda, Development of a biofidelic 2.5 kg infant dummy and its application to assessing infant head trauma during violent shaking, in: Proc. 30th Int. Work. Hum. Subj. Biomech. Res., 2002: pp. 129–41.

[40] M.T. Prange, B. Coats, A.-C. Duhaime, S.S. Margulies, Anthropomorphic simulations of falls, shakes, and inflicted impacts in infants, J. Neurosurg. 99 (2003) 143–150. doi:10.3171/jns.2003.99.1.0143.

[41] C.A. Jenny, G. Bertocci, T. Fukuda, N. Rangarajan, T. Shams, Biomechanical response of the infant head to shaking: an experimental investigation, J. Neurotrauma. 34 (2017) 1–10. doi:10.1089/neu.2016.4687.

[42] S. Lazoritz, V.J. Palusci, The Shaken Baby Syndrome: a multidisciplinary approach, Taylor and Francis, 2002.

# Inflicted Head Injury by Shaking Trauma in Infants

## Part II: the importance of spatiotemporal variation of the rotation center when modelling external head-dynamics

L.A.H. Schiks, J. Dankelman, A.J. Loeve
Department of BioMedical Engineering, Delft University of Technology, The Netherlands

**Abstract**

Computational model simulations are extensively used to analyze inflicted head injury by shaking trauma in infants (IHI-ST). Infant head models are usually excited by dynamic inputs, which are applied to a specific point with respect to the head. In existing studies the load application point is assumed to be fixed over time; thereby neglecting spatiotemporal variation of the rotation center during shaking. Therefore, this assumption may be inappropriate, because the location of the heads' rotation center is in fact not constant over time during shaking. It is unknown to what extent head dynamics are correctly simulated when using a fixed rotation center, hence simulation results regarding injury thresholds and shaking trauma assessment could be invalid.

In this study, loading-methods used in IHI-ST simulations were evaluated for their temporal accuracy in replicating external head-dynamics. First, a mathematical model incorporating spatiotemporal variation of the head's rotation center was proposed. Secondly, head dynamics were calculated using the proposed mathematical model and existing model-loading methods. Finally, the calculated head dynamics were compared to a reference dataset.

Key findings: in all of the 29 cases from the reference dataset, implementation of a time-varying load application point resulted in an improved temporal replication of shaking dynamics compared to existing model-loading methods. Accelerations of the head in x- and z-direction had a two and four times smaller absolute error over a typical shake cycle than any previously existing finite element model (FEM) for IHI-ST. It remains unclear how implementation of a time-varying load application point affects the dynamics of fluids and tissues inside the skull. Future research should therefore focus on re-evaluating the results of IHI-ST assessment studies and injury threshold studies employing FEM head-models.

**Keywords**

Closed head injuries—child abuse—biomechanics—finite element models.

### Introduction

Each year 14-41 per 100.000 infants up to 1 year of age are diagnosed with inflicted head injuries [1–3]. Retinal hemorrhage, subdural hemorrhage, diffuse axonal injury, and neck injury are symptoms often associated with violent shaking of an infant. The diagnosis of inflicted head injury by shaking trauma (IHI-ST) based on the presence of such symptoms is often debated because these symptoms can also be caused by events other than abusive shaking [4–7]. However, no consensus has been reached yet regarding the question if shaking alone can actually result in loading anatomy beyond its failure thresholds [8–11].

Dynamic parameters such as angular acceleration or angular velocity, and biomechanical tissue properties such as ultimate strength, are examples of thresholds that are currently used to estimate injury risk [12,13]. Injury thresholds and head dynamics are hard to obtain directly from infants due to ethical considerations and hence are based on experiments with surrogates [14–16], mathematical models [15,17,18] or on extrapolated or scaled adult- or animal data [10,11,19]. Such studies investigate the effects of head dynamics during shaking on loading—and subsequent deformation—of anatomical structures; which is essential knowledge to determine whether or not violent shaking may cause damage to an infant's anatomy. However, the literature study preceding this thesis (submitted) showed that many infant shaking trauma assessment studies use inappropriate injury thresholds which did not match shaking loading conditions [12] (Appendix I).

Computational models, such as finite element models (FEM) and rigid body models (RBM) of an infant's anatomy, are commonly subjected to dynamics that have been measured in physical model studies [10,15,16,20–26]. A good model accurately mimics anatomical geometry and tissue properties to provide insights in the biomechanical behavior of the brain and skull during shaking. Evidently, the outcome of a simulation not only

depends on the model itself, but also on accurate formulation of the model's input.

Where in RBMs the load applied to the chest is often a translation/linear acceleration [25–28], loads applied to FEMs are often more complex. The head may be subjected to a uniaxial sinusoidal displacement [29–31], or to—whether or not a combination of—linear or angular accelerations or velocities [32–37]. The center of rotation of an infant's head in IHI-ST FEM simulations is usually defined somewhere at the cervical spine; e.g. the base of the skull, the C5-C6 junction or the base of the neck [32–37]. However, in Part I of this study it was found that the infant's head does not rotate around a fixed pivoting point during shaking. Both the radius of curvature and the location of the rotation center are highly variable over time. It is currently unknown to what extent this would affect the outcome obtained from existing IHI-ST computational simulations in terms of accurately replicating the dynamics acting on the infant's head and internal anatomical structures.

Therefore, the aim of the present study is to analyze different loading methods for computational IHI-ST simulations and to evaluate their temporal accuracy in replicating external head-dynamics. A mathematical model is proposed to accurately head-dynamics and inertial effects in IHI-ST, using a spatiotemporal variation of the head's rotation center. Next, the head-dynamics will be calculated using the proposed mathematical model and existing model-loading methods. Finally, results of these calculations will be compared to a reference dataset.

## Methods

### Moving ICOR model

Every motion of a rigid body can be expressed as a translation combined with a rotation. Based on this, Loeve and Stray-Pedersen [38] proposed a model for the head dynamics related to shake-doll experiments. The moving instantaneous center of rotation (ICOR) in their model was assumed to be located at the z-axis of the head (Figure 1), colinear with the center of gravity (COG). However, the ICOR varies both in x- and z-direction over time due to the flexible character of the human neck, and the external imposed shaking motion from the arms and wrists of the perpetrator, as was found in Part I (Figure 2).

Therefore, a mathematical model was derived in which spatiotemporal variations of the ICOR were implemented in both x- and z-direction (Moving ICOR Model; Figure 1), using the model of Loeve and Stray-Pedersen [38] as a starting point. The Equations of Motion (EOM), which analytically define the Moving ICOR Model, are presented in the results section. Accelerations in y-direction were negligible compared to other accelerations [39] (under submission) and hence were neglected.

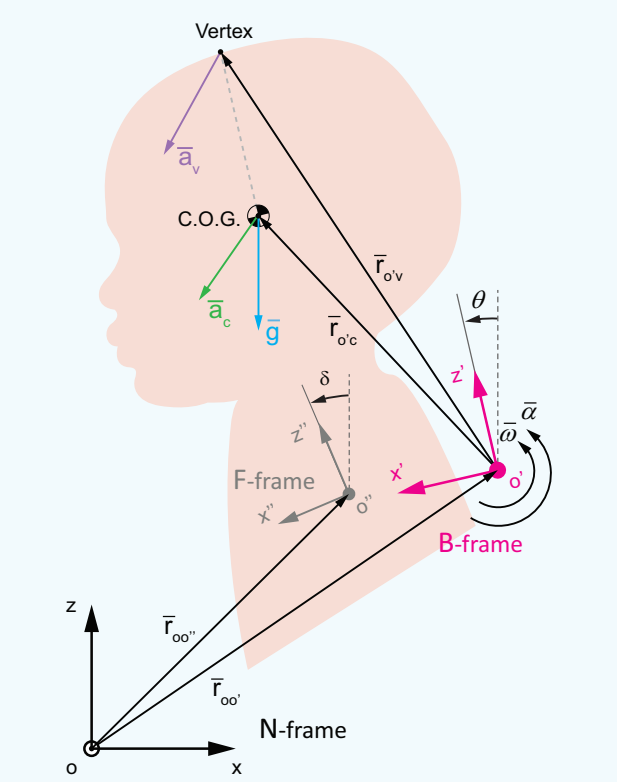


**Figure 1.** Free body diagram of the infant's head. Inertial reference frame N is defined by the xyz triad. Moving reference frame B rotates with the head and is defined by the x'y'z' triad. The B-frame is tilted by angle $\theta$ with respect to the z-axis of the inertial reference frame N, and its origin o' corresponds with the ICOR. Torso reference frame F is defined by the x"y"z" triad and is tilted with respect to the z-axis by angle $\delta$. Other variables are further explained in Equation 1.

### Existing models

An overview of existing IHI-ST FEM studies [13] was used to identify studies incorporating head-dynamics. The model-loading methods reported in sagittal plane studies [29–37] were categorized according to loading direction (Table 1).

**Table 1.** Categories assigned to model-loading methods used in existing IHI-ST FEM studies.

| Loading direction | Model-loading category |
|---|---|
| Rotation around y-axis | CAT I |
| Translation in x-direction | CAT II |
| Combined rotation around y-axis and translation in x-direction | CAT III |

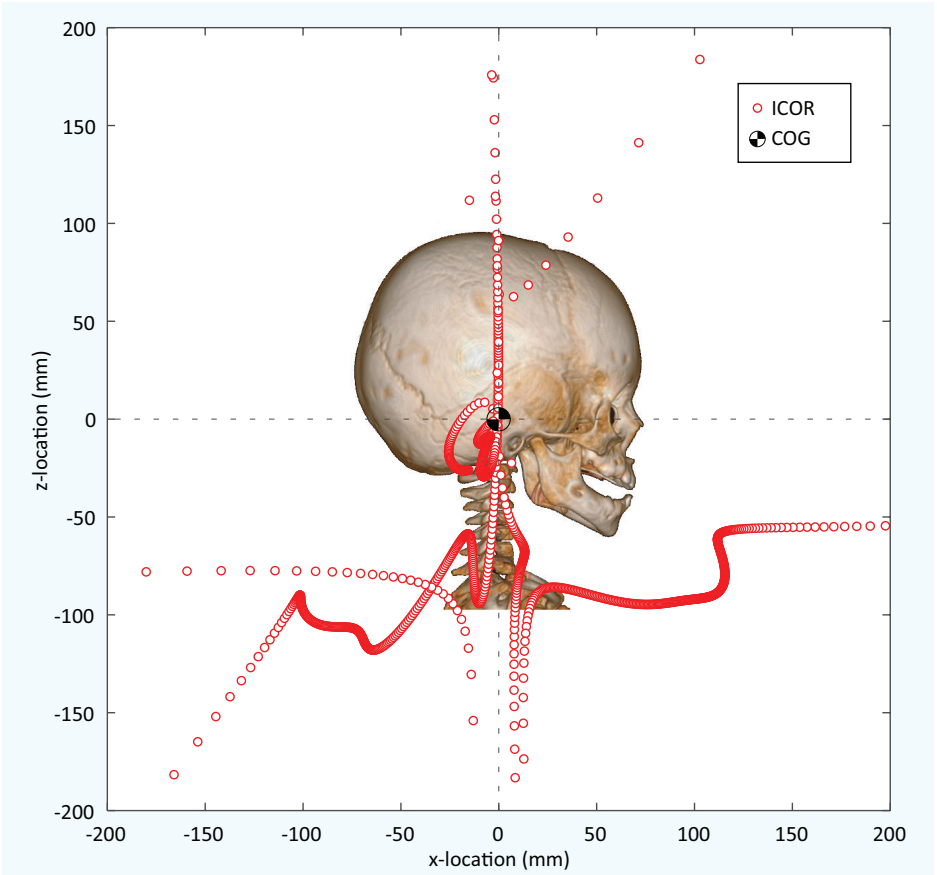


**Figure 2.** Spatiotemporal variation of the instantaneous center of rotation (ICOR) with respect to the center of gravity (COG) of the head, during a single typical shake cycle (Part I). 3D CT-scan of a 6-week old infant.

Load application points differed among the studies that incorporated combined rotation and translation (CAT III). Therefore, model-loading category III was subclassified according to the employed load application point; i.e. the base of the neck (CAT III-A) or the base of the skull (CAT III-B).

The EOM for the vertex and COG were derived for each model-loading category. The EOM of existing models are in fact simplified versions of the EOM of the Moving ICOR Model; neglecting either translation or rotation of the head, and variations in the location of the ICOR of the head. Some of the variables thus were disregarded or simplified: e.g. $\omega = 0$ and $\alpha = 0$ in case of translation only; $r_{oc} = constant$, $\dot{r}_{oc} = 0$ and $\ddot{r}_{oc} = 0$ in case of a fixed rotation center. Therefore, the EOM for each model-loading category were obtained easily by filling in the EOM of the Moving ICOR Model, using the simplifications for each category.

## Model-loading method evaluation

The performance of each model-loading category, for replicating IHI-ST head-dynamics, was evaluated by comparing calculated accelerations[1] of the head's COG and vertex to reference values measured in Part I. To justify the use of measured accelerations of the COG and vertex as a reference, the input for the EOMs were defined by values (e.g. angular velocity or torso acceleration) taken from the same dataset.

The absolute root-mean-square error (RMSE) between the calculated and measured vertex acceleration was calculated as a quantitative measure to evaluate the overall performance—over a single shake cycle—of each model-loading category. A plot of the residual accelerations over time (i.e. the difference between the reference value and the calculated value), was used to visually compare the temporal accuracy of each model-loading category within a shake cycle.

[1] Using the Equations of Motion

## Results

### Equations of Motion for the Moving ICOR Model

The Equations of Motion of the Moving ICOR model are defined by Equation 1.

$$\begin{cases} \bar{a}_v = \bar{\ddot{r}}_{oo'} + \bar{\alpha} \times \bar{r}_{o'v} + \bar{\omega} \times (\bar{\omega} \times \bar{r}_{o'v}) + \bar{\ddot{r}}_{o'v} + 2\bar{\omega} \times \bar{\dot{r}}_{o'v} + \bar{g} \\ \bar{a}_c = \bar{\ddot{r}}_{oo'} + \bar{\alpha} \times \bar{r}_{o'c} + \bar{\omega} \times (\bar{\omega} \times \bar{r}_{o'c}) + \bar{\ddot{r}}_{o'c} + 2\bar{\omega} \times \bar{\dot{r}}_{o'c} + \bar{g} \end{cases} \quad (1)$$

| | |
|---|---|
| $\bar{a}_v$ | inertial acceleration of the vertex (m/s²) |
| $\bar{a}_c$ | inertial acceleration of the COG (m/s²) |
| $\bar{\ddot{r}}_{oo'}$ | inertial acceleration of the origin *o'* (m/s²) |
| $\bar{r}_{o'v}$ | position vector from the origin *o'* to the vertex (m) |
| $\bar{r}_{o'c}$ | position vector from the origin *o'* to the COG (m) |
| $\bar{\dot{r}}_{o'v}$ | velocity of the vertex relative to the origin *o'* (m/s) |
| $\bar{\dot{r}}_{o'c}$ | velocity of the COG relative to the origin *o'* (m/s) |
| $\bar{\ddot{r}}_{o'v}$ | acceleration of the vertex relative to the origin *o'* (m/s²) |
| $\bar{\ddot{r}}_{o'c}$ | acceleration of the COG relative to the origin *o'* (m/s²) |
| $\bar{\omega}$ | angular velocity of the head (rad/s) |
| $\bar{\alpha}$ | angular acceleration of the head (rad/s²) |
| $\bar{g}$ | gravitational acceleration (m/s²) |

### Categorization of existing model-loading methods

An overview of the (sub)categories assigned to model-loading methods reported in existing IHI-ST model studies is presented in Table 2.

### Equations of Motion for existing model-loading categories

#### Category I – Rotation only

Roth et al. [33] and Raul et al. [34] incorporated only rotation in their simulation, around the point o' (Figure 1) which was kept fixed over time (Equation 2). The C5-C6 junction of the cervical spine was defined as the rotation center of the head (Figure 3). In this special case, the origin o' and z' axis were aligned with the vertex and COG (Figure 1).

$$\begin{cases} \bar{a}_v = \bar{\alpha} \cdot \bar{r}_{o'v} + \bar{\omega} \times (\bar{\omega} \cdot \bar{r}_{o'v}) \\ \bar{a}_c = \bar{\alpha} \cdot \bar{r}_{o'c} + \bar{\omega} \times (\bar{\omega} \cdot \bar{r}_{o'c}) \end{cases} \quad (2)$$

| | |
|---|---|
| $\bar{a}_v$ | inertial acceleration of the vertex (m/s²) |
| $\bar{a}_c$ | inertial acceleration of the COG (m/s²) |
| $\bar{r}_{o'v}$ | distance from origin o' to vertex (m) |
| $\bar{r}_{o'c}$ | distance from origin o' to COG (m) |
| $\bar{\omega}$ | angular velocity of the head (rad/s) |
| $\bar{\alpha}$ | angular acceleration of the head (rad/s²) |

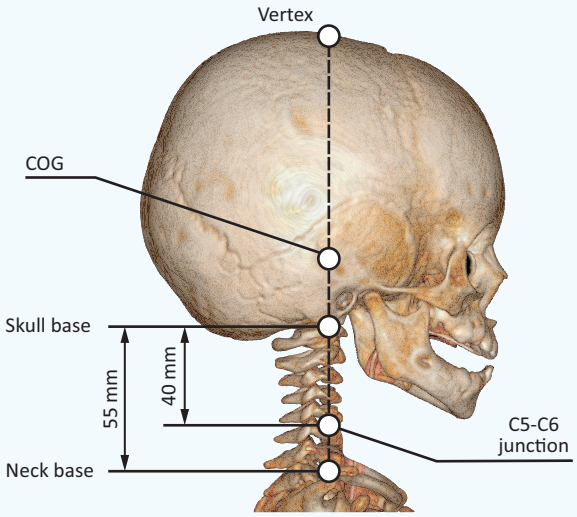


**Figure 3.** Locations of fixed rotation centers used in existing models. 3D CT-scan of a 6-week old infant, the neck length of 55 mm corresponds with the Q0-dummy.

#### Category II – Translation only

Cheng et al. [29,31] and Batterbee et al. [30] incorporated only translation of the head in their simulations, and only in horizontal direction (Equation 3). The torso acceleration magnitude from a physical model study [24] was used as inertial acceleration of the head. The load application point may be disregarded; per definition, every point on a purely translating rigid body has the same acceleration.

$$\begin{cases} \bar{a}_v = \bar{\ddot{r}}_{oo'} \\ \bar{a}_c = \bar{\ddot{r}}_{oo'} \end{cases} \quad (3)$$

| | |
|---|---|
| $\bar{a}_v$ | inertial acceleration of the vertex (m/s²) |
| $\bar{a}_c$ | inertial acceleration of the COG (m/s²) |
| $\bar{\ddot{r}}_{oo'}$ | inertial acceleration of the origin *o'* (m/s²); i.e. torso acceleration in this specific case |

#### Category III – Combined rotation and translation

Morison [32], Hans et al. [35], Couper and Albermani [36] and Batterbee et al. [37] incorporated combined rotation and translation in their simulations (Equation 4). The load application point o' (Figure 1) varied per study; Morison [32] and Hans et al. [35] used the base of the neck (subcategory III-A), whereas Couper and Albermani [36] and Batterbee et al. [37] applied the load to the base of the brainstem—approximately the base of the skull—(subcategory III-B) (Figure 3). All studies used the torso acceleration vector as inertial linear acceleration of the head's load application point o' (Figure 1), and assumed that the torso did not rotate with respect to the inertial reference frame N; the angle $\delta$ between the torso and the z-axis, and its time derivatives, thus were disregarded (Figure 1). Therefore, torso accelerations that were

**Table 2.** Existing studies were each assigned a model-loading category according to their loading type, loading direction and load application point. *Loading directions correspond to the skull-fixed reference frame (Figure 1).

| Study | Purpose | Loading type (and reference if available) | Loading direction* | Load application point | Model-loading category |
|---|---|---|---|---|---|
| Morison [32] | Examine bridging vein strain in a shaking scenario | Head rotation combined with torso acceleration | Rotation around y-axis and translation in sagittal plane | Rotation center at the base of the neck | III-A |
| Roth et al. [33] | Compare intracerebral mechanical response for impact and shaking | Head rotation [22] | Rotation around y-axis | Rotation center at C5-C6 junction | I |
| Cheng et al. [29] | Effect of anterior fontanelle in IHI-ST | Torso acceleration [24] | Translation in x-direction | N/A | II |
| Raul et al. [34] | Examine influence of the benign enlargement of the subarachnoid space on child head injury | Head rotation [22] | Rotation around y-axis | Rotation center at C5-C6 junction | I |
| Hans et al. [35] | Compare retinal forces for impact and shaking | Head rotation combined with torso acceleration [32] | Rotation around y-axis and translation in sagittal plane x- and z-direction | Rotation center at the base of the neck | III-A |
| Batterbee et al. [30] | Development of simplified FEM model and influence of anterior fontanelle | Not clear. Based on magnitude; probably torso acceleration | Translation in x-direction | N/A | II |
| Cheng et al. [31] | Examine influence of anterior fontanelle and brain-skull interface on intracranial brain movement | Torso acceleration [24] | Translation in x-direction | N/A | II |
| Couper and Albermani [36] | Examine the loading–injury relationship of infant shaking and the related deterministic parameters | Head rotation combined with torso acceleration [20,22,25,40] | Rotation around y-axis and translation in sagittal plane | At the base of the brainstem (approx. skull base) | III-B |
| Batterbee et al. [37] | Uncertainty analysis of a finite element model of an infant's head subject to shaking | Head rotation combined with torso acceleration | Rotation around y-axis and translation in sagittal plane | At the base of the brainstem (approx. skull base) | III-B |

measured (in Part I) with respect to the torso reference frame F must be mapped to the skull reference frame B (Equation 5). The other variables in Equation 4 were already measured or calculated with respect to the B-frame in Part I. The vertex and COG were aligned with the origin o' and the z' axis (Figure 3).

$$\begin{cases} \bar{a}_v = \ddot{\bar{r}}_{oo'} + \bar{\alpha} \cdot \bar{r}_{o'v} + \bar{\omega} \times (\bar{\omega} \cdot \bar{r}_{o'v}) \\ \bar{a}_c = \ddot{\bar{r}}_{oo'} + \bar{\alpha} \cdot \bar{r}_{o'c} + \bar{\omega} \times (\bar{\omega} \cdot \bar{r}_{o'c}) \end{cases} \quad (4)$$

$\bar{a}_v$ inertial acceleration of the vertex (m/s²)
$\bar{a}_c$ inertial acceleration of the COG (m/s²)
$\ddot{\bar{r}}_{oo'}$ inertial acceleration of the origin o' (m/s²); i.e. torso acceleration $\bar{a}_t$
$\bar{r}_{o'c}$ distance from origin o' to COG (m)
$\bar{r}_{o'v}$ distance from origin o' to vertex (m)
$\bar{\omega}$ angular velocity of the head (rad/s)
$\bar{\alpha}$ angular acceleration of the head (rad/s²)

$$^{B}\bar{a}_t = \begin{bmatrix} \cos\theta & 0 & -\sin\theta \\ 0 & 1 & 0 \\ \sin\theta & 0 & \cos\theta \end{bmatrix} {}^{F}\bar{a}_t \quad (5)$$

$^{B}\bar{a}_t$ torso acceleration expressed in the skull reference frame *B* (m/s²)
$^{F}\bar{a}_t$ torso acceleration expressed in the torso reference frame *F* (m/s²)
$\theta$ angle between the skull reference frame *B* and the z-axis of the inertial reference frame *N* (rad)

## Model-loading method evaluation

The Moving ICOR Model outperformed other model-loading categories in terms of temporal replication shaking dynamics.

### Root-mean-square error

The mean absolute root-mean-square error (RMSE)—across results for each participant—over the full shake cycle varied a lot across all model-loading methods (Table 3). The CAT-II methods, which incorporated horizontal

**Table 3.** Mean absolute root-mean-square error (RMSE) between the models and the measured accelerations of the vertex and center of gravity (COG) for a single shake cycle. The RMSE-Z was not calculated for CAT-II because this model-type only involved horizontal accelerations.

| | Vertex | | COG | |
|---|---|---|---|---|
| | RMSE-X ($m/s^2$) | RMSE-Z ($m/s^2$) | RMSE-X ($m/s^2$) | RMSE-Z ($m/s^2$) |
| CAT I | 49.8 | 40.3 | 46.8 | 38.9 |
| CAT II | 114.1 | N/A | 54.4 | N/A |
| CAT III-A | 48.3 | 40.6 | 44.0 | 39.2 |
| CAT III-B | 36.7 | 44.4 | 33.0 | 44.4 |
| New model | 13.7 | 6.4 | 0.0 | 0.0 |

translation only, performed far worse than other model-loading categories. The Moving ICOR Model had the smallest RMSE in both x- and z-direction, indicating a good temporal accuracy of the model.

### Acceleration residuals

Replication of the inertial vertex acceleration in x- and z-direction during a shake cycle varied a lot across all model-loading methods (Figures 4 and 5). The acceleration residuals of the Moving ICOR Model were smaller and more constant over the entire shake cycle for x- and z-direction compared to the other model-loading categories. Particularly the CAT-II methods had large residuals at acceleration peaks in x-direction (Figure 4). Except for the Moving ICOR Model, all other model-loading methods had large residuals for the acceleration in z-direction (Figure 5). Similar results—as to those described above for replication of the vertex acceleration—were found for replication of the inertial COG acceleration.

## Discussion

### Model-loading method comparison

The results demonstrated that using a spatiotemporal variation of the load application point resulted in a better temporal replication of head accelerations in both x- and z-direction, as compared to currently existing model-loading methods. The head accelerations that are related to IHI-ST were analytically defined by the EOM (Equation 1), from which it becomes clear that multiple variables contribute to the dynamic behavior of the head during shaking. Each simplification regarding the EOM might result in deviation of the model with respect to the actual head dynamics. Rotation-only methods (CAT-I) disregard translational accelerations, translation-only methods (CAT-II) disregard centripetal accelerations, etc. At first sight, the implementation of combined rotation and acceleration in CAT-III methods seems to provide a reasonable replication of head dynamics, yet the absolute error is over

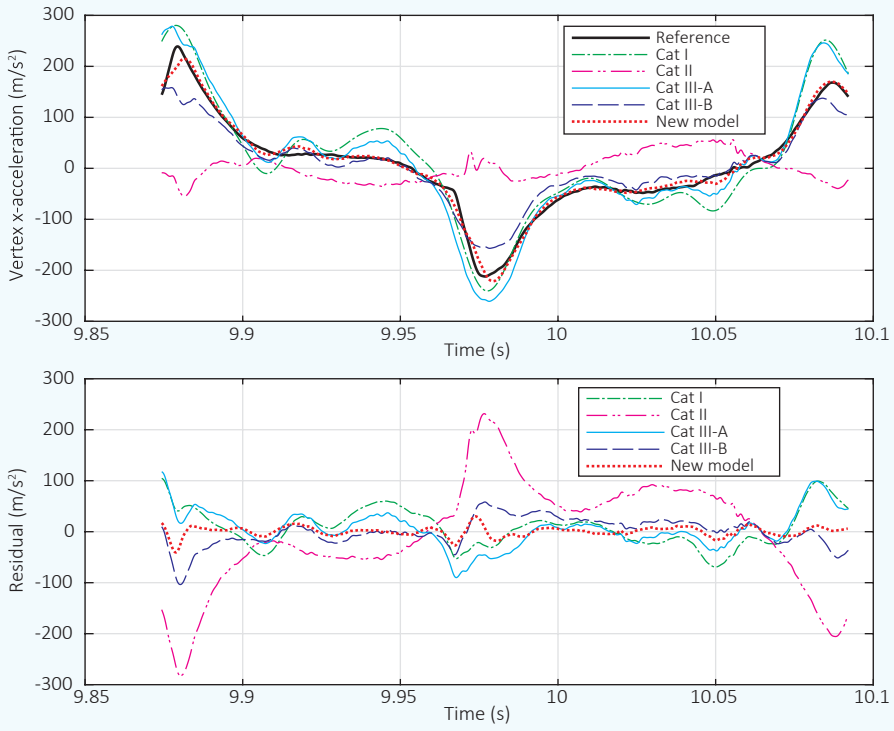


**Figure 4.** Replication of vertex acceleration of the head in x-direction for a typical shake cycle. (Top) inertial vertex acceleration in x-direction. (Bottom) residual acceleration.

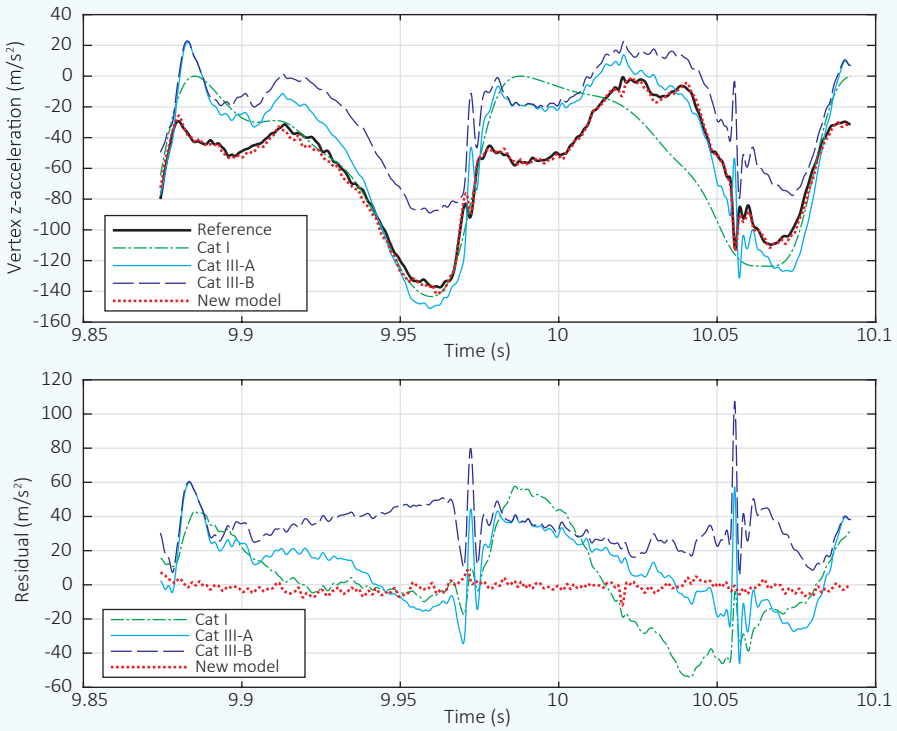


**Figure 5.** Replication of vertex acceleration of the head in z-direction for a typical shake cycle. (Top) inertial vertex acceleration in z-direction. (Bottom) residual acceleration.

twice as large as for the Moving ICOR Model; caused by the simplification of taking the ICOR fixed over time. Moreover, because the acceleration of the ICOR itself was not taken into account, at some points CAT-II methods describe positive accelerations while the measured acceleration was negative instead (Figure 5).

The acceleration of the origin o' in Part I of this study was calculated using the measured COG acceleration. Therefore, the COG acceleration in the new model had an RMSE equal to zero.

## Implications for modeling IHI-ST

Accurate temporal replication of shaking dynamics is of major importance when modeling biomechanics of viscoelastic tissues such as brain tissue because the tissue response is not only dependent on loading magnitude, but also on the loading rate and loading repetitions [12,41]. Therefore, the head's accelerations, and consequently the simulation results, are calculated wrongly if temporal replication of shaking dynamics is inaccurate. Model output is also highly dependent on the excitation type [37]. This further underlines the importance of implementing a spatiotemporal load application. In the subsections following hereafter, the implications of parameter assumptions in existing IHI-ST models are discussed separately for each model category.

### Category I – Rotation only

Roth et al. [33] compared the intracerebral mechanical response for impact and shaking and found that both shaking and impact may result in a subdural hematoma due to rupture of bridging veins. Raul et al. [34] investigated the effect of the be benign enlargement of the subarachnoid space on bridging vein stretch during shaking. Both studies used the C5-C6 junction as rotation center and did not model linear accelerations. Consequently, rotation of the brain with respect to the skull may be highly over- or underestimated depending on the true ICOR.

### Category II – Translation only

Cheng et al. [29,31] modeled IHI-ST using a horizontal-translation-only model-loading method (CAT-II). Their experiments were aimed to examine intracranial brain movement of the infant's head during violent shaking, and to evaluate the performance of several brain-skull interfaces; including fluid-structural interaction (FSI) between anatomical structures. To do so, they subjected the head directly to the horizontal accelerations earlier measured to be experienced by the torso. However, the results demonstrated that such methods had extremely high acceleration residuals. This is a direct consequence of leaving out the phase difference and orientation between the torso and head accelerations during shaking caused by interaction with the neck. Furthermore, because CAT-II methods disregard rotational effects, the high magnitude

accelerations in z-direction were not modeled at all. Yet, accelerations in z-direction are a considerable and essential factor in FSI, because it forces the brain against the skull[2] [32]; thereby displacing the cerebrospinal fluid (CSF). Other results of Cheng et al. [31]—regarding the comparison of CSF modeling methods—were based on motion of the brain within the skull and on the interaction effects between the brain and the anterior fontanelle. However, brain motion effects due to z-acceleration were disregarded, while those accelerations were found to be large (Part I) and possibly interact with the anterior fontanelle. The conclusions that were drawn thus could be incorrect.

Likewise, Batterbee et al. [30] studied the influence of the anterior fontanelle on stresses in brain tissue and performed frequency response simulations of the brain during shaking using the horizontal-translation-only method (CAT-II). As mentioned above, CAT-II methods disregarded brain motion effects due to z-acceleration, whereas accelerations of the brain in z-direction might cause interactions between the brain and the anterior fontanelle. Similarly, the phase difference between motion of the head and the torso affects the frequency response analysis. Unfortunately, the phase timing of the oscillations was not mentioned. Also, it was not entirely clear what acceleration was used to excite the head model, but the magnitude of about 30 m/s$^2$ corresponds to the torso acceleration as measured in Part I. Therefore, the conclusions regarding the effect of the anterior fontanelle on tissue stresses may be underestimated. Furthermore, the frequency response of the brain might be inaccurate, if the torso acceleration was used to excite the head model.

Couper and Albermani [42,43] stated, without further substantiation, that using only anterior/posterior accelerations suffices for modeling the qualitative mechanics of the head in oscillatory motion. A transverse plane 2D model of the brain was used for this purpose. However, this qualitative description might be inaccurate because of multiple factors:

1) the inertial acceleration experienced by each particle within the head is related to the ROC [32], which is highly variable during a shaking cycle (Part I), and causes each particle in the 2D slice to have a unique acceleration instead of the same acceleration for each particle (Equation 1).
2) displacement of the brain with respect to the skull is mainly rotational rather than translational [32].
3) accelerations in z-direction are quite large and should not be disregarded, whereas these are not considered at all in translation-only model-loading methods.

Therefore, transverse plane 2D brain models are deemed inappropriate for modeling brain injuries in IHI-ST.

#### Category III – Combined rotation and translation

The load application point o' was fixed over time for CAT-III methods but varied per study, resulting in different simulation outputs. The CAT-III method output for accelerations in x-direction showed reasonable agreement with the measured accelerations in Part I. Yet in general, CAT-III methods underestimated accelerations in z-direction and at some points in the shake cycle even indicating positive- instead of negative accelerations. This has severe consequences for simulations regarding intracranial pressure build-up due to blood accumulation and CSF displacements. Morison [32], Hans et al. [35], Couper and Albermani [36] and Batterbee et al. [37] all used a fixed ICOR. Therefore, similar to the rotation-only methods (CAT-I), rotation of the brain with respect to the skull might be over- or underestimated depending on the actual ICOR.

### Limitations

The scope of the present study was limited to external head dynamics. Hence, the effect of spatiotemporal variation of the ICOR on dynamics *inside* the skull could not be quantified.

### Recommendations for future research

Future research should be focused on quantifying the effect of spatiotemporal variation of the load application point in finite element and rigid body models on the dynamics of fluids and tissues inside the skull; e.g. bridging vein strain, intracranial brain movement, fluid-structural interaction, bridging vein strain or brain frequency response. Shaking variables based on extensive measurements (Part I) such as those used in this study can be used as model input for future studies.

## Conclusion

The Moving ICOR Model presented in this study provided an improved temporal replication of shaking dynamics compared to existing model-loading methods. Accelerations in x- and z-direction had a two and four times smaller absolute error over a typical shake cycle than any previously existing FEM for IHI-ST.

[2] Because brain tissue is more dense than cerebrospinal fluid [44,45]

The results showed the importance of modeling spatiotemporal variation of the load application point in simulations for replicating infant skull dynamics during violent shaking. In particular accelerations in z-direction were largely underestimated in existing studies that used a fixed rotation center. Therefore, it is strongly suggested that future IHI-ST simulation studies incorporate a spatiotemporal variation of the rotation center to improve the temporal accuracy of simulated head dynamics during shaking. Shaking variables that were measured and calculated in Part I of this study can serve as a solid basis for future modeling of IHI-ST.

## Acknowledgments

The authors would like to thank Prof.Dr. Rick van Rijn from the Department of Radiology and Nuclear Medicine (Amsterdam University Medical Center, Amsterdam, The Netherlands) for providing DICOM data of the pediatric skull and cervical spine.

## Abbreviations

| | |
|---|---|
| **IHI-ST** | Inflicted head injuries by shaking trauma in infants |
| **FEM** | Finite elements model |
| **RBM** | Rigid body model |
| **ICOR** | Instantaneous center of rotation |
| **COG** | Center of gravity |
| EOM | Equations of motion |

## References

[1] M. Fanconi, U. Lips, Shaken baby syndrome in Switzerland: results of a prospective follow-up study, 2002-2007, Eur. J. Pediatr. 169 (2010) 1023–28. doi:10.1007/s00431-010-1175-x.

[2] K.D. Ellingson, J.M. Leventhal, H.B. Weiss, Using Hospital Discharge Data to Track Inflicted Traumatic Brain Injury, Am. J. Prev. Med. 34 (2008) S157–S162. doi:10.1016/j.amepre.2007.12.021.

[3] I. Talvik, T. Metsvaht, K. Leito, H. Põder, P. Kool, M. Väli, M. Lintrop, A. Kolk, T. Talvik, Inflicted traumatic brain injury (ITBI) or shaken baby syndrome (SBS) in Estonia, Acta Paediatr. 95 (2006) 799–804. doi:10.1111/j.1651-2227.2006.tb02343.x.

[4] M. Mian, J. Shah, A. Dalpiaz, R. Schwamb, Y. Miao, K. Warren, S. Khan, Shaken baby syndrome: A review, Fetal Pediatr. Pathol. 34 (2015) 169–75. doi:10.3109/15513815.2014.999394.

[5] M. Vinchon, O. Noizet, S. Defoort-Dhellemmes, G. Soto-Ares, P. Dhellemmes, Infantile subdural hematomas due to traffic accidents, Pediatr. Neurosurg. 37 (2002) 245–53. doi:10.1159/000066216.

[6] G. Elinder, A. Eriksson, B. Hallberg, N. Lynøe, P.M. Sundgren, M. Rosén, I. Engström, B.E. Erlandsson, Traumatic shaking: The role of the triad in medical investigations of suspected traumatic shaking, Acta Paediatr. Int. J. Paediatr. 107 (2018) 3–23. doi:10.1111/apa.14473.

[7] M. Laghmari, H. Skiker, H. Handor, B. Mansouri, K. Ouazzani Chahdi, R. Lachkar, Y. Salhi, O. Cherkaoui, B. Ouazzani Tnacheri, W. Ibrahimy, H. Alami, R. Bezad, S. Ahid, R. Abouqal, R. Daoudi, [Birth-related retinal hemorrhages in the newborn: incidence and relationship with maternal, obstetric and neonatal factors. Prospective study of 2,031 cases], J. Fr. d Opthalmologie. 37 (2014) 313–9. doi:http://dx.doi.org/10.1016/j.jfo.2013.06.005.

[8] S.C. Gabaeff, Challenging the Pathophysiologic Connection between Subdural Hematoma, Retinal Hemorrhage and Shaken Baby Syndrome, West. J. Emerg. Med. 12 (2011) 144–58.

[9] W. Squier, Shaken baby syndrome: The quest for evidence, Dev. Med. Child Neurol. 50 (2008) 10–4. doi:10.1111/j.1469-8749.2007.02004.x.

[10] C.Z. Cory, M.D. Jones, Can shaking alone cause fatal brain injury? A biomechanical assessment of the Duhaime shaken baby syndrome model, Med. Sci. Law. 43 (2003) 317–33. doi:10.1258/rsmmsl.43.4.317.

[11] T.O. Lintern, M.P. Nash, P. Kelly, F.H. Bloomfield, A.J. Taberner, P.M.F. Nielsen, Probabilistic description of infant head kinematics in abusive head trauma, Comput. Methods Biomech. Biomed. Engin. 20 (2017) 1633–42. doi:10.1080/10255842.2017.1403593.

[12] L.A.H. Schiks, J. Dankelman, A.J. Loeve, Thresholds for the assessment of inflicted head injury by shaking trauma in infants: a systematic review, Forensic Sci. Int. (2019) Submitted.

[13] J.P. van Zandwijk, M.E.M. Vester, R.A. Bilo, R.R. van Rijn, A.J. Loeve, Modeling of inflicted head injury by shaking trauma in children: what can we learn? Part II: A systematic review of mathematical and physical models, Forensic Sci. Med. Pathol. (2019). doi:10.1007/s12024-019-00093-7.

[14] T. Koizumi, N. Tsujiuchi, K. Hara, Y. Miyazaki, Dynamic response and damage estimation of infant brain for vibration, in: Proc. Soc. Exp.

Mech. Ser., 2013: pp. 11–8. doi:10.1007/978-1-4614-6546-1_2.

[15] J. Lloyd, E.N. Willey, J.G. Galaznik, W.E. Lee, S.E. Luttner, Biomechanical Evaluation of Head Kinematics During Infant Shaking Versus Pediatric Activities of Daily Living, J. Forensic Biomech. 2 (2011) 1–9. doi:10.4303/jfb/f110601.

[16] S. Cirovic, M. Freddolini, R. Goodwin, D. Zimarev, Shaken Mannequin Experiments: Head Motion Pattern and Its Potential Effect on Blood Pressure, J. Forensic Biomech. 3 (2012). doi:10.4303/jfb/235476.

[17] L. Ren, D. Baumgartner, J. Yang, J. Davidsson, R. Willinger, Investigation of diffuse axonal injury induced by rotational acceleration via numerical reconstructions of in vivo rat head impact experiments, Int. J. Crashworthiness. 20 (2015) 602–12. doi:10.1080/13588265.2015.1073132.

[18] B. Coats, S.A. Eucker, S. Sullivan, S.S. Margulies, Finite element model predictions of intracranial hemorrhage from non-impact, rapid head rotations in the piglet, Int. J. Dev. Neurosci. 30 (2012) 191–200. doi:10.1016/j.ijdevneu.2011.12.009.

[19] S.A. Pasquesi, S.S. Margulies, Failure and fatigue properties of immature human and porcine parasagittal bridging veins, Ann. Biomed. Eng. 45 (2017) 1877–1889. doi:10.1007/s10439-017-1833-5.

[20] A.C. Duhaime, T.A. Gennarelli, L.E. Thibault, D.A. Bruce, S.S. Margulies, R. Wiser, The shaken baby syndrome. A clinical, pathological, and biomechanical study, J. Neurosurg. 66 (1987) 409–15. doi:10.3171/jns.1987.66.3.0409.

[21] C.A. Jenny, T. Shams, N. Rangarajan, T. Fukuda, Development of a biofidelic 2.5 kg infant dummy and its application to assessing infant head trauma during violent shaking, in: Proc. 30th Int. Work. Hum. Subj. Biomech. Res., 2002: pp. 129–41.

[22] M.T. Prange, B. Coats, A.-C. Duhaime, S.S. Margulies, Anthropomorphic simulations of falls, shakes, and inflicted impacts in infants, J. Neurosurg. 99 (2003) 143–150. doi:10.3171/jns.2003.99.1.0143.

[23] C.A. Jenny, G. Bertocci, T. Fukuda, N. Rangarajan, T. Shams, Biomechanical response of the infant head to shaking: an experimental investigation, J. Neurotrauma. 34 (2017) 1–10. doi:10.1089/neu.2016.4687.

[24] J. Cheng, Shaken Baby Syndrome: simulation via computational and physical modelling (PhD thesis), The University of Sheffield, 2008.

[25] D.R. Wolfson, D.S. McNally, M.J. Clifford, M. Vloeberghs, Rigid-body modelling of shaken baby syndrome, Proc. Inst. Mech. Eng. Part H J. Eng. Med. 219 (2005) 63–70. doi:10.1243/095441105X9237.

[26] M. Bondy, W. Altenhof, X. Chen, A. Snowdon, B. Vrkljan, Development of a finite element/multi-body model of a newborn infant for restraint analysis and design, Comput. Methods Biomech. Biomed. Engin. 17 (2014) 149–162. doi:10.1080/10255842.2012.672563.

[27] M.D. Jones, P.S. Martin, J.M. Williams, A.M. Kemp, P. Theobald, Development of a computational biomechanical infant model for the investigation of infant head injury by shaking, Med. Sci. Law. 55 (2014) 291–299. doi:10.1177/0025802414564495.

[28] T.O. Lintern, N.T. Puhulwelle Gamage, F.H. Bloomfield, P. Kelly, M.C. Finch, A.J. Taberner, M.P. Nash, P.M.F. Nielsen, Head kinematics during shaking associated with abusive head trauma, J. Biomech. 48 (2015) 3123–3127. doi:10.1016/j.jbiomech.2015.07.016.

[29] J. Cheng, D. Batterbee, A. Yoxall, N.D. Sims, J. Rowson, I.C. Howard, D.W. Katholieke Univ Leuven, D.M.E. Katholieke Univ Leuven, D.M.E.S.S.J.D.S.Y.E. Univ Sheffield, Shaken baby syndrome: a structural dynamics perspective, in: Int. Conf. Noise Vib. Eng., 2008: pp. 2003–14.

[30] D. Batterbee, N. Sims, J. Rowson, Finite element modelling of shaken baby syndrome: a frequency response approach, in: Proc. IMAC, 2009.

[31] J. Cheng, I.C. Howard, M. Rennison, Study of an infant brain subjected to periodic motion via a custom experimental apparatus design and finite element modelling, J. Biomech. 43 (2010) 2887–96. doi:10.1016/j.jbiomech.2010.07.023.

[32] C.N. Morison, The dynamics of shaken baby syndrome, University of Birmingham, 2002.

[33] S. Roth, J.S. Raul, B. Ludes, R. Willinger, Finite element analysis of impact and shaking inflicted to a child, Int. J. Legal Med. 121 (2007) 223–8. doi:10.1007/s00414-006-0129-3.

[34] J.S. Raul, S. Roth, B. Ludes, R. Willinger, Influence of the benign enlargement of the subarachnoid space on the bridging veins strain during a shaking event: A finite element study, Int. J. Legal Med. 122 (2008) 337–40. doi:10.1007/s00414-008-0242-6.

[35] S.A. Hans, S.Y. Bawab, M.L. Woodhouse, A finite element infant eye model to investigate retinal

forces in shaken baby syndrome, Graefe's Arch. Clin. Exp. Ophthalmol. 247 (2009) 561–71. doi:10.1007/s00417-008-0994-1.

[36] Z. Couper, F. Albermani, Mechanical response of infant brain to manually inflicted shaking, Proc. Inst. Mech. Eng. Part H J. Eng. Med. 224 (2010) 1–15. doi:10.1243/09544119JEIM587.

[37] D.C. Batterbee, N.D. Sims, W. Becker, K. Worden, J. Rowson, Computational model of an infant brain subjected to periodic motion simplified modelling and bayesian sensitivity analysis, in: Proc. Inst. Mech. Eng. Part H J. Eng. Med., 2011: pp. 1136–49. doi:10.1177/0954411911420002.

[38] A.J. Loeve, A. Stray-Pedersen, Shaken baby model: head dynamics, Unpublished Work, 2015.

[39] A. Stray-Pedersen, A.J. Loeve, L.A.H. Schiks, Violent infant surrogate shaking: Continuous high magnitude centripetal force and abrupt shift in tangential acceleration may explain high risk for subdural haemorrhage (under submission), (2019).

[40] Z. Couper, F. G. Albermani, Biomechanics of shaken baby syndrome: physical testing and numerical modeling, in: A.J. Deeks, H. Hao (Eds.), Proc. 18th Australas. Conf. Mech. Struct. Mater., Perth, Australia, 2005: pp. 213–218.

[41] R. Raghupathi, M.F. Mehr, M.A. Helfaer, S.S. Margulies, Traumatic Axonal Injury is Exacerbated following Repetitive Closed Head Injury in the Neonatal Pig, J. Neurotrauma. 21 (2004) 307–16. doi:10.1089/089771504322972095.

[42] Z. Couper, F. Albermani, Infant brain subjected to oscillatory loading: Material differentiation, properties, and interface conditions, Biomech. Model. Mechanobiol. 7 (2008) 105–125.

[43] Z. Couper, F. Albermani, Infant brain subjected to oscillatory loading, Aust. J. Mech. Eng. 6 (2008) 79–85.

[44] A.C. Lui, T.Z. Polis, N.J. Cicutti, Densities of cerebrospinal fluid and spinal anaesthetic solutions in surgical patients at body temperature, Can. J. Anaesth. 45 (1998) 297–303.

[45] T.W. Barber, J.A. Brockway, L.S. Higgins, The density of tissues in and about the head, Acta Neurol. Scand. 46 (1970) 85–92. doi:10.1111/j.1600-0404.1970.tb05606.x.

# Appendix I

Literature study
(submitted to the Forensic Science International journal)

# Thresholds for the assessment of inflicted head injury by shaking trauma in infants: a systematic review

**Abstract**

In order to investigate potential causal relations between the shaking of infants and injuries, biomechanical studies compare brain and skull dynamic behavior during shaking to injury thresholds. However, performing shaking tolerance research on infants, either in vivo or ex vivo, is extremely difficult, if not impossible. Therefore, infant injury thresholds are usually estimated by scaling or extrapolating adult or animal data obtained from crash tests or whiplash experiments. However, it is doubtful whether such data accurately matches the biomechanics of shaking in an infant. Hence some thresholds may be inappropriate to be used for the assessment of inflicted head injury by shaking trauma in infants.

A systematic literature review was conducted to 1) provide an overview of existing thresholds for head- and neck injuries related to violent shaking, and 2) to identify and discuss which thresholds have been used or could be used for the assessment of inflicted head injury by shaking trauma in infants.

Key findings: the majority of studies establishing or proposing injury thresholds were found to be based on loading cycle durations and loading cycle repetitions that did not resemble those occurring during shaking, or had experimental conditions that were insufficiently documented in order to evaluate the applicability of such thresholds. Injury thresholds that were applied in studies aimed at assessing whether an injury could occur under certain shaking conditions were all based on experiments that did not properly replicate the loading characteristics of shaking. Somewhat validated threshold scaling methods only exist for scaling concussive injury thresholds from adult primate to adult human. Scaling methods that have been used for scaling other injuries, or for scaling adult injury thresholds to infants were not validated. There is a clear and urgent need for new injury thresholds established by accurately replicating the loading characteristics of shaking.

*Keywords: forensic science; child abuse; head injury; shaking trauma; injury tolerance*

## 1. Introduction

Retinal hemorrhage, subdural hemorrhage, diffuse axonal injury, and neck injury are symptoms often associated with violent shaking of an infant. However, the diagnosis of inflicted head injury based on the presence of such symptoms is often debated, because these symptoms can also be caused by events other than abusive shaking [1–4]. No consensus has been reached yet regarding the question if shaking alone can actually cause these symptoms [5–8].

Direct evidence or witnesses are often lacking in lawsuits regarding inflicted head injury by shaking trauma in infants (IHI-ST) [9,10]. Instead, expert witnesses and scientific studies are currently being used as corroborative evidence [11–13]. Scientific evidence for IHI-ST may include studies that investigate brain and skull dynamic behavior during violent shaking. The obtained data are compared to injury thresholds for bulk dynamical aspects, such as rotational acceleration of the skull, in order to assess the probability of injury [7,8,14]. Such injury thresholds and head dynamics are hard to obtain directly from infants due to ethical considerations and hence are based on experiments with surrogates [15–17], mathematical models [8,18,19] or on extrapolated or scaled adult- or animal data [7,8,20].

The thresholds that are used for the assessment of IHI-ST thus originate from various experiments, not all of which resembling the specific characteristics—e.g. loading conditions and test subject properties—for the assessment of IHI-ST. To the best of the authors' knowledge, no overview is available of which injury thresholds have been *used in studies on the assessment* of IHI-ST, or which thresholds could be *considered appropriate* for the assessment of IHI-ST.

Therefore, the purpose of this study was to identify and assess thresholds that have up to now been used for the assessment of IHI-ST. A systematic literature review was conducted to address the following research questions: are the thresholds that have been used in IHI-ST assessment studies appropriate? Which thresholds—available in literature—resemble the specific characteristics of IHI-ST? A framework was proposed and applied to score the applicability of injury thresholds for the assessment of IHI-ST.

## 2. Methods

A systematic search for literature was conducted in the databases of Scopus, PubMed and Web of Science to retrieve relevant literature published until March 4th, 2018.

### *2.1. Search strategy*

Studies regarding accidental falls, car crashes, and sports accidents may have constructed thresholds that are suitable for the assessment of IHI-ST. However, the loading conditions—e.g. impact of the head against an object—used in such studies often differ from the trauma mechanisms involved in IHI-ST. Another source for suitable injury thresholds are studies on material properties of tissues involved in IHI-ST. It was decided to construct a search query focused on the injuries often associated with IHI-ST—i.e. retinal hemorrhage, subdural hemorrhage, diffuse axonal injury and neck injury—and loading type—i.e. shaking or rotational loading without impact—rather than on the type of study they were established or used in. The search query is presented in Table 1.

**Table 1**
Database search query in general syntax.

| Category | Syntax |
|---|---|
| Threshold related terms | (criteria OR criterion OR limit* OR boundar* OR threshold* OR tolerance OR ((maxim* OR peak) AND (stress OR strain OR acceleration OR velocity))) |
| | AND |
| Experimental conditions | ((shake* OR shaking OR rotational OR whiplash AND NOT "head impact") AND (infant OR baby OR primate OR animal OR pig OR piglet OR goat)) |
| | AND |
| Types of injury | (("neck injury" OR "neck trauma" OR "subdural h*ematoma" OR "diffuse axonal" OR "subdural h*emorrhage" OR "cerebral concussion" OR "retinal h*emorrhage" OR "bridging vein*") OR ((craniocerebral OR retinal OR "diffuse axonal") AND (bleeding OR trauma OR injury))) |

Only literature in English or Dutch language was searched for. Duplicate records were removed after the database searches.

The reference lists of full-text articles were screened for relevant titles, and relevant citations were evaluated as well (backward snowballing). After three iterations of backward snowballing no more relevant articles were found. The articles identified in the database searches and the additional articles were put through the selection process described in *section 2.2.*

### *2.2. Selection criteria*

Articles were selected using the PRISMA methodology [21]; subsequently, the title, abstract and full-text were screened according to predefined selection criteria (Table 2). When there was any doubt about whether the article should be excluded, the article was put to the next step of the selection process.

**Table 2**
Selection criteria.

| | | Criteria |
|---|---|---|
| **Title** | *Inclusion* | Title contains terms related to research on- or evaluation of biomechanics, injury mechanisms, injury criteria, pathology or pathophysiology of head- and neck injuries concerning IHI-ST.<br>Or title contains terms concerning phenomena related to IHI-ST in an infant, animal, surrogate, or mathematical model.<br>Or title indicates potential relevance in any other way. |
| | *Exclusion* | Title is exclusively related to epidemiological research, penetrating trauma, blunt trauma /mechanical impact to the head/direct head impact , lateral/side impact, rear-end impact, drug or biochemical research, or injury diagnosis with- or evaluation of imaging techniques. |
| **Abstract** | *Inclusion* | Abstract shows that research was done regarding quantitative injury criteria, tissue properties, mechanical injury characteristics (e.g. forces, loads, stresses, strains) or kinematic injury characteristics (e.g. velocities, accelerations) related to head- and neck injuries concerning IHI-ST.<br>Or abstract shows that a quantitative analysis or an experiment—on (the assessment or probability of) head- and neck injuries related to IHI-ST—was conducted or reviewed.<br>Or "abstract shows that research was done using a child, animal, physical model or mathematical model to understand or explain (aspects of) IHI-ST" [22]. |
| | *Exclusion* | Abstract shows that the paper is exclusively related to qualitative criteria, diagnosis, treatment or to the after effects of head- and neck injuries. |
| **Full-text** | *Inclusion* | Injury thresholds were found regarding head- and neck injuries concerning IHI-ST.<br>Or injury thresholds were used for the assessment of IHI-ST related injuries. |
| | *Exclusion* | Axial or coronal plane angular accelerations, direct impact of or to the head and rear-impact studies—since the brain might have been injured from the blunt force impact (i.e. headrest or piston or similar objects) prior to the rotational acceleration. |

### *2.3. Data structuring*

In order to structure this systematic review, a distinction was made between 1) studies in which existing thresholds have been applied in order to assess IHI-ST; hereafter called *assessment studies* and 2) research on or development of thresholds for injuries seen in IHI-ST; hereafter called *threshold studies*.

Five categories, each with sub-categories, were used to classify the identified thresholds according to the type of injury:

- Axonal injuries
  - Diffuse axonal injury
  - Axotomy
  - Moderate and severe traumatic brain injury
- Concussive injuries
  - Cerebral concussion
  - Mild traumatic brain injury
- Intracranial bleedings
  - Ruptured bridging veins
  - Subdural hemorrhage
  - Subdural hematoma
- Retinal injuries
  - Retinal hemorrhage
- Neck injuries
  - Structural failure
  - Functional failure

*2.4. Data extraction*

A pre-defined data extraction table was used to extract all relevant data from the included literature. The following data were extracted from *threshold studies*; subject type, subject's actual age, subject's representative age, subject state, test type, loading type, loading cycle repetitions, loading cycle duration, injury type, threshold type, threshold property, scaling type, scaling reference, non-infant threshold value and infant threshold value. The following data were extracted from the *assessment studies*; threshold source, references used, injury type, threshold type, threshold property, non-infant threshold value, infant threshold value and assessed infant age. In the present study, the age range for an 'infant' is defined to be from newborn up to the age of 1 year.

*2.5. Threshold applicability framework*

Threshold scaling methods and experimental variables are major determinants for the applicability of a threshold for IHI-ST assessment, e.g. because injury tolerance is not equal among species and depends on the loading conditions used in experiments. Hence the experimental variables found in the identified threshold studies were evaluated for their role in the assessment of IHI-ST by reviewing relevant literature. Furthermore, the original papers of any scaling methods were evaluated for applicability in IHI-ST assessment. A threshold applicability framework was proposed and applied in order to indicate to what extent the variables of threshold experiments match the conditions seen in IHI-ST and to compare the agreement to IHI-ST conditions between the thresholds for each IHI-ST injury category.

## 3. Results

A total of 2269 unique records were identified, of which 47 articles were included in this systematic review. Figure 1 shows the PRISMA flowchart of the study selection process and the reasons for exclusion of the excluded full-text articles.

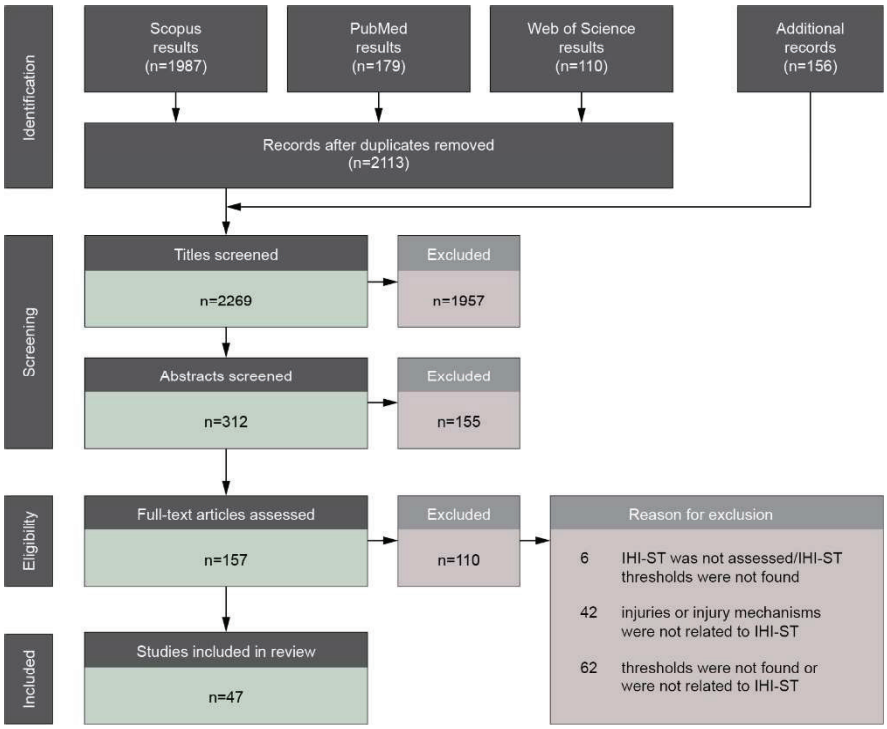


**Figure 1.** PRISMA flowchart of the literature selection process.

### 3.1. Threshold experimental variables

*Test subject properties*

Interspecies variations in both anatomy and mechanical properties of tissues result in specific injury tolerance [20,23,24]. Non-human primates are the closest relatives to humans. Therefore, this group of test subjects is considered preferable over non-primate species, although still sub-optimal compared to human test subjects.

Mechanical properties of tissues affect injury tolerance because the loading response of the tissue depends directly on these mechanical properties. Stiffness and ultimate strength of the cervical spine are age-dependent [25–27], and the elastic properties of brain tissue are age-dependent as well [28–30], in both animals and humans. However, it is unclear to what extent the mechanical properties of bridging veins vary with age [20,31].

Cadaveric specimens show a different mechanical response to loading than living or fresh specimens, e.g. due to preservation methods, rigor mortis effects, preconditioning and preloading [32–34].

*Loading conditions*

Dynamics of the head during shaking are different than during impact, because the loading conditions differ. Impact is characterized by a single (often high) load with a short loading-cycle duration, whereas shaking is characterized by successive (lower) load cycles of longer cycle durations. These different loading conditions affect the response—and thus the tolerance—of the infants head to the load.

Some of the tissues inside the skull, such as brain tissue, exhibit viscoelastic behavior [35,36]. The strain and stiffness of such viscoelastic materials are loading-rate-dependent. After loading, these tissues need a certain period of time to return to the undeformed state. However, when a subsequent load is applied before the tissue could return to its initial state, this subsequent load may cause a cumulative effect on the deformation of the tissue.

Characteristic for shaking is that the consecutive rotational-loading cycles are causing a persistent high magnitude centripetal acceleration of the head [37]. This may cause an increase of both the intracranial- and arterial pressure [38], which may in turn lead to additional stresses and strains in vessel walls and surrounding tissue.

Hence stating all the above, the mechanical response of a test subject will be different in cyclic loading than in single loads, which is reflected in the injury tolerance to such motions [20,39–41]. Therefore, studies using cyclic loading (n > 1) in threshold experiments have a better resemblance of shaking than single load experiments and are therefore more appropriate to use for IHI-ST assessment.

Studies also have shown that the tolerance of the head to angular acceleration varies with the duration of the acceleration pulse [42,43]. The duration of a single loading-cycle for shaking was derived from shaking frequencies reported in biomechanical research and was estimated to be half the period time. The reported shaking frequencies—exerted by participants—are in the range of 2–5 Hz [14,16,17,44–46]; i.e. one loading cycle for shaking has a duration of 100-250 ms for the reported frequency range.

### 3.2. Threshold scaling methods applied in IHI-ST assessment studies

The threshold scaling methods from the following studies were found to be used in IHI-ST assessment studies: Ommaya et al. [47], Margulies et al. [48], Klinich et al. [49] and Thibault [28].

Ommaya et al. [47] proposed an angular acceleration scaling relation for concussion in brains with similar properties and shapes (Equation 1), based on an unpublished letter of Holbourn [50]. The scaling relation was developed for predicting the angular acceleration required to produce a concussion in the human, based on experiments with primate test subjects. However, they emphasized that the proposed scaling relation was only a “working theory, and not a factual demonstration”. Experiments were announced to validate the scaling relation on squirrel monkeys and chimpanzees.

$$\ddot{\theta}_P = \ddot{\theta}_m \left(\frac{M_m}{M_P}\right)^{2/3} \quad (1)$$

The scaling relation of Ommaya et al. [47] (Equation 1) was eventually checked in primate experiments performed by Ommaya and Hirsch [24]. In that same study, a level of angular acceleration causing a concussion in the human was predicted using the scaling relation. This prediction was compared to a single case-history—in Ommaya and Yarnell [51]; human subject—in which cerebral concussion was not described, but "the production of a large subdural hematoma suggests a level of injury reasonably close to the threshold for cerebral concussion" [24]. Ommaya and Hirsch [24] found reasonable agreement between their prediction, and the level of angular acceleration in the—assumed concussion—case of Ommaya and Yarnell [51].

Margulies et al. [48] used Holbourn's scaling relation [47, 50] for scaling diffuse axonal injury tolerance data from primates to humans, for *coronal plane rotations*, using Equations 2 and 3. In these equations primate and human are denoted by the subscripts *"model M"* and *"prototype P"* respectively, and angular acceleration and angular velocity are denoted by $\ddot{\theta}$ and $\dot{\theta}$ respectively. Equation 2 is the same as in Ommaya et al. [47]. The origin and validity of Equation 3 could not be traced.

$$\ddot{\theta}_P = \ddot{\theta}_M \left(\frac{M_M}{M_P}\right)^{2/3} \quad (2)$$

$$\dot{\theta}_P = \dot{\theta}_M \left(\frac{M_M}{M_P}\right)^{1/3} \quad (3)$$

Klinich et al. [49] proposed a method for scaling adult protection reference values (PRVs) to the child. However, PRVs apply specifically to crash test dummies and are usually different from injury criteria, which apply to humans [49].

An angular acceleration ratio was derived from the ratio of the brain modulus of elasticity and the ratio of brain mass between adult and child. Klinich et al. [49] emphasized that PRVs are not equal to injury criteria for humans. The scaling relation of Klinich et al. [49] was rearranged to the form of Equation 4 in order to enable comparison with other scaling methods. Variables $A_{child}$ and $A_{adult}$ represent the angular accelerations, $E_{child}$ and $E_{adult}$ represent the brain elasticities and $M_{child}$ and $M_{adult}$ represent the brain masses of the child and the adult respectively.

$$A_{child} = A_{adult} \cdot \frac{\mathrm{M}_{adult}}{\mathrm{M}_{child}} \cdot \frac{\mathrm{E}_{child}}{\mathrm{E}_{adult}} \quad (4)$$

Thibault [28] proposed a method for scaling angular acceleration of the adult $\ddot{\theta}_{adult}$ to the infant $\ddot{\theta}_{infant}$. The difference in brain mass *M* and viscoelastic properties of brain tissue *G'* were included in the scaling method (Equation 5). This scaling law could not be found to be validated.

$$\ddot{\theta}_{infant} = \ddot{\theta}_{adult} \left(\frac{M_{adult}}{M_{infant}}\right)^{2/3} \cdot \left(\frac{G'_{infant}}{G'_{adult}}\right) \quad (5)$$

### *3.3. Threshold applicability for IHI-ST assessment*

Test subject type, subject state, loading cycle repetitions, loading cycle duration and scaling methods were found to be major determinants for the applicability (*sections 3.1* and *3.2)*. Also the subject's age may affect tolerance to certain injuries. However, because the effect of age on the injury tolerance is not yet known for *every* injury category covered in the present study, it was decided for now to exclude subject age from the threshold applicability framework presented hereafter.

Using the results from *sections 3.1 and 3.2* a threshold applicability framework was proposed (Table 3) in order to score thresholds for agreement with the conditions of IHI-ST in *sections 3.4 and 3.5*. The following applicability determinants were implemented in the framework; test subject type, subject state, loading cycle repetitions, loading cycle duration and scaling method. Each condition superior to another was rewarded one point per level of superiority in order to indicate to what extent the experimental conditions match the conditions seen in IHI-ST.

**Table 3**
Threshold applicability framework.

| | | Applicability score 2 | 1 | 0 |
|---|---|---|---|---|
| Applicability determinant | *Subject type* | Human | Non-human primate (model) | Non-primate (model) |
| | *Subject state* | - | Living or fresh | Non-living |
| | *Loading cycles [n]* | - | Multiple | Single |
| | *Loading duration (if n=1) or frequency (if n>1)* | - | IHI-ST related (100-250 ms or 2-5 Hz) | Other |
| | *Scaling method* | Not scaled | Thibault [28] or Ommaya et al. [47] | Other method |

*3.4. Identified threshold studies*

A total of 73 threshold values related to IHI-ST were found in a total of 37 studies [7,8,31,34,42,43,47,52–56,14,57–66,18,67–73,19,20,23,24,26,27]. Most thresholds were found for neck injuries and intracranial bleedings, while thresholds for retinal injuries were scarce. An overview of the thresholds found for each injury category is presented in Figure 2. The complete data extraction table from the included thresholds is provided as supplementary material.

An overview of the characteristics of experiments in which IHI-ST related thresholds were found is presented in Figure 3. Some results of particular interest were:

- The majority of retinal injury and axonal injury thresholds is based on non-primate test subjects.
- The majority of all thresholds is based on a single loading cycle.
- Multiple loading cycles were only used for intracranial bleeding thresholds.
- Loading cycle duration was not reported for the majority of the thresholds and could often not be deduced from the reported data either.
- An IHI-ST related loading cycle duration was only used for intracranial bleeding thresholds.
- Most thresholds were not scaled to infant values, but were thresholds for non-infant humans or animals.

In order to visualize to what extent the experimental conditions in threshold experiments agree with the conditions in IHI-ST, all thresholds were assigned an applicability score according to the threshold applicability framework (Table 3). A normalized overview of the applicability scores that were assigned to the 73 IHI-ST related thresholds is presented in Figure 4.

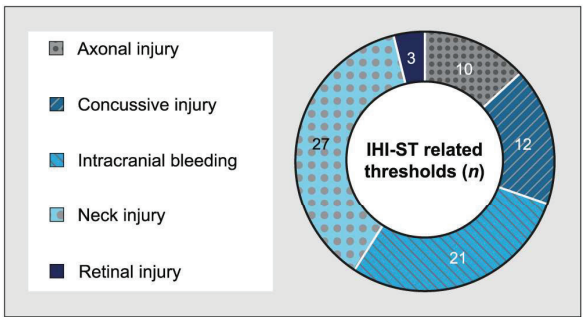


**Figure 2.** Number of thresholds (*n*) available in literature for each injury category.

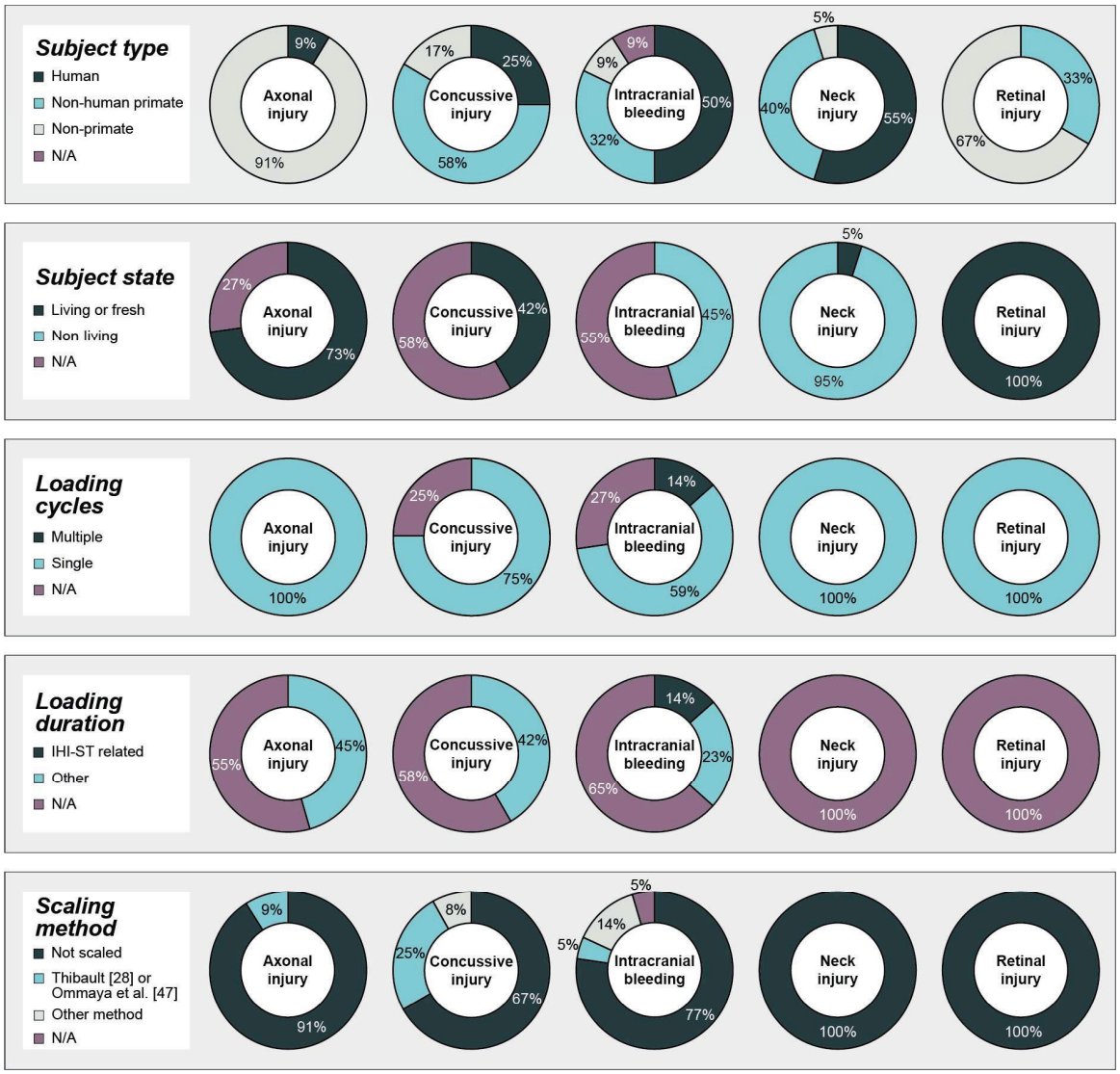


**Figure 3.** Overview of the characteristics of experimental conditions in threshold studies for IHI-ST related head- and neck injuries.

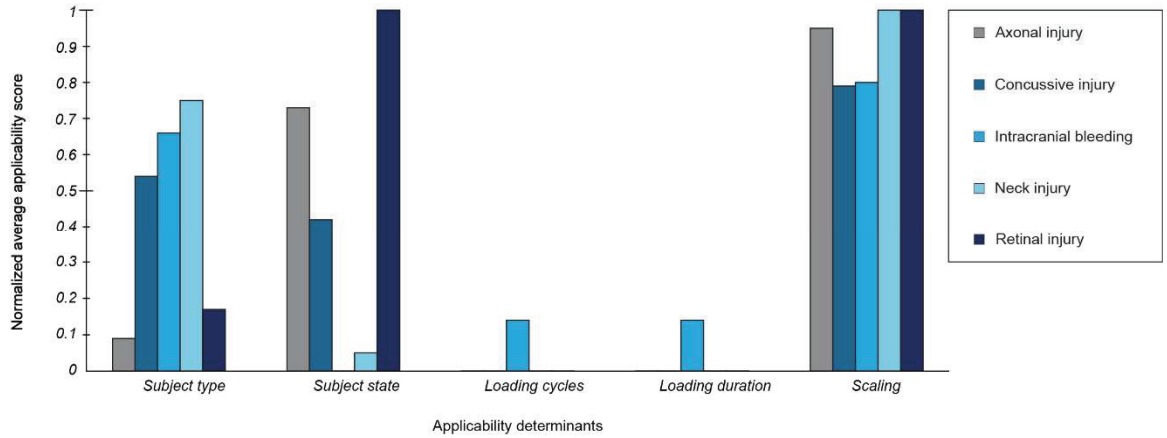


**Figure 4.** Average applicability scores assigned to the 73 thresholds for IHI-ST related head- and neck injuries, per applicability determinant. The average score of each applicability determinant was divided by the maximum score possible for that determinant to obtain a normalized maximum score of 1.

### 3.5. Identified assessment studies

Some of the found assessment studies used multiple thresholds for the assessment of a single injury; this was counted as a single assessment of the injury. An overview of the assessments of IHI-ST injuries is presented in Figure 5. Intracranial bleeding was assessed most, while neck injury and retinal injury were least frequently assessed in IHI-ST studies.

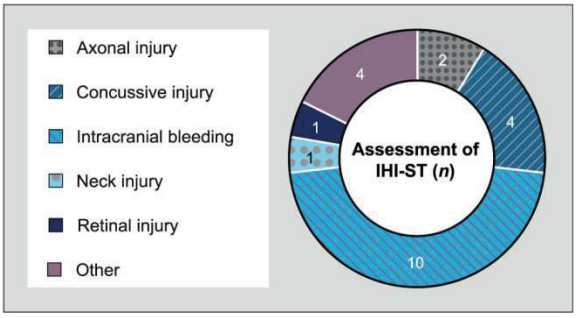


**Figure 5.** Number of times (*n*) that each IHI-ST injury was assessed in literature. The category 'other' was appointed when a study used more general definitions such as 'head injury' or 'neck injury'.

A total of 14 IHI-ST assessment studies [7,8,77–80,14–16,23,46,74–76] were found. In these studies 25 unique injury thresholds were used for the 35 times that an IHI-ST injury was assessed.

In 13 out of the 35 injury assessments a threshold was used that was deemed unsuitable for IHI-ST according to the considerations stated above, because the thresholds were based on experiments in which impact to the head was part of the motion or in which rotations were not mainly in the sagittal plane. In Appendix I, an overview is provided of: the identified IHI-ST assessment studies, the thresholds that were used in these studies and their threshold applicability scores—or the reason for exclusion. The complete data extraction table from the included assessment studies is provided as supplementary material.

## 4. Discussion

### 4.1. Threshold scaling methods

Four injury threshold scaling methods were identified in the IHI-ST assessment studies. These scaling methods were originally developed only for scaling tolerance data of a specific injury, under specific loading conditions, in specific species. However, these scaling methods have been used by several studies far beyond their originally intended purpose.

The scaling relation of Ommaya et al. [47] was proposed for scaling concussion thresholds between brains with similar properties and shapes but was merely a "working theory, and not a factual demonstration" [47]. Later Ommaya and Hirsch [24] found a good agreement between experimental concussion data from three primate species—rhesus monkey, squirrel monkey and chimpanzee—and the predictions from the scaling method of Ommaya et al. [47]. Furthermore, a reasonable agreement was found between their prediction of a concussion threshold for the human and a single case-history in Ommaya and Yarnell [51]. However, the viscoelastic properties of human brain tissue were found to be age-dependent [30]. Thibault [28] and Thibault and Margulies [29] found that adult and infant porcine brain properties are not similar and that the age-dependent material properties of brain tissue "affect the mechanical response of the brain to inertial loading" [29]. Thus if the same relation between material properties and the mechanical response of the brain holds for human brain tissue, then the threshold scaling method proposed by Ommaya et al. [47] cannot be used directly for scaling human adult thresholds to the infant.

Margulies et al. [48] used the method of Ommaya et al. [47] and Holbourn [50] for scaling diffuse axonal injury angular acceleration and angular velocity thresholds for coronal plane head rotations, in order to predict injury thresholds for humans based on primate experiments. Although Margulies et al. [48] reported that the results were in agreement with other physical model studies, the experiments only included head rotations in the coronal plane, while injury tolerance is specific to

the plane of rotation, and tolerance for axonal injury is significantly higher for angular accelerations of the head in the coronal plane than in the sagittal plane [81,82]. Rotations of the head in IHI-ST are mainly in the sagittal plane and it is not known whether the scaling relation holds for both coronal and sagittal plane head rotations.

The scaling relation of Klinich et al. [49] was developed for scaling adult PRVs for dummies to the infant, it was not developed for scaling injury thresholds for humans. PRVs apply specifically to crash test dummies and are usually different from injury criteria that apply to humans [49]. It is not known if the scaling relation for dummies also holds for scaling human concussion tolerance data between adult and infant.

Thibault [28] used the scaling relation of Ommaya et al. [47]—originally intended for scaling concussion thresholds between primate species and human—and incorporated the different material properties of adult and infant brain in order to scale concussion tolerance data from the adult to the infant. Thibault [28] assumed that the scaling method of Ommaya et al. [47] was also valid for scaling between adult and infant if it would be accounted for that the material properties of the adult and infant brain are not equal—because Ommaya et al. [47] assumed equal brain properties. The improved scaling relation of Thibault [28] is the most comprehensive one compared to the other scaling methods discussed in this section.

### *4.2. Validation of threshold scaling methods*

The scaling relation of Ommaya et al. [47] for concussion thresholds was validated in primate experiments and reasonable agreement was found for scaling primate concussion tolerance data to the human adult. Therefore, this scaling relation can be used only for scaling concussion thresholds between primate species, or for scaling between primate and human—not for scaling thresholds from adult to infant.

Validation of scaling methods between animals does not justify the use of these scaling methods for scaling animal injury thresholds to the human adult or to the infant, which would require further validation. However, experimental data from fresh or cadaveric pediatric specimens are hard to obtain. In addition to ethical considerations, there is only limited availability of pediatric cadaveric specimens. Adult to infant scaling methods can currently hardly be validated with the use of finite element models for the same reasons. Hence it remains unclear if existing methods for scaling between adults and infants are appropriate.

Because adult and infant brain material properties are not the same—adult brain is found to be 3-4 times stiffer than the brain of a 5 months old infant [30]—it must be emphasized that the difference in mechanical properties between adult and infant brain tissue must not be neglected when scaling injury thresholds. After all, the loading response of the brain directly depends on its material properties. Validated scaling methods that incorporate the different material properties of adult and infant brains thus would be most useful for IHI-ST assessment.

### *4.3. Threshold studies*

The identified thresholds for the head- and neck injuries related to IHI-ST were evaluated for their agreement with the rather specific conditions of IHI-ST. The identified injury threshold experiments were only occasionally focused specifically on IHI-ST, more often the thresholds were developed in studies with a focus on whiplash experiments or on tissue strength properties. This may also be a valid reason for the over-represented neck injury- and bridging vein rupture thresholds, compared to the only few retinal injury thresholds.

The experimental variables that were used in these studies differ a lot from the conditions that are required for a good agreement with IHI-ST conditions. Furthermore, experimental variables that are important for evaluating the agreement with IHI-ST conditions were often not reported in the threshold studies, most likely because they were simply not relevant for the kind of application those studies were intended for. This is reflected by the fact that the majority of the identified thresholds is based on a single loading cycle and the loading cycle duration was shorter than in IHI-ST—or was not reported at all.

Furthermore, the majority of thresholds for neck injuries and retinal injuries—and a fewer number for axonal injuries—proposed an ultimate or structural failure value, while functional failure might occur already on lower levels. Such thresholds might still be useful for the assessment of IHI-ST, although it must be taken into account that these thresholds represent a rather liberal threshold, which in turn may cause an overestimated tolerance to shaking.

Most of the identified thresholds were applicable only for adult injury assessment. The few thresholds that were found for infants were almost always scaled from animal tolerance data while it remains unclear if these scaling methods are valid.

*4.4. Assessment studies*

Retinal hemorrhage, subdural hemorrhage, diffuse axonal injury and neck injury all are symptoms that are often associated with violent shaking of an infant. However, the distribution of the assessment of each injury category was found to be far from balanced. The majority of the IHI-ST assessment studies assessed concussive injury and intracranial bleeding, while only a few studies assessed axonal injury, neck injury or retinal bleeding. This may be explained by the fact that the thresholds for axonal- and retinal injury were all based on animal data, and no scaling methods exist for scaling thresholds for these injuries. The thresholds that were identified for neck injury and retinal injury all describe an ultimate failure threshold; e.g. neck distraction force or retinal detachment force. This could explain the lack of assessment of such injuries because the injuries following from shaking trauma are less extreme.

In several studies thresholds were used for the assessment of IHI-ST that were excluded from the present study. In these threshold experiments impact of the head or to the head was part of the motion or motions were not mainly in the sagittal plane, while injury tolerance under these conditions is not the same as in IHI-ST. Although linear acceleration of the brain due to direct impact of the head or to the head has the potential of causing similar injuries—e.g. concussion—as angular acceleration, the tolerance to linear acceleration is higher than to angular acceleration [24,83]. Adoption of such thresholds in IHI-ST assessment studies may result in an overestimated tolerance to shaking.

Thresholds that were used in IHI-ST assessment studies were often based on a single loading cycle with a loading duration that was not related to IHI-ST—or was not reported at all. It was already emphasized that injury tolerance and the mechanical response of the brain are dependent on the loading duration and loading cycle repetitions.

The majority of the infant injury thresholds that were used in IHI-ST assessment studies was scaled from adult or animal data. In some cases, it was not reported which scaling methods were applied, or scaling methods were used outside the originally intended purpose. Although for most studies scaling methods were used—either directly or indirectly—that were in good agreement with the intended purpose of the scaling method, the validity of these scaling methods is still not known.

*4.5. Limitations*

The applicability scores that were assigned in *section 3.3* merely indicate a level of superiority *within* that specific applicability determinant. By no means, is the presented qualitative applicability score meant to be used as a definitive grade. Additional weighting for experimental conditions within each applicability determinant and amongst the other applicability determinants would first be required.

Whenever certain information on experimental variables was not reported in a threshold- or assessment study, the assigned applicability score was 0 because the applicability of such a threshold for the assessment of IHI-ST could not be appraised. This does not refer to the quality of the study concerned.

The purpose of the present study was to identify and discuss which thresholds have been used for the assessment of IHI-ST; not to identify all injury threshold scaling methods that exist in general. Therefore, methods for scaling injury thresholds were identified only if they have ever been used within the included threshold- or assessment

studies. Hence, it could be that some scaling methods that would be suitable for scaling injury thresholds were not identified in the current study.

*4.6. Future research*

It is suggested that future research investigates the effect of each individual applicability determinant on the applicability of the threshold for IHI-ST assessment, in order to quantify the consequences of the disagreement that was found between the conditions in currently available injury thresholds and the rather specific conditions of IHI-ST. Furthermore, future research should be directed towards the selection or development of injury thresholds specifically for the conditions as seen in IHI-ST and on validation of the methods for scaling animal or human adult injury tolerance data to infants.

## 5. Conclusion

An applicability framework was proposed and applied in order to examine to what extent the variables of head- and neck injury threshold experiments match the conditions seen in IHI-ST. As hardly any existing thresholds linking bulk dynamics to injury are based on actual infant data or on tests with dynamics similar to shaking, the identified thresholds for the head- and neck injuries related to IHI-ST, as well as the thresholds applied in IHI-ST assessment studies, generally do not match the conditions of IHI-ST.

Validated scaling methods were only found for scaling concussive injury thresholds from primate to human. Scaling methods that were used for scaling other injuries, or for scaling adult injury thresholds to the infant could not be found to be validated. Therefore it is suggested to not use these thresholds for IHI-ST assessment.

## Abbreviations

| | |
|---|---|
| **IHI-ST** | Inflicted Head Injury by Shaking Trauma |
| **PRV** | Protection Reference Value |

## Declarations of interests

The authors have no conflicts of interest to declare.

## Funding

This research did not receive any specific grant from funding agencies in the public, commercial, or not-for-profit sectors.

## References

[1] M. Mian, J. Shah, A. Dalpiaz, R. Schwamb, Y. Miao, K. Warren, S. Khan, Shaken baby syndrome: A review, Fetal Pediatr. Pathol. 34 (2015) 169–75. doi:10.3109/15513815.2014.999394.

[2] M. Vinchon, O. Noizet, S. Defoort-Dhellemmes, G. Soto-Ares, P. Dhellemmes, Infantile subdural hematomas due to traffic accidents, Pediatr. Neurosurg. 37 (2002) 245–53. doi:10.1159/000066216.

[3] G. Elinder, A. Eriksson, B. Hallberg, N. Lynøe, P.M. Sundgren, M. Rosén, I. Engström, B.E. Erlandsson, Traumatic shaking: The role of the triad in medical investigations of suspected traumatic shaking, Acta Paediatr. Int. J. Paediatr. 107 (2018) 3–23. doi:10.1111/apa.14473.

[4] M. Laghmari, H. Skiker, H. Handor, B. Mansouri, K. Ouazzani Chahdi, R. Lachkar, Y. Salhi, O. Cherkaoui, B. Ouazzani Tnacheri, W. Ibrahimy, H. Alami, R. Bezad, S. Ahid, R. Abouqal, R. Daoudi, [Birth-related retinal hemorrhages in the newborn: incidence and relationship with maternal, obstetric and neonatal factors. Prospective study of 2,031 cases], J. Fr. d Opthalmologie. 37 (2014) 313–9. doi:http://dx.doi.org/10.1016/j.jfo.2013.06.005.

[5] S.C. Gabaeff, Challenging the Pathophysiologic Connection between Subdural Hematoma, Retinal Hemorrhage and Shaken Baby Syndrome, West. J. Emerg. Med. 12 (2011) 144–58.

[6] W. Squier, Shaken baby syndrome: The quest for evidence, Dev. Med. Child Neurol. 50 (2008) 10–4. doi:10.1111/j.1469-8749.2007.02004.x.

[7] C.Z. Cory, M.D. Jones, Can shaking alone cause fatal brain injury? A biomechanical assessment of the Duhaime shaken baby syndrome model, Med. Sci. Law.

43 (2003) 317–33. doi:10.1258/rsmmsl.43.4.317.

[8] T.O. Lintern, M.P. Nash, P. Kelly, F.H. Bloomfield, A.J. Taberner, P.M.F. Nielsen, Probabilistic description of infant head kinematics in abusive head trauma, Comput. Methods Biomech. Biomed. Engin. 20 (2017) 1633–42. doi:10.1080/10255842.2017.1403593.

[9] R.W. Byard, "Shaken baby syndrome" and forensic pathology: An uneasy interface, Forensic Sci. Med. Pathol. 10 (2014) 239–41. doi:10.1007/s12024-013-9514-7.

[10] D. Tuerkheimer, Flawed convictions: "Shaken baby syndrome" and the inertia of injustice, 2014.

[11] C. Dyer, Court hears shaken baby cases, BMJ. (2005). doi:10.1136/bmj.330.7506.1463-a.

[12] M. Vinchon, S. De Foort-Dhellemmes, M. Desurmont, I. Delestret, Confessed abuse versus witnessed accidents in infants: Comparison of clinical, radiological, and ophthalmological data in corroborated cases, Child's Nerv. Syst. 26 (2010) 637–45. doi:10.1007/s00381-009-1048-7.

[13] A.K. Choudhary, S. Servaes, T.L. Slovis, V.J. Palusci, G.L. Hedlund, S.K. Narang, J.A. Moreno, M.S. Dias, C.W. Christian, M.D. Nelson, V.M. Silvera, S. Palasis, M. Raissaki, A. Rossi, A.C. Offiah, Consensus statement on abusive head trauma in infants and young children, Pediatr. Radiol. 48 (2018) 1048–65. doi:10.1007/s00247-018-4149-1.

[14] A.C. Duhaime, T.A. Gennarelli, L.E. Thibault, D.A. Bruce, S.S. Margulies, R. Wiser, The shaken baby syndrome. A clinical, pathological, and biomechanical study, J. Neurosurg. 66 (1987) 409–15. doi:10.3171/jns.1987.66.3.0409.

[15] T. Koizumi, N. Tsujiuchi, K. Hara, Y. Miyazaki, Dynamic response and damage estimation of infant brain for vibration, in: Conf. Proc. Soc. Exp. Mech. Ser., 2013: pp. 11–8. doi:10.1007/978-1-4614-6546-1_2.

[16] J. Lloyd, E.N. Willey, J.G. Galaznik, W.E. Lee, S.E. Luttner, Biomechanical Evaluation of Head Kinematics During Infant Shaking Versus Pediatric Activities of Daily Living, J. Forensic Biomech. 2 (2011) 1–9. doi:10.4303/jfb/f110601.

[17] S. Cirovic, M. Freddolini, R. Goodwin, D. Zimarev, Shaken Mannequin Experiments: Head Motion Pattern and Its Potential Effect on Blood Pressure, J. Forensic Biomech. 3 (2012). doi:10.4303/jfb/235476.

[18] L. Ren, D. Baumgartner, J. Yang, J. Davidsson, R. Willinger, Investigation of diffuse axonal injury induced by rotational acceleration via numerical reconstructions of in vivo rat head impact experiments, Int. J. Crashworthiness. 20 (2015) 602–12. doi:10.1080/13588265.2015.1073132.

[19] B. Coats, S.A. Eucker, S. Sullivan, S.S. Margulies, Finite element model predictions of intracranial hemorrhage from non-impact, rapid head rotations in the piglet, Int. J. Dev. Neurosci. 30 (2012) 191–200. doi:10.1016/j.ijdevneu.2011.12.009.

[20] S.A. Pasquesi, S.S. Margulies, Failure and Fatigue Properties of Immature Human and Porcine Parasagittal Bridging Veins, Ann. Biomed. Eng. 45 (2017) 1877–89. doi:10.1007/s10439-017-1833-5.

[21] D. Moher, A. Liberati, J. Tetzlaff, D.G. Altman, T.P. Group, Preferred Reporting Items for Systematic Reviews and Meta-Analyses: The PRISMA Statement, PLoS Med. 6 (2009) e1000097. doi:10.1371/journal.pmed.1000097.

[22] J.P. van Zandwijk, M.E.M. Vester, R.A. Bilo, R.R. van Rijn, A.J. Loeve, Modeling of inflicted head injury by shaking trauma in children: what can we learn?, Forensic Sci. Med. Pathol. (2019). doi:10.1007/s12024-019-00093-7.

[23] C.N. Morison, The dynamics of shaken baby syndrome, University of Birmingham, 2002.

[24] A.K. Ommaya, A.E. Hirsch, Tolerances for cerebral concussion from head impact and whiplash in primates, J. Biomech. 4 (1971) 13–21. doi:10.1016/0021-9290(71)90011-X.

[25] R. Mayer, F.P. Pintar, N. Yoganandan, Pediatric neck tensile strength characteristics using a caprine model, in: Inj. Biomech. Res. Proc. 27th Int. Work. Hum. Subj. Biomech., San Diego, 1999: pp. 87–92.

[26] J. Ouyang, Q. Zhu, W. Zhao, Y. Xu, W. Chen, S. Zhong, Biomechanical assessment of the pediatric cervical spine under bending and tensile loading, Spine (Phila. Pa. 1976). 30 (2005) E716-23. doi:10.1097/01.brs.0000192280.53831.70.

[27] R.P. Ching, D.J. Nuckley, S.M. Hertsted, M.P. Eck, F.A. Mann, E.A. Sun, Tensile mechanics of the developing cervical spine, Stapp Car Crash J. 1 (2001) 329–36. doi:10.4271/2001-22-0015.

[28] K.L. Thibault, Pediatric head injuries: the influence of brain and skull mechanical properties, University of Pennsylvania, 1997.

[29] K.L. Thibault, S.S. Margulies, Age-dependent material properties of the porcine cerebrum: Effect on pediatric inertial head injury criteria, J. Biomech. 31 (1998) 1119–26. doi:10.1016/S0021-9290(98)00122-5.

[30] S. Chatelin, J. Vappou, S. Roth, J.S. Raul, R. Willinger,

Towards child versus adult brain mechanical properties, J. Mech. Behav. Biomed. Mater. 6 (2012) 166–73. doi:10.1016/j.jmbbm.2011.09.013.

[31] D.F. Meaney, Biomechanics of acute subdural hematoma in the subhuman primate and man, University of Pennsylvania, 1991.

[32] E. Hohmann, N. Keough, V. Glatt, K. Tetsworth, R. Putz, A. Imhoff, The mechanical properties of fresh versus fresh/frozen and preserved (Thiel and Formalin) long head of biceps tendons: A cadaveric investigation, Ann. Anat. 221 (2019) 186–191. doi:10.1016/j.aanat.2018.05.002.

[33] C.C. Van Ee AL; Myers, BS, Quantifying skeletal muscle properties in cadaveric test specimens: Effects of mechanical loading, postmortem time, and freezer storage, J. Biomech. Eng. 122 (2000) 9–14.

[34] K.L. Monson, W. Goldsmith, N.M. Barbaro, G.T. Manley, Significance of source and size in the mechanical response of human cerebral blood vessels, J. Biomech. 38 (2005) 737–44. doi:10.1016/j.jbiomech.2004.05.004.

[35] S. Budday, G. Sommer, C. Birkl, C. Langkammer, J. Haybaeck, J. Kohnert, M. Bauer, F. Paulsen, P. Steinmann, E. Kuhl, G.A. Holzapfel, Mechanical characterization of human brain tissue, Acta Biomater. 48 (2017) 319–40. doi:10.1016/j.actbio.2016.10.036.

[36] K.K. Darvish, J.R. Crandall, Nonlinear viscoelastic effects in oscillatory shear deformation of brain tissue, Med. Eng. Phys. 23 (2001) 633–45. doi:10.1016/S1350-4533(01)00101-1.

[37] A. Stray-Pedersen, Violent infant surrogate shaking: Continuous high magnitude centripetal force and abrupt shift in tangential acceleration may explain high risk for subdural haemorrhage, Unpubl. Results. (2019).

[38] T.A. Rochetti Bezerra, D.L. Spavieri Júnior, G. Frigieri, R. Brunell, S.M. de Oliveira, In-flight analysis of intracranial pressure in pilots undergoing variation in Gz, Aeronaut. Aerosp. Open Access J. 2 (2018) 126–131. doi:10.15406/aaoaj.2018.02.00042.

[39] B.M. Knowles, S.R. MacGillivray, J.A. Newman, C.R. Dennison, Influence of rapidly successive head impacts on brain strain in the vicinity of bridging veins, J. Biomech. 59 (2017) 59–70. doi:10.1016/j.jbiomech.2017.05.016.

[40] R. Raghupathi, M.F. Mehr, M.A. Helfaer, S.S. Margulies, Traumatic Axonal Injury is Exacerbated following Repetitive Closed Head Injury in the Neonatal Pig, J. Neurotrauma. 21 (2004) 307–16. doi:10.1089/089771504322972095.

[41] N. Rangarajan, S.B. Kamalakkannan, V. Hasija, T. Shams, C. Jenny, I. Serbanescu, J. Ho, M. Rusinek, A. V. Levin, Finite element model of ocular injury in abusive head trauma, J. AAPOS. 13 (2009) 364–9. doi:10.1016/j.jaapos.2008.11.006.

[42] T.A. Gennarelli, L.E. Thibault, Biomechanics of acute subdural hematoma, J. Trauma - Inj. Infect. Crit. Care. 22 (1982) 680–6. doi:10.1097/00005373-198208000-00005.

[43] G.N. Bycroft, Mathematical model of a head subjected to an angular acceleration, J. Biomech. 6 (1973) 487–95. doi:10.1016/0021-9290(73)90007-9.

[44] C.A. Jenny, T. Shams, N. Rangarajan, T. Fukuda, Development of a biofidelic 2.5 kg infant dummy and its application to assessing infant head trauma during violent shaking, in: Proc. 30th Int. Work. Hum. Subj. Biomech. Res., 2002: pp. 129–41.

[45] C.A. Jenny, G. Bertocci, T. Fukuda, N. Rangarajan, T. Shams, Biomechanical response of the infant head to shaking: an experimental investigation, J. Neurotrauma. 34 (2017) 1–10. doi:10.1089/neu.2016.4687.

[46] M.T. Prange, B. Coats, A.-C. Duhaime, S.S. Margulies, Anthropomorphic simulations of falls, shakes, and inflicted impacts in infants, J. Neurosurg. 99 (2003) 143–150. doi:10.3171/jns.2003.99.1.0143.

[47] A.K. Ommaya, P.R. Yarnell, A.E. Hirsch, E.H. Harris, Scaling of experimental data on cerebral concussion in sub-human primates to concussion threshold for man, in: Proc. 11th Stapp Car Crash Conf., 1967: pp. 73–80. doi:10.4271/670906.

[48] S.S. Margulies, L.E. Thibault, T.A. Gennarelli, Physical model simulations of brain injury in the primate, J. Biomech. 23 (1990) 823–36. doi:10.1016/0021-9290(90)90029-3.

[49] K.D. Klinich, R. Saul, G. Auguste, S. Backaitis, M. Kleinberger, Techniques for developing child dummy protection reference values, 1996.

[50] A. Holbourn, Personal communication to Dr Sabina Stritch 13 October, 1956.

[51] A.K. Ommaya, P.R. Yarnell, Subdural hæmatoma after whiplash injury, Lancet. 294 (1969) 237–39. doi:10.1016/s0140-6736(69)90005-1.

[52] A.C. Bain, D.F. Meaney, Thresholds for mechanical injury to the in vivo white matter, in: 43rd Stapp Car Crash Conf., 1999: pp. 295–302. doi:10.4271/99sc19.

[53] A.C. Bain, D.F. Meaney, Tissue-level thresholds for axonal damage in an experimental model of central nervous system white matter injury, J. Biomech. Eng.

122 (2000) 615–22. doi:10.1115/1.1324667.

[54] J. Davidsson, M. Angeria, M.G. Risling, Injury threshold for sagittal plane rotational induced diffuse axonal injuries, in: Proc. Int. Res. Conf. Biomech. Impact, 2009.

[55] H. Delye, J. Goffin, P. Verschueren, J. Vander Sloten, G. Van der Perre, H. Alaerts, I. Verpoest, D. Berckmans, Biomechanical properties of the superior sagittal sinus-bridging vein complex., Stapp Car Crash J. 50 (2006) 625–36.

[56] J.M. Duncan, Laboratory note: On the tensile strengthof the fresh adult fœtus, Br. Med. J. 2 (1874) 763–4. doi:10.1136/bmj.2.729.763.

[57] B.S. Elkin, B. Morrison, Region-specific tolerance criteria for the living brain., Stapp Car Crash J. 51 (2007) 127–38.

[58] H.M. Huang, M.C. Lee, W.T. Chiu, C.T. Chen, S.Y. Lee, Three-dimensional finite element analysis of subdural hematoma, J. Trauma - Inj. Infect. Crit. Care. 47 (1999) 538–44. doi:10.1097/00005373-199909000-00019.

[59] H. Kimpara, M. Iwamoto, Mild traumatic brain injury predictors based on angular accelerations during impacts, Ann. Biomed. Eng. 40 (2012) 114–26. doi:10.1007/s10439-011-0414-2.

[60] M. Kita, M.F. Marmor, Retinal adhesive force in living rabbit, cat, and monkey eyes: Normative data and enhancement by mannitol and acetazolamide, Investig. Ophthalmol. Vis. Sci. 33 (1992) 1879–82.

[61] M.C. Lee, R.C. Haut, Insensitivity of tensile failure properties of human bridging veins to strain rate: Implications in biomechanics of subdural hematoma, J. Biomech. 22 (1989) 537–42. doi:10.1016/0021-9290(89)90005-5.

[62] M.C. Lee, J.W. Melvin, K. Ueno, Finite Element Analysis of Traumatic Subdural Hematoma, in: 31st Stapp Car Crash Conf., 1987: pp. 67–77. doi:10.4271/872201.

[63] H.J. Mertz, L.M. Patrick, Strength and Response of the Human Neck, in: 15th Stapp Car Crash Conf., 1971: pp. 207–55. doi:10.4271/710855.

[64] A.G. Monea, K. Baeck, E. Verbeken, I. Verpoest, J. Vander Sloten, J. Goffin, B. Depreitere, The biomechanical behaviour of the bridging vein-superior sagittal sinus complex with implications for the mechanopathology of acute subdural haematoma, J. Mech. Behav. Biomed. Mater. 32 (2014) 155–65. doi:10.1016/j.jmbbm.2013.12.007.

[65] B. Morrison, H.L. Cater, C.C.-B. Wang, F.C. Thomas, C.T. Hung, G.A. Ateshian, L.E. Sundstrom, A Tissue Level Tolerance Criterion for Living Brain Developed with an In Vitro Model of Traumatic Mechanical Loading, in: 47th Stapp Car Crash Conf., 2003: pp. 93–105. doi:10.4271/2003-22-0006.

[66] R.W. Nightingale, V. Carol Chancey, D. Ottaviano, J.F. Luck, L. Tran, M. Prange, B.S. Myers, Flexion and extension structural properties and strengths for male cervical spine segments, J. Biomech. 40 (2007) 535–42. doi:10.1016/j.jbiomech.2006.02.015.

[67] A.K. Ommaya, F. Faas, P.R. Yarnell, Whiplash Injury and Brain Damage: An Experimental Study, JAMA J. Am. Med. Assoc. 204 (1968) 285–9. doi:10.1001/jama.1968.03140170001001.

[68] J.A. Pramudita, K. Watanabe, Y. Tanabe, Strength of porcine cervical facet joint capsular ligament under vertebral axial tensile loading, J. Biomech. Sci. Eng. 8 (2013) 293–305. doi:10.1299/jbse.8.293.

[69] K.P. Quinn, B.A. Winkelstein, Cervical facet capsular ligament yield defines the threshold for injury and persistent joint-mediated neck pain, J. Biomech. 40 (2007) 2299–306. doi:10.1016/j.jbiomech.2006.10.015.

[70] A. Singh, Y. Lu, C. Chen, S. Kallakuri, J.M. Cavanaugh, A New Model of Traumatic Axonal Injury to Determine the Effects of Strain and Displacement Rates, in: 50th Stapp Car Crash Conf., 2006: pp. 601–23. doi:10.4271/2006-22-0023.

[71] D.H. Smith, J.A. Wolf, T.A. Lusardi, V.M. Lee, D.F. Meaney, High tolerance and delayed elastic response of cultured axons to dynamic stretch injury., J. Neurosci. 19 (1999) 4263–9.

[72] N. Yoganandan, S. Kumaresan, F.A. Pintar, Geometric and Mechanical Properties of Human Cervical Spine Ligaments, J. Biomech. Eng. 122 (2000) 623–9. doi:10.1115/1.1322034.

[73] N. Yoganandan, F.A. Pintar, D.J. Maiman, J.F. Cusick, A. Sances, P.R. Walsh, Human head-neck biomechanics under axial tension, Med. Eng. Phys. 18 (1996) 289–94. doi:10.1016/1350-4533(95)00054-2.

[74] F.A. Bandak, Shaken baby syndrome: A biomechanics analysis of injury mechanisms, Forensic Sci. Int. 151 (2005) 71–9. doi:10.1016/j.forsciint.2005.02.033.

[75] Z. Couper, F. Albermani, Mechanical response of infant brain to manually inflicted shaking, Proc. Inst. Mech. Eng. Part H J. Eng. Med. 224 (2010) 1–15. doi:10.1243/09544119JEIM587.

[76] S.A. Hans, S.Y. Bawab, M.L. Woodhouse, A finite element infant eye model to investigate retinal forces in shaken baby syndrome, Graefe's Arch. Clin. Exp. Ophthalmol. 247 (2009) 561–71. doi:10.1007/s00417-

008-0994-1.

[77] T. Koizumi, N. Tsujiuchi, K. Hara, Infant brain response against shaking vibration using finite element analysis, in: Conf. Proc. Soc. Exp. Mech. Ser., 2014: pp. 1–11. doi:10.1007/978-3-319-04753-9_1.

[78] E. Ponce, D. Ponce, Modeling neck and brain injuries in infants, IEEE Comput. Graph. Appl. 31 (2011) 90–6. doi:10.1109/MCG.2011.99.

[79] S. Roth, J.S. Raul, B. Ludes, R. Willinger, Finite element analysis of impact and shaking inflicted to a child, Int. J. Legal Med. 121 (2007) 223–8. doi:10.1007/s00414-006-0129-3.

[80] D.R. Wolfson, D.S. McNally, M.J. Clifford, M. Vloeberghs, Rigid-body modelling of shaken baby syndrome, Proc. Inst. Mech. Eng. Part H J. Eng. Med. 219 (2005) 63–70. doi:10.1243/095441105X9237.

[81] S. Sullivan, S.A. Eucker, D. Gabrieli, C. Bradfield, B. Coats, M.R. Maltese, J. Lee, C. Smith, S.S. Margulies, White matter tract-oriented deformation predicts traumatic axonal brain injury and reveals rotational direction-specific vulnerabilities, Biomech. Model. Mechanobiol. 14 (2015) 877–96. doi:10.1007/s10237-014-0643-z.

[82] S.A. Eucker, C. Smith, J. Ralston, S.H. Friess, S.S. Margulies, Physiological and histopathological responses following closed rotational head injury depend on direction of head motion, Exp. Neurol. 227 (2011) 79–88. doi:10.1016/j.expneurol.2010.09.015.

[83] A.K. Ommaya, A.E. Hirsch, J.L. Martinez, The Role of Whiplash in Cerebral Concussion, in: 10th Stapp Car Crash Conf., 1966. doi:10.4271/660804.

# Appendix II

Letter of approval – Human Research Ethics Committee

Date 16-04-2019
Contact person Ir. J.B.J. Groot Kormelink, secretary HREC
Telephone +31 152783260
E-mail j.b.j.grootkormelink@tudelft.nl


Human Research Ethics Committee
TU Delft
(http://hrec.tudelft.nl/)

Visiting address
Jaffalaan 5 (building 31)
2628 BX Delft

Postal address
P.O. Box 5015
2600 GA Delft
The Netherlands

*Ethics Approval Application: Shake Doll 01*
*Applicant: Loeve, Arjo*

Dear Arjo Loeve,

It is a pleasure to inform you that your application mentioned above has been approved.

Good luck with your research!

Sincerely,

Prof. Dr. Sabine Roeser
Chair Human Research Ethics Committee TU Delft

**Prof.dr. Sabine Roeser**
**TU Delft**
Head of the Ethics and Philosophy of Technology Section
Department of Values, Technology, and Innovation
Faculty of Technology, Policy and Management
Jaffalaan 5
2628 BX Delft
The Netherlands
+31 (0) 15 2788779
S.Roeser@tudelft.nl
www.tbm.tudelft.nl/sroeser

# Appendix III

Custom made sensor bracket and modified Q0-dummy

## Sensor bracket design

The custom made accelerometer bracket (Figure A2.1) was designed to match the dimensions and inertial properties of the original load cell as close as possible to not compromise the biofidelity of the dummy. However, due to the use of extra sensors and associated mountings the weight of the new bracket was inevitably higher than the original load cell (273 g and 194 g respectively). Corresponding to an increase of 6.7% of the total head weight (1176 g). Technical drawings of the new sensor bracket are provided in the end of this appendix.

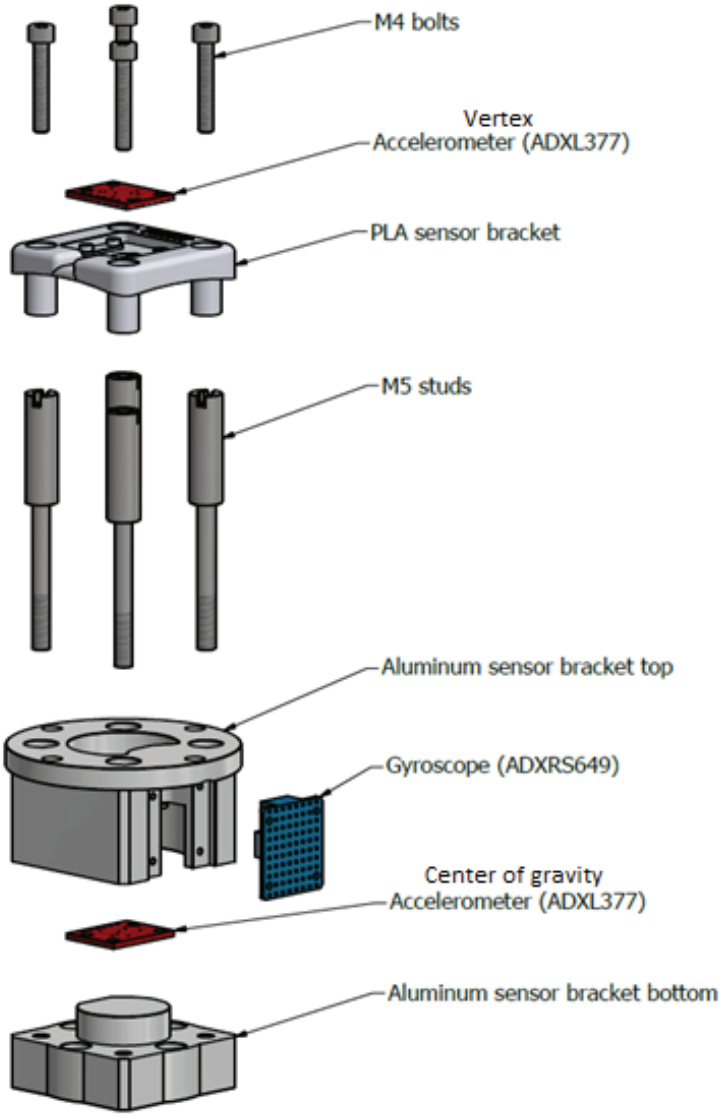


*Figure A2.1 - Parts of the new sensor bracket*

The location of the center of gravity of the new bracket in x- and y- direction was equal to the original load cell. However, the center of gravity of the new bracket was shifted 4 mm towards the vertex compared to the original load cell (Figure A3.2).

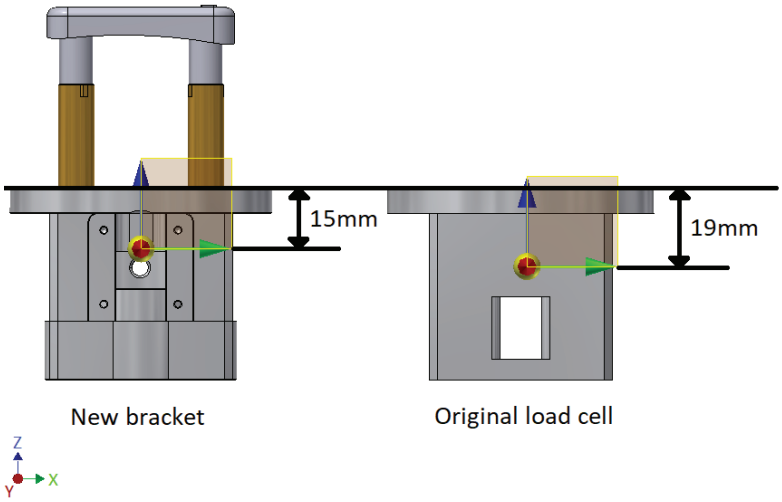


*Figure A2.2 - Center of gravity of the new and original sensor brackets*

## Modified Q0-dummy

A Q0 crash-test dummy (First Technology Safety Systems, Delft, The Netherlands) was used as an infant surrogate in the shake experiment. A vertex accelerometer, center of gravity accelerometer and gyroscope were mounted to the dummy's head as part of the previously described sensor bracket (Figure A2.1). Reflective markers for the motion capture system were mounted to the dummy's head (Figure A2.3). An additional accelerometer was placed in the dummy's torso (Figure A2.4). See Figure A2.5 for an overview of the dummy's head components.

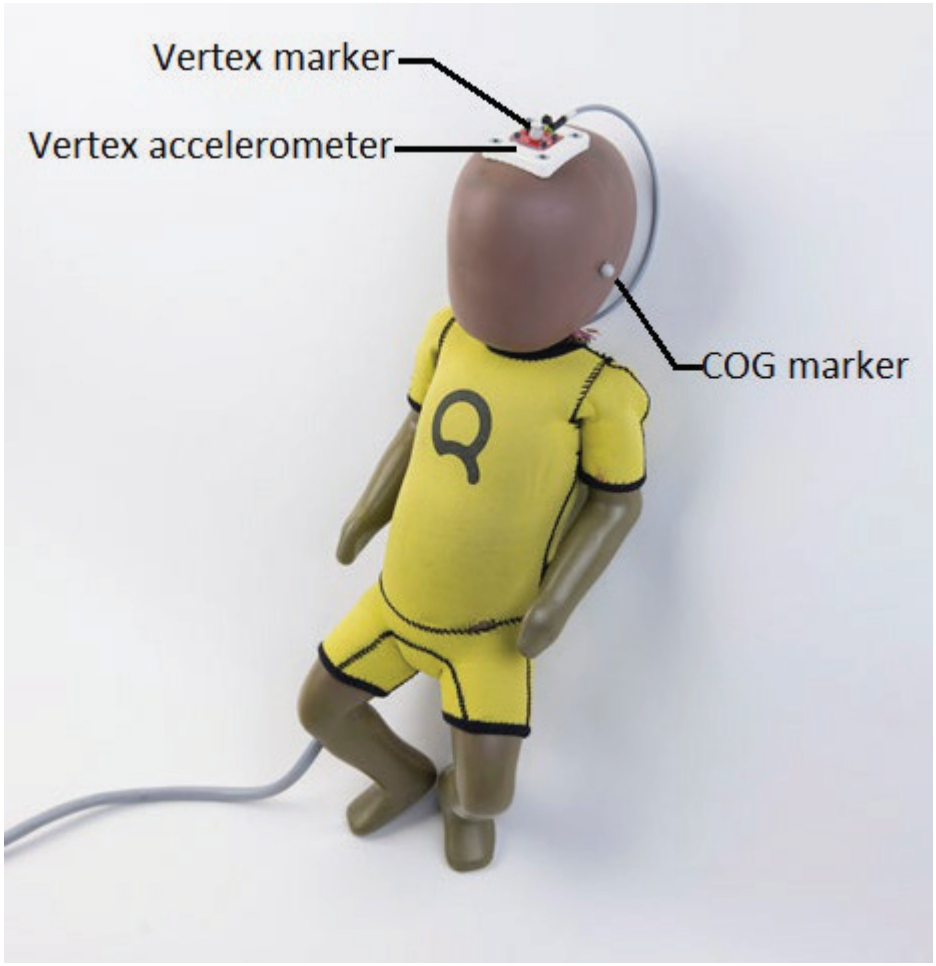


*Figure A2.3 - Full assembly of the modified Q0-dummy. COG: Center of gravity*

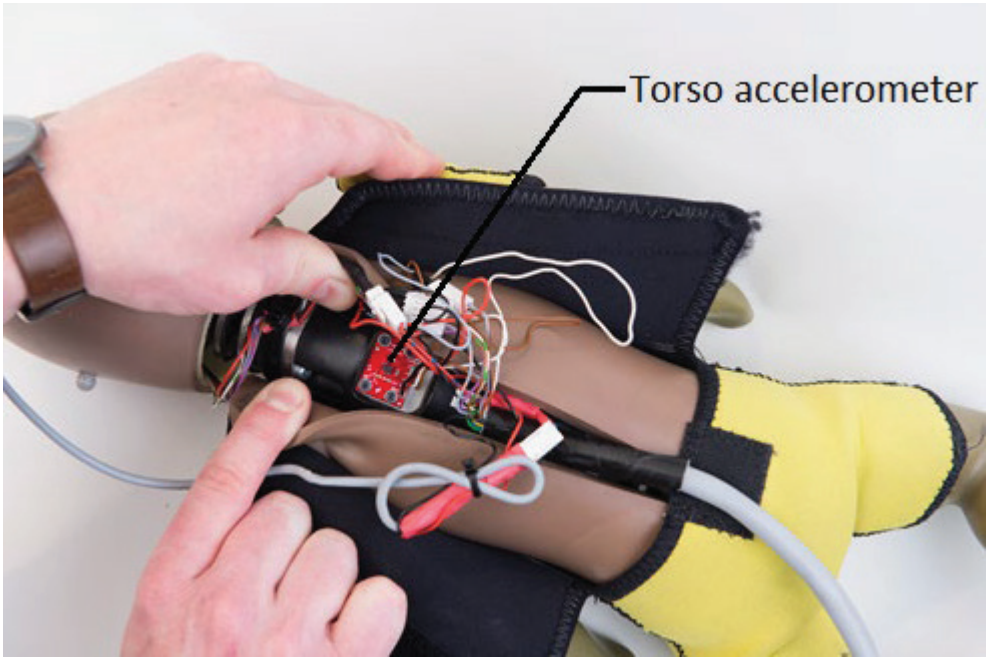


*Figure A2.4 - Position of the torso accelerometer*

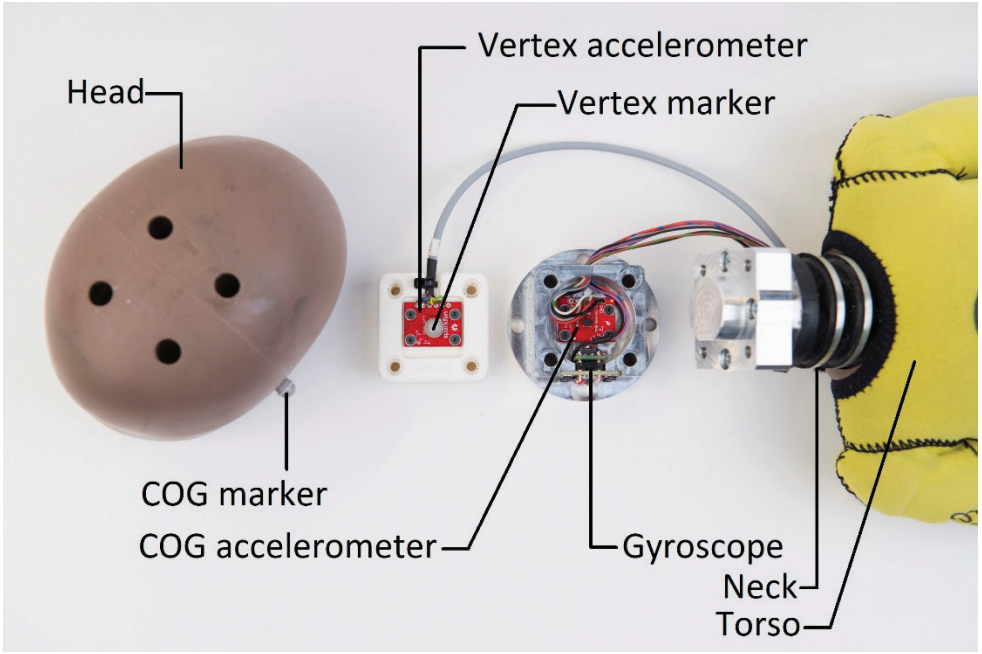


*Figure A2.5 – Components of the dummy's head*

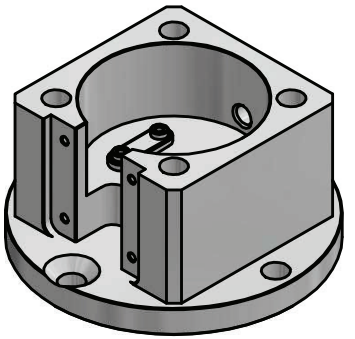

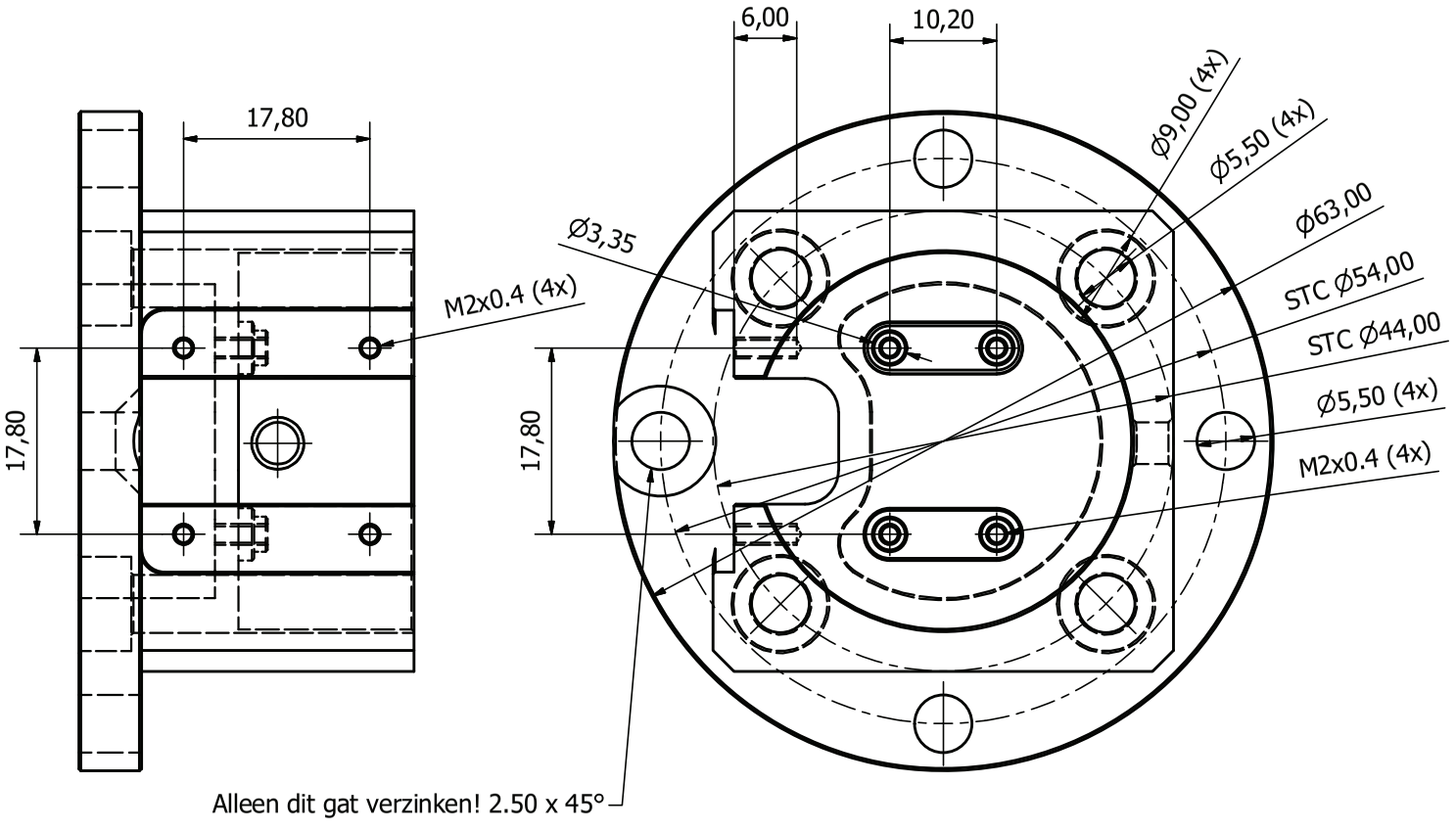


| Form- and placetolerance acc. NEN-ISO 1101 | General measure- and formtolerances acc. NEN-ISO 2768-mK | Registration measuretolerances acc. NEN-ISO 406 | Roughness acc. NEN 3634 | Weldsymbols acc. NEN-ISO 2553 |
|---|---|---|---|---|


**L.A.H. Schiks**
van Galenstraat 27 2518EN Den Haag
Tel. +31(0)6 16 30 27 22
E-Mail: l.a.h.schiks@student.tudelft.nl


Title:

Material: Aluminum 6061

Remarks:

Projection:

| Scale: 2:1 | Drawn by: L.A.H. Schiks | Date: 10-Mar-19 |
|---|---|---|
| Measurement: mm | Checked by: | Date: |

Drawing no.:

# Q0 BRACKET TOP

Weight: N/A

Area: N/A

Rev:

Size: **A3**

Sheet: 1 of 1

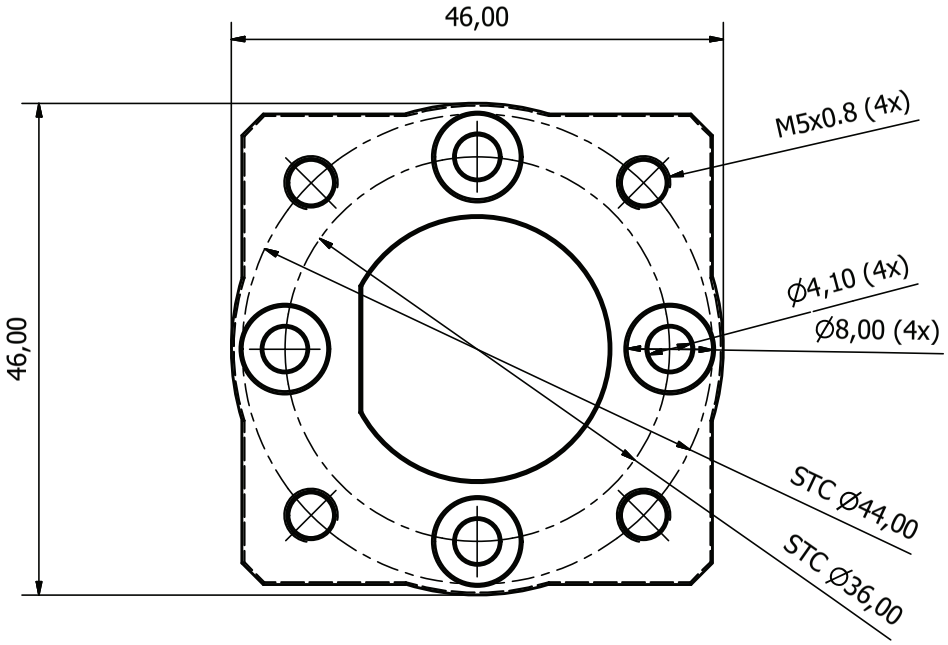


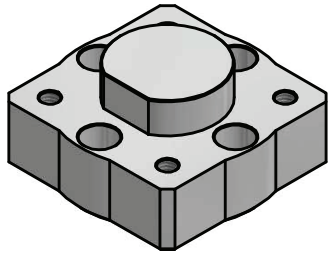

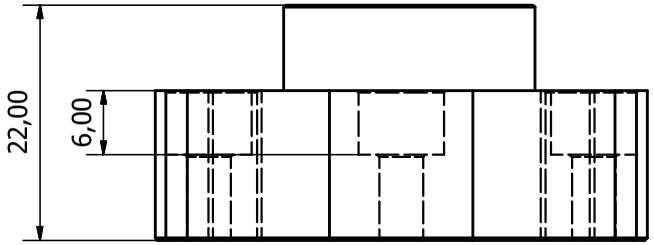


| Form- and placetolerance acc. NEN-ISO 1101 | General measure- and formtolerances acc. NEN-ISO 2768-mK | Registration measuretolerances acc. NEN-ISO 406 | Roughness acc. NEN 3634 | Weldsymbols acc. NEN-ISO 2553 |
|---|---|---|---|---|

**L.A.H. Schiks**
van Galenstraat 27 2518EN Den Haag
Tel. +31(0)6 16 30 27 22
E-Mail: l.a.h.schiks@student.tudelft.nl

Title:

Material: Aluminum 6061

| Scale: 2:1 | Drawn by: L.A.H. Schiks | Date: 10-Mar-19 |
|---|---|---|
| Measurement: mm | Checked by: | Date: |

Drawing no.:

# Q0 BRACKET BOTTOM

Weight: N/A

Area: N/A

Remarks:

Projection:

Rev:

Size: A3

Sheet: 1 - 1

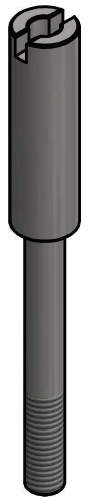

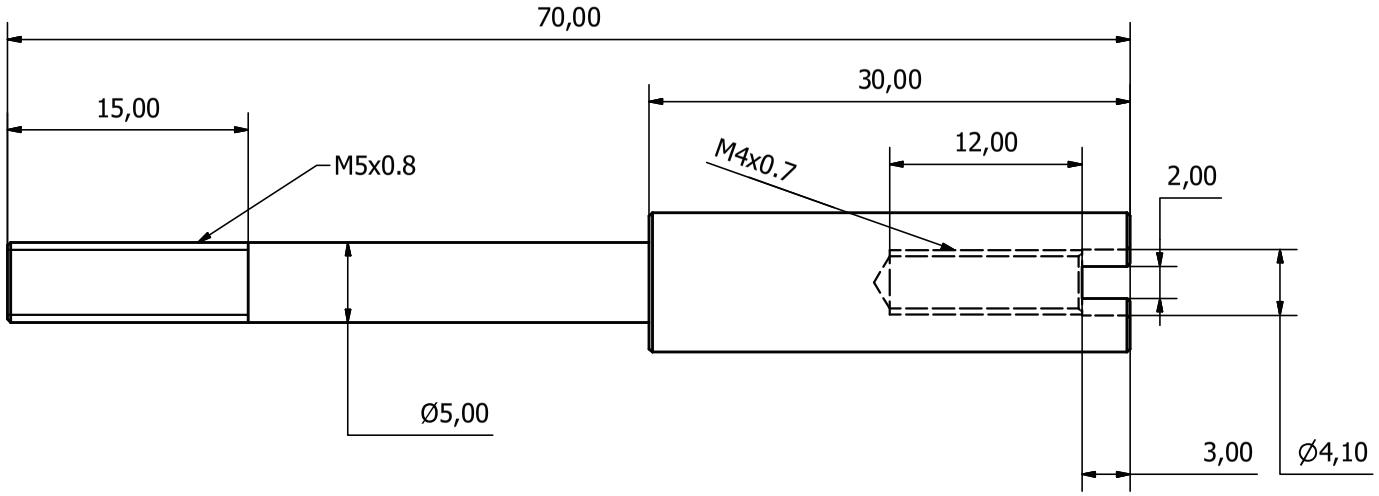


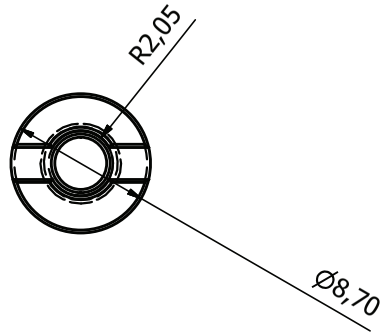


| Form- and placetolerance acc. NEN-ISO 1101 | General measure- and formtolerances acc. NEN-ISO 2768-mK | Registration measuretolerances acc. NEN-ISO 406 | Roughness acc. NEN 3634 | Weldsymbols acc. NEN-ISO 2553 |
|---|---|---|---|---|


**L.A.H. Schiks**
van Hasseltlaan 56 2625 HC Delft
Tel. +31(0)6 16 30 27 22
E-Mail: l.a.h.schiks@student.tudelft.nl


Title:

Material: Steel

Remarks:

Projection:

| Scale: 2:1 | Drawn by: L.A.H. Schiks | Date: 10-Mar-19 |
|---|---|---|
| Measurement: mm | Checked by: | Date: |

Drawing no.: **Stud**

Weight: 0.02 kg

Area: 1722.77 mm^2

Rev:

Size: **A3**

Sheet: 1 - 1

# Appendix IV

Camera settings – Motion capture system

Camera settings used for the Oqus 700 motion capture system (Qualysis, Göteborg, Sweden) are provided in Table A4.1.

*Table A4.1 – Camera settings for the motion capture system*

| *Camera no.* | *Exposure time (µs)* | *Marker threshold (-)* | *Focus distance (m)* | *Aperture (mm)* |
|---|---|---|---|---|
| 1 | 100 | 20 | 4 | 2.2 |
| 2 | 100 | 20 | 5 | 2.8 |
| 3 | 100 | 39 | 3.5 | 2.8 |
| 4 | 100 | 19 | 4 | 2 |
| 5 | 100 | 10 | 5 | 4 |
| 7 | 100 | 15 | 2 | 2.8 |
| 8 | 100 | 20 | 3 | 2.8 |
| 10 | 100 | 18 | 3 | 2.8 |
| 11 | 100 | 23 | 2 | 2.8 |
| 12 | 100 | 31 | 4.5 | 2.8 |
| 13 | 100 | 29 | 5 | 4 |
| 14 | 100 | 10 | 3 | 2.2 |

# Appendix V

Connection diagram – Data acquisition setup

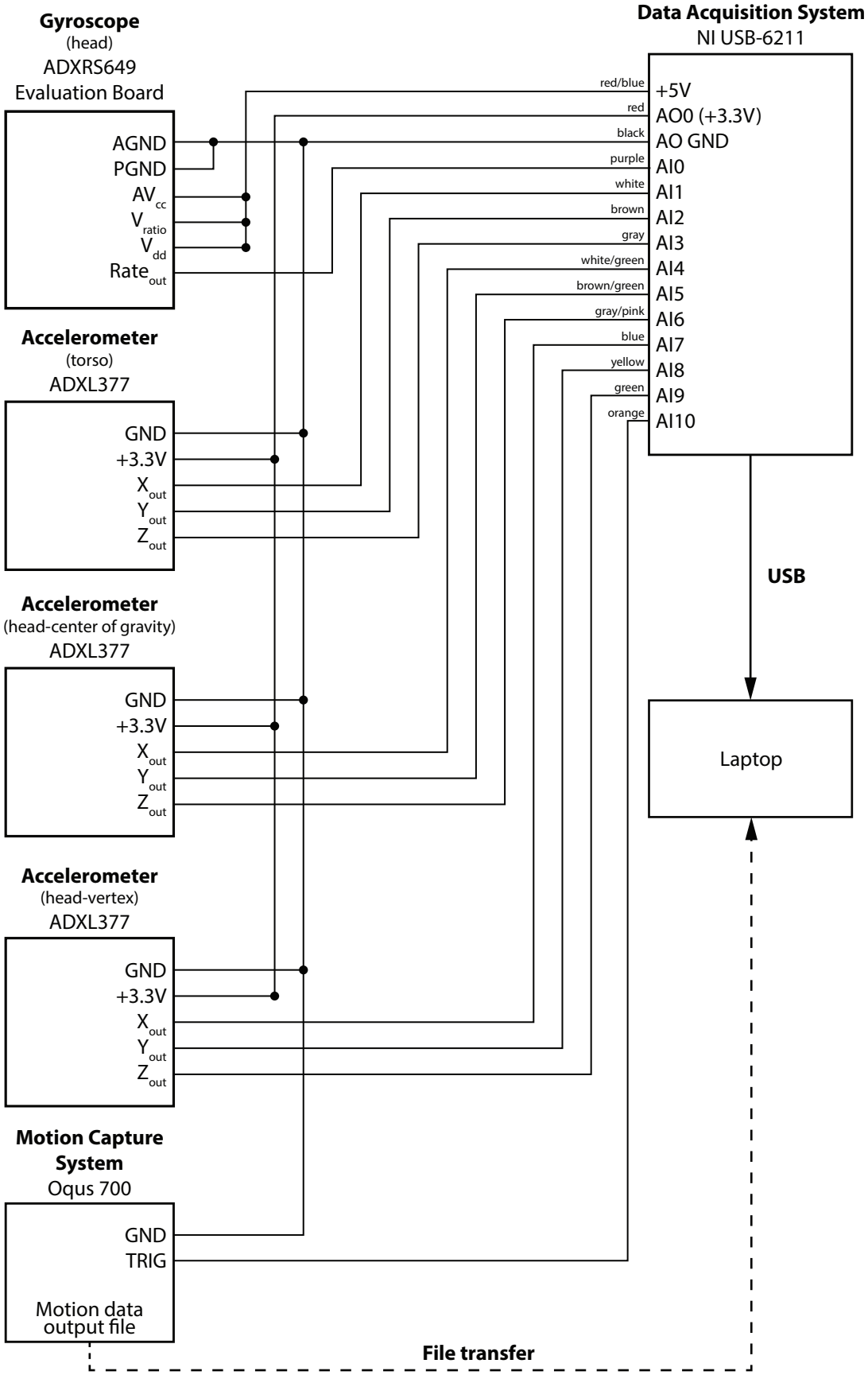

# Appendix VI

Data processing algorithm – Mathworks Matlab

# MATLAB DATA PROCESSING SCRIPT

```
% Author: L.A.H. Schiks
% Reviewed by:
% Version: 2019, July 18th
% Explore IHI-ST experimental data

close all
clear all
clc

% Some administration
acc_sensitivity     = 6.5;                      % mV/g --> datasheet ADXL377
gyr_sensitivity     = 0.1;                      % mV/g --> datasheet ADXRS649
g                   = 9.81;                     % Gravity acceleration
subjects            = [ 'SUBJ01'                % Participants
                        'SUBJ02'
                        'SUBJ03'
                        'SUBJ04'
                        'SUBJ05'
                        'SUBJ06'
                        'SUBJ07'
                        'SUBJ08'
                        'SUBJ09'
                        'SUBJ10'
                        'SUBJ11'
                        'SUBJ12'
                        'SUBJ13'
                        'SUBJ14'
                        'SUBJ15'
                        'SUBJ16'
                        'SUBJ17'
                        'SUBJ18'
                        'SUBJ19'
                        'SUBJ20'
                        'SUBJ21'
                        'SUBJ22'
                        'SUBJ23'
                        'SUBJ24'
                        'SUBJ25'
                        'SUBJ26'
                        'SUBJ27'
                        'SUBJ28'
                        'SUBJ29'];
%                         'SUBJ30'
%                         'SUBJ31'
%                         'SUBJ32'
%                         'SUBJ33'];
dirname             = 'testdata\';              % Directory containing experimental data and calibration files
gender = [0;0;1;0;0;0;0;0;1;1;0;0;0;1;1;0;0;0;0;0;0;0;1;1;1;0;0;0;0;0;0;0;0;0]; %male=0, female=1

% Import sensor data
for i=1:size(subjects,1)

    % Load calibration data
    cal_file_date       = xlsread([dirname subjects(i,:) '.csv'],1,'D1');
    cal_file_name       = strcat('calibration_',num2str(cal_file_date));
    fprintf('Initializing %s...\n', cal_file_name)
    [cal, labels]       = xlsread([dirname char(cal_file_name) '.csv']);
    labels              = labels(2,1:11);
    cal                 = cal(3:end,1:10);


    % Calculate calibration values and store them in a data structure using label names
    fprintf('Calculate calibration values...\n')
        for j = 1:length(labels)-1                                  % Minus 1 because not applicable to trigger signal
            c.(labels{j}) = mean(cal(100:end-1,j));
        end
    fprintf('Done\n')

```

```
69      % Load excel data
70      fprintf('Initializing %s sensor data...\n', subjects(i,:))
71
72      [data, labels]  = xlsread([dirname subjects(i,:) '.csv']);       % Read excel sensor
            data and labels
73      data            = data(3:end,1:11);
74      labels          = labels(2,1:11);
75
76      % Create data structure using label names
77          for j = 1:length(labels)
78              d.(subjects(i,:)).(labels{j}) = data(:,j);
79          end
80
81      % Calibrate raw data
82      fprintf('Apply calibration values...\n')
83
84          for j = 1:length(labels)-1                                    % Minus 1 because
                not applicable to trigger signal
85              if j==1
86                  d.(subjects(i,:)).(labels{j}) = deg2rad((d.(subjects(i,:)).(labels{j})-c
                        .(labels{j}))/(gyr_sensitivity/1000)); % [rad/s]
87              else
88                  d.(subjects(i,:)).(labels{j}) = (d.(subjects(i,:)).(labels{j})-c.(labels{
                        j}))/(acc_sensitivity/1000)*g;        % [m/s^2]
89              end
90          end
91      fprintf('Done\n')
92
93      % Switch sensor orientation to dummy orientation and apply gravity
94      w.(subjects(i,:)).gy    = - d.(subjects(i,:)).gy;
95      a.(subjects(i,:)).tx    = -(d.(subjects(i,:)).tz)+g;
96      a.(subjects(i,:)).ty    = - d.(subjects(i,:)).ty;
97      a.(subjects(i,:)).tz    = - d.(subjects(i,:)).tx;
98
99      a.(subjects(i,:)).cx    =   d.(subjects(i,:)).cy;
100     a.(subjects(i,:)).cy    =   d.(subjects(i,:)).cx;
101     a.(subjects(i,:)).cz    = -(d.(subjects(i,:)).cz)-g;
102
103     a.(subjects(i,:)).vx    = - d.(subjects(i,:)).vx;
104     a.(subjects(i,:)).vy    =   d.(subjects(i,:)).vy;
105     a.(subjects(i,:)).vz    = -(d.(subjects(i,:)).vz)-g;
106
107     % Synchronize sensor data with trigger signal of motion capture system
108     Fs      = xlsread([dirname subjects(i,:) '.csv'],1,'B1');           % Read sample
            frequency of the sensor data [Hz]
109     dt      = 1/Fs;
110     delay   = 0.02;                                                     % Delay between
            trigger and start of motion capture [s] (settings Qualisys)
111     sync    = find(d.(subjects(i,:)).trig<0.1,1) + delay/dt;            % Find
            synchronization point; the first point at which trigger signal (5V) is under 0.1
            volts
112
113         for j = 1:length(labels)-1
114             if j==1
115                 sen.(subjects(i,:)).w.(labels{j}) = w.(subjects(i,:)).gy(sync:end);
                                            % [rad/s]
116             else
117                 sen.(subjects(i,:)).a.(labels{j}) = a.(subjects(i,:)).(labels{j})(sync:
                        end);                % [m/s2]
118             end
119         end
120
121     % Create time vector
122     t.(subjects(i,:)) = linspace(0,length(sen.(subjects(i,:)).a.vx)/(Fs),length(sen.(
            subjects(i,:)).a.vx)); % [s]
123
124     % Some administration for filter
125     T   = dt*length(t.(subjects(i,:)));       % Obeservation time [s]
126     N   = T/dt;                               % Number of samples [-]
127     F   = (0:N-1)' / T;                       % Frequency vector [Hz]
128     Fc_gyr = 50;                              % Cutoff frequency for gyroscope data [Hz]
129     Fc_acc = 500;                             % Cutoff frequency for accelerometer data [Hz
```

```
        ]

    % Plot the power spectral density
    ACC = fft(sen.(subjects(i,:)).a.vx,N);  %Fourier transform
    Pyy = ACC.*conj(ACC)/N;

    % Apply low-pass filter on accelerometer and gyroscope signals
    [B,A]=butter(6,(Fc_gyr/(Fs/2)),'low');  %6th order butterworth filter results in
                                            %a 12th order filter. Filter order is
                                            %doubled because of the filtfilt (see
                                            %reference page for filtfilt)
    [D,C]=butter(6,(Fc_acc/(Fs/2)),'low');

        for j = 1:length(labels)-1
            if j==1
                sen.(subjects(i,:)).w.(labels{j})= filtfilt(B,A,sen.(subjects(i,:)).w.(
                    labels{j}));     % [rad/s]
            else
                sen.(subjects(i,:)).a.(labels{j}) = filtfilt(D,C,sen.(subjects(i,:)).a.(
                    labels{j}));    % [m/s2]
            end
        end
end
clear ACC GYR Pyy Pgg h1 h2 A B C D Fc_gyr Fc_acc Fc_gyr F N T a acc_sensitivity c cal
    cal_file_date cal_file_name d data delay g gyr_sensitivity sync w i j

% Import motion tracking data
for i=1:size(subjects,1)
    load ([dirname subjects(i,:)])                          % Load test data for each
        subject
end

m.SUBJ01.v = SUBJ01.Trajectories.Labeled.Data(1,:,:);     % Extract vertex data
m.SUBJ01.c = SUBJ01.Trajectories.Labeled.Data(2,:,:);     % Extract COG data
m.SUBJ02.v = SUBJ02.Trajectories.Labeled.Data(1,:,:);     % Extract vertex data
m.SUBJ02.c = SUBJ02.Trajectories.Labeled.Data(2,:,:);     % Extract COG data
m.SUBJ03.v = SUBJ03.Trajectories.Labeled.Data(1,:,:);     % Extract vertex data
m.SUBJ03.c = SUBJ03.Trajectories.Labeled.Data(2,:,:);     % Extract COG data
m.SUBJ04.v = SUBJ04.Trajectories.Labeled.Data(1,:,:);     % Extract vertex data
m.SUBJ04.c = SUBJ04.Trajectories.Labeled.Data(2,:,:);     % Extract COG data
m.SUBJ05.v = SUBJ05.Trajectories.Labeled.Data(1,:,:);     % Extract vertex data
m.SUBJ05.c = SUBJ05.Trajectories.Labeled.Data(2,:,:);     % Extract COG data
m.SUBJ06.v = SUBJ06.Trajectories.Labeled.Data(1,:,:);     % Extract vertex data
m.SUBJ06.c = SUBJ06.Trajectories.Labeled.Data(2,:,:);     % Extract COG data
m.SUBJ07.v = SUBJ07.Trajectories.Labeled.Data(1,:,:);     % Extract vertex data
m.SUBJ07.c = SUBJ07.Trajectories.Labeled.Data(2,:,:);     % Extract COG data
m.SUBJ08.v = SUBJ08.Trajectories.Labeled.Data(1,:,:);     % Extract vertex data
m.SUBJ08.c = SUBJ08.Trajectories.Labeled.Data(2,:,:);     % Extract COG data
m.SUBJ09.v = SUBJ09.Trajectories.Labeled.Data(1,:,:);     % Extract vertex data
m.SUBJ09.c = SUBJ09.Trajectories.Labeled.Data(2,:,:);     % Extract COG data
m.SUBJ10.v = SUBJ10.Trajectories.Labeled.Data(1,:,:);     % Extract vertex data
m.SUBJ10.c = SUBJ10.Trajectories.Labeled.Data(2,:,:);     % Extract COG data
m.SUBJ11.v = SUBJ11.Trajectories.Labeled.Data(1,:,:);     % Extract vertex data
m.SUBJ11.c = SUBJ11.Trajectories.Labeled.Data(2,:,:);     % Extract COG data
m.SUBJ12.v = SUBJ12.Trajectories.Labeled.Data(1,:,:);     % Extract vertex data
m.SUBJ12.c = SUBJ12.Trajectories.Labeled.Data(2,:,:);     % Extract COG data
m.SUBJ13.v = SUBJ13.Trajectories.Labeled.Data(1,:,:);     % Extract vertex data
m.SUBJ13.c = SUBJ13.Trajectories.Labeled.Data(2,:,:);     % Extract COG data
m.SUBJ14.v = SUBJ14.Trajectories.Labeled.Data(1,:,:);     % Extract vertex data
m.SUBJ14.c = SUBJ14.Trajectories.Labeled.Data(2,:,:);     % Extract COG data
m.SUBJ15.v = SUBJ15.Trajectories.Labeled.Data(1,:,:);     % Extract vertex data
m.SUBJ15.c = SUBJ15.Trajectories.Labeled.Data(2,:,:);     % Extract COG data
m.SUBJ16.v = SUBJ16.Trajectories.Labeled.Data(1,:,:);     % Extract vertex data
m.SUBJ16.c = SUBJ16.Trajectories.Labeled.Data(2,:,:);     % Extract COG data
m.SUBJ17.v = SUBJ17.Trajectories.Labeled.Data(1,:,:);     % Extract vertex data
m.SUBJ17.c = SUBJ17.Trajectories.Labeled.Data(2,:,:);     % Extract COG data
m.SUBJ18.v = SUBJ18.Trajectories.Labeled.Data(1,:,:);     % Extract vertex data
m.SUBJ18.c = SUBJ18.Trajectories.Labeled.Data(2,:,:);     % Extract COG data
m.SUBJ19.v = SUBJ19.Trajectories.Labeled.Data(1,:,:);     % Extract vertex data
m.SUBJ19.c = SUBJ19.Trajectories.Labeled.Data(2,:,:);     % Extract COG data
m.SUBJ20.v = SUBJ20.Trajectories.Labeled.Data(1,:,:);     % Extract vertex data
m.SUBJ20.c = SUBJ20.Trajectories.Labeled.Data(2,:,:);     % Extract COG data
```

```
m.SUBJ21.v = SUBJ21.Trajectories.Labeled.Data(1,:,:);    % Extract vertex data
m.SUBJ21.c = SUBJ21.Trajectories.Labeled.Data(2,:,:);    % Extract COG data
m.SUBJ22.v = SUBJ22.Trajectories.Labeled.Data(1,:,:);    % Extract vertex data
m.SUBJ22.c = SUBJ22.Trajectories.Labeled.Data(2,:,:);    % Extract COG data
m.SUBJ23.v = SUBJ23.Trajectories.Labeled.Data(1,:,:);    % Extract vertex data
m.SUBJ23.c = SUBJ23.Trajectories.Labeled.Data(2,:,:);    % Extract COG data
m.SUBJ24.v = SUBJ24.Trajectories.Labeled.Data(1,:,:);    % Extract vertex data
m.SUBJ24.c = SUBJ24.Trajectories.Labeled.Data(2,:,:);    % Extract COG data
m.SUBJ25.v = SUBJ25.Trajectories.Labeled.Data(1,:,:);    % Extract vertex data
m.SUBJ25.c = SUBJ25.Trajectories.Labeled.Data(2,:,:);    % Extract COG data
m.SUBJ26.v = SUBJ26.Trajectories.Labeled.Data(1,:,:);    % Extract vertex data
m.SUBJ26.c = SUBJ26.Trajectories.Labeled.Data(2,:,:);    % Extract COG data
m.SUBJ27.v = SUBJ27.Trajectories.Labeled.Data(1,:,:);    % Extract vertex data
m.SUBJ27.c = SUBJ27.Trajectories.Labeled.Data(2,:,:);    % Extract COG data
m.SUBJ28.v = SUBJ28.Trajectories.Labeled.Data(1,:,:);    % Extract vertex data
m.SUBJ28.c = SUBJ28.Trajectories.Labeled.Data(2,:,:);    % Extract COG data
m.SUBJ29.v = SUBJ29.Trajectories.Labeled.Data(1,:,:);    % Extract vertex data
m.SUBJ29.c = SUBJ29.Trajectories.Labeled.Data(2,:,:);    % Extract COG data
% m.SUBJ30.v = SUBJ30.Trajectories.Labeled.Data(1,:,:);    % Extract vertex data
% m.SUBJ30.c = SUBJ30.Trajectories.Labeled.Data(2,:,:);    % Extract COG data
% m.SUBJ31.v = SUBJ31.Trajectories.Labeled.Data(1,:,:);    % Extract vertex data
% m.SUBJ31.c = SUBJ31.Trajectories.Labeled.Data(2,:,:);    % Extract COG data
% m.SUBJ32.v = SUBJ32.Trajectories.Labeled.Data(1,:,:);    % Extract vertex data
% m.SUBJ32.c = SUBJ32.Trajectories.Labeled.Data(2,:,:);    % Extract COG data
% m.SUBJ33.v = SUBJ33.Trajectories.Labeled.Data(1,:,:);    % Extract vertex data
% m.SUBJ33.c = SUBJ33.Trajectories.Labeled.Data(2,:,:);    % Extract COG data

for i=1:size(subjects,1)
    % Store directions separately, reshape and convert from milimeters to meters
    mot.(subjects(i,:)).s.cx = m.(subjects(i,:)).c(1,1,:)/1000; % [m]
    mot.(subjects(i,:)).s.cx = reshape(mot.(subjects(i,:)).s.cx,[1,length(mot.(subjects(i
        ,:)).s.cx)]);
    mot.(subjects(i,:)).s.cy = m.(subjects(i,:)).c(1,2,:)/1000; % [m]
    mot.(subjects(i,:)).s.cy = reshape(mot.(subjects(i,:)).s.cy,[1,length(mot.(subjects(i
        ,:)).s.cy)]);
    mot.(subjects(i,:)).s.cz = m.(subjects(i,:)).c(1,3,:)/1000; % [m]
    mot.(subjects(i,:)).s.cz = reshape(mot.(subjects(i,:)).s.cz,[1,length(mot.(subjects(i
        ,:)).s.cz)]);

    mot.(subjects(i,:)).s.vx = m.(subjects(i,:)).v(1,1,:)/1000; % [m]
    mot.(subjects(i,:)).s.vx = reshape(mot.(subjects(i,:)).s.vx,[1,length(mot.(subjects(i
        ,:)).s.vx)]);
    mot.(subjects(i,:)).s.vy = m.(subjects(i,:)).v(1,2,:)/1000; % [m]
    mot.(subjects(i,:)).s.vy = reshape(mot.(subjects(i,:)).s.vy,[1,length(mot.(subjects(i
        ,:)).s.vy)]);
    mot.(subjects(i,:)).s.vz = m.(subjects(i,:)).v(1,3,:)/1000; % [m]
    mot.(subjects(i,:)).s.vz = reshape(mot.(subjects(i,:)).s.vz,[1,length(mot.(subjects(i
        ,:)).s.vz)]);

    % Resample signals
    Fs_motion = 1000;
    mot.(subjects(i,:)).s.cx = interp(mot.(subjects(i,:)).s.cx,Fs/Fs_motion);
    mot.(subjects(i,:)).s.cy = interp(mot.(subjects(i,:)).s.cy,Fs/Fs_motion);
    mot.(subjects(i,:)).s.cz = interp(mot.(subjects(i,:)).s.cz,Fs/Fs_motion);
    mot.(subjects(i,:)).s.vx = interp(mot.(subjects(i,:)).s.vx,Fs/Fs_motion);
    mot.(subjects(i,:)).s.vy = interp(mot.(subjects(i,:)).s.vy,Fs/Fs_motion);
    mot.(subjects(i,:)).s.vz = interp(mot.(subjects(i,:)).s.vz,Fs/Fs_motion);
    time_motion = linspace(0,length(mot.(subjects(i,:)).s.cx)/(Fs),length(mot.(subjects(i
        ,:)).s.cx)); % [s]

    % Some administration for filter
    Fc_mot = 10;

    % Apply low-pass filter
    [B,A]=butter(6,(Fc_mot/(Fs_motion/2)),'low');   %6th order butterworth filter results
         in
                                                    %a 12th order filter!!!! Filter order
                                                        is
                                                    %doubled because of the filtfilt (see
                                                    %reference page for filtfilt)

    mot.(subjects(i,:)).s.cx = filtfilt(B,A,mot.(subjects(i,:)).s.cx);
```

```
260     mot.(subjects(i,:)).s.cy = filtfilt(B,A,mot.(subjects(i,:)).s.cy);
261     mot.(subjects(i,:)).s.cz = filtfilt(B,A,mot.(subjects(i,:)).s.cz);
262     mot.(subjects(i,:)).s.vx = filtfilt(B,A,mot.(subjects(i,:)).s.vx);
263     mot.(subjects(i,:)).s.vy = filtfilt(B,A,mot.(subjects(i,:)).s.vy);
264     mot.(subjects(i,:)).s.vz = filtfilt(B,A,mot.(subjects(i,:)).s.vz);
265
266     % Trim sensor data to the length of the motion data
267     sen.(subjects(i,:)).a.tx = sen.(subjects(i,:)).a.tx(1:length(mot.(subjects(i,:)).s.cx
            ));
268     sen.(subjects(i,:)).a.ty = sen.(subjects(i,:)).a.ty(1:length(mot.(subjects(i,:)).s.cx
            ));
269     sen.(subjects(i,:)).a.tz = sen.(subjects(i,:)).a.tz(1:length(mot.(subjects(i,:)).s.cx
            ));
270     sen.(subjects(i,:)).a.cx = sen.(subjects(i,:)).a.cx(1:length(mot.(subjects(i,:)).s.cx
            ));
271     sen.(subjects(i,:)).a.cy = sen.(subjects(i,:)).a.cy(1:length(mot.(subjects(i,:)).s.cx
            ));
272     sen.(subjects(i,:)).a.cz = sen.(subjects(i,:)).a.cz(1:length(mot.(subjects(i,:)).s.cx
            ));
273     sen.(subjects(i,:)).a.vx = sen.(subjects(i,:)).a.vx(1:length(mot.(subjects(i,:)).s.cx
            ));
274     sen.(subjects(i,:)).a.vy = sen.(subjects(i,:)).a.vy(1:length(mot.(subjects(i,:)).s.cx
            ));
275     sen.(subjects(i,:)).a.vz = sen.(subjects(i,:)).a.vz(1:length(mot.(subjects(i,:)).s.cx
            ));
276     t.(subjects(i,:)) = t.(subjects(i,:))(1:length(mot.(subjects(i,:)).s.cx));
277
278     for k=1:length(mot.(subjects(i,:)).s.vx) % Calculate angle between dummy and z-axis (
            clockwise = positive w.r.t. inertial ref frame. Range + and - 180.
279
280         if      (mot.(subjects(i,:)).s.vx(k)-mot.(subjects(i,:)).s.cx(k))>=0 & (mot.(
                subjects(i,:)).s.vz(k)-mot.(subjects(i,:)).s.cz(k))>0 %first quadrant
281             theta.(subjects(i,:))(k) = atan((mot.(subjects(i,:)).s.vx(k)-mot.(subjects(i
                    ,:)).s.cx(k))/(mot.(subjects(i,:)).s.vz(k)-mot.(subjects(i,:)).s.cz(k)));
282         elseif  (mot.(subjects(i,:)).s.vx(k)-mot.(subjects(i,:)).s.cx(k))>0 & (mot.(
                subjects(i,:)).s.vz(k)-mot.(subjects(i,:)).s.cz(k))<=0 %second quadrant
283             theta.(subjects(i,:))(k) = -atan((mot.(subjects(i,:)).s.vz(k)-mot.(subjects(i
                    ,:)).s.cz(k))/(mot.(subjects(i,:)).s.vx(k)-mot.(subjects(i,:)).s.cx(k)))
                    +(pi()/2);
284         elseif  (mot.(subjects(i,:)).s.vx(k)-mot.(subjects(i,:)).s.cx(k))<=0 & (mot.(
                subjects(i,:)).s.vz(k)-mot.(subjects(i,:)).s.cz(k))<0 %third quadrant
285             theta.(subjects(i,:))(k) = -atan((mot.(subjects(i,:)).s.vz(k)-mot.(subjects(i
                    ,:)).s.cz(k))/(mot.(subjects(i,:)).s.vx(k)-mot.(subjects(i,:)).s.cx(k)))
                    -(pi()/2);
286         elseif  (mot.(subjects(i,:)).s.vx(k)-mot.(subjects(i,:)).s.cx(k))<0 & (mot.(
                subjects(i,:)).s.vz(k)-mot.(subjects(i,:)).s.cz(k))>=0 %fourth quadrant
287             theta.(subjects(i,:))(k) = atan((mot.(subjects(i,:)).s.vx(k)-mot.(subjects(i
                    ,:)).s.cx(k))/(mot.(subjects(i,:)).s.vz(k)-mot.(subjects(i,:)).s.cz(k)));
288         else
289             fprintf('Error in calculation of theta\n')
290             pause;
291         end
292     end
293
294     % Calculate angular data
295     theta.(subjects(i,:))       = -theta.(subjects(i,:)); %Theta in moving B frame is in
            oposite direction of inertial N frame (from which we derive theta)
296     calc.(subjects(i,:)).w.gy   = gradient(theta.(subjects(i,:)),dt).';
297     calc.(subjects(i,:)).alpha  = gradient(calc.(subjects(i,:)).w.gy,dt).';
298 end
299
300 clear A B N F Fc T dirname dt_motion Fs_motion SUBJ01 SUBJ02 SUBJ03 SUBJ04 SUBJ05 SUBJ06
        SUBJ07 SUBJ08 SUBJ09 SUBJ10 SUBJ11 SUBJ12 SUBJ13 SUBJ14 SUBJ15 m SUBJ16 SUBJ17 SUBJ18
         SUBJ19 SUBJ20 SUBJ21 SUBJ22 SUBJ24 SUBJ25 SUBJ26 SUBJ27 SUBJ28 SUBJ29
301
302 % Data analyse
303 for i=1:size(subjects,1)
304
305     % Find maximum vertex acceleration in x-direction
306     maximum=[max(sen.(subjects(i,:)).a.vx) min(sen.(subjects(i,:)).a.vx)];
307     if abs(maximum(2))>=maximum(1)
308         maximum=maximum(2);
```

```
309     else
310         maximum=maximum(1);
311     end
312     loc=find(sen.(subjects(i,:)).a.vx==maximum);
313 
314     % Calculate velocities
315     mot.(subjects(i,:)).v.cx = gradient(mot.(subjects(i,:)).s.cx,dt);
                                        % [m/s]
316     mot.(subjects(i,:)).v.cz = gradient(mot.(subjects(i,:)).s.cz,dt);
                                        % [m/s]
317     mot.(subjects(i,:)).v.c_abs = sqrt(mot.(subjects(i,:)).v.cx.^2+mot.(subjects(i,:)).v.
        cz.^2);    % [m/s]
318     v_cog_abs_max(i) = max(mot.(subjects(i,:)).v.c_abs);
319 
320     mot.(subjects(i,:)).v.vx = gradient(mot.(subjects(i,:)).s.vx,dt);
                                        % [m/s]
321     mot.(subjects(i,:)).v.vz = gradient(mot.(subjects(i,:)).s.vz,dt);
                                        % [m/s]
322     mot.(subjects(i,:)).v.v_abs = sqrt(mot.(subjects(i,:)).v.cx.^2+mot.(subjects(i,:)).v.
        cz.^2);    % [m/s]
323 
324     mot.(subjects(i,:)).a.vx = gradient(mot.(subjects(i,:)).v.vx,dt);
                                        % [m/s]
325     mot.(subjects(i,:)).a.vz = gradient(mot.(subjects(i,:)).v.vz,dt);
                                        % [m/s]
326 
327     %Calculate absolute accelerations from motion data
328     mot.(subjects(i,:)).a.v_abs = sqrt(mot.(subjects(i,:)).a.vx.^2+mot.(subjects(i,:)).a.
        vz.^2);
329     % and from sensor data
330     sen.(subjects(i,:)).a.t_abs = sqrt(sen.(subjects(i,:)).a.tx.^2+sen.(subjects(i,:)).a.
        tz.^2);    % [m/s]
331     sen.(subjects(i,:)).a.c_abs = sqrt(sen.(subjects(i,:)).a.cx.^2+sen.(subjects(i,:)).a.
        cz.^2);    % [m/s]
332     sen.(subjects(i,:)).a.v_abs = sqrt(sen.(subjects(i,:)).a.vx.^2+sen.(subjects(i,:)).a.
        vz.^2);    % [m/s]
333 
334     %Calculate maximum value for each participant
335     % Calculate a_t_abs max
336     if abs(min(sen.(subjects(i,:)).a.t_abs))>max(sen.(subjects(i,:)).a.t_abs)
337         acc_t_max(i) = min(sen.(subjects(i,:)).a.t_abs);
338     else
339         acc_t_max(i) = max(sen.(subjects(i,:)).a.t_abs);
340     end
341 
342     % Calculate a_c_abs max
343     if abs(min(sen.(subjects(i,:)).a.c_abs))>max(sen.(subjects(i,:)).a.c_abs)
344         acc_c_max(i) = min(sen.(subjects(i,:)).a.c_abs);
345     else
346         acc_c_max(i) = max(sen.(subjects(i,:)).a.c_abs);
347     end
348 
349     if abs(min(sen.(subjects(i,:)).a.cx))>max(sen.(subjects(i,:)).a.cx)
350         acc_cx_max(i) = min(sen.(subjects(i,:)).a.cx);
351     else
352         acc_cx_max(i) = max(sen.(subjects(i,:)).a.cx);
353     end
354 
355     if abs(min(sen.(subjects(i,:)).a.cz))>max(sen.(subjects(i,:)).a.cz)
356         acc_cz_max(i) = min(sen.(subjects(i,:)).a.cz);
357     else
358         acc_cz_max(i) = max(sen.(subjects(i,:)).a.cz);
359     end
360 
361     % Calculate a_v max
362     if abs(min(sen.(subjects(i,:)).a.v_abs))>max(sen.(subjects(i,:)).a.v_abs)
363         acc_v_max(i) = min(sen.(subjects(i,:)).a.v_abs);
364     else
365         acc_v_max(i) = max(sen.(subjects(i,:)).a.v_abs);
366     end
367 
368     if abs(min(sen.(subjects(i,:)).a.vx))>max(sen.(subjects(i,:)).a.vx)
```

```
369         acc_vx_max(i) = min(sen.(subjects(i,:)).a.vx);
370     else
371         acc_vx_max(i) = max(sen.(subjects(i,:)).a.vx);
372     end
373 
374     if abs(min(sen.(subjects(i,:)).a.vz))>max(sen.(subjects(i,:)).a.vz)
375         acc_vz_max(i) = min(sen.(subjects(i,:)).a.vz);
376     else
377         acc_vz_max(i) = max(sen.(subjects(i,:)).a.vz);
378     end
379 
380     % Calculate omega max
381     if abs(min(calc.(subjects(i,:)).w.gy))>max(calc.(subjects(i,:)).w.gy)
382         omega_max(i) = min(calc.(subjects(i,:)).w.gy);
383     else
384         omega_max(i) = max(calc.(subjects(i,:)).w.gy);
385     end
386 
387     % Calculate alpha max
388     if abs(min(calc.(subjects(i,:)).alpha))>max(calc.(subjects(i,:)).alpha)
389         alpha_max(i) = min(calc.(subjects(i,:)).alpha);
390     else
391         alpha_max(i) = max(calc.(subjects(i,:)).alpha);
392     end
393 
394     % Calculate vertex tangential velocity max
395     if abs(min(mot.(subjects(i,:)).v.vx))>max(mot.(subjects(i,:)).v.vx)
396         v_ver_max(i) = min(mot.(subjects(i,:)).v.vx);
397     else
398         v_ver_max(i) = max(mot.(subjects(i,:)).v.vx);
399     end
400 
401     % Calculate average shake frequency during the trial
402     [pks,locs]    = findpeaks(sen.(subjects(i,:)).a.vx,'MinPeakHeight',0.4*max(sen.(
        subjects(i,:)).a.vx),'MinPeakDistance',100);   % Find other peaks 400
403     for n=1:length(locs)-1
404         intervals(n)=(locs(n+1)-locs(n))*dt;                              % Calculate the
            perdiod time of 1 shake cycle
405     end
406     freq_shake(i,:)=1/mean(intervals);                                    % Calculate
        average shaking frequency [Hz]
407     clear intervals pks locs
408 end
409 
410     % Calculate maximum value amongst all participants
411     % Calculate a_t_abs max
412     if abs(min(acc_t_max))>max(acc_t_max)
413         acc_t_max_max = min(acc_t_max);
414     else
415         acc_t_max_max = max(acc_t_max);
416     end
417 
418     % Calculate a_c_abs max
419     if abs(min(acc_c_max))>max(acc_c_max)
420         acc_c_max_max = min(acc_c_max);
421     else
422         acc_c_max_max = max(acc_c_max);
423     end
424 
425     if abs(min(acc_cx_max))>max(acc_cx_max)
426         acc_cx_max_max = min(acc_cx_max);
427     else
428         acc_cx_max_max = max(acc_cx_max);
429     end
430 
431     if abs(min(acc_cz_max))>max(acc_cz_max)
432         acc_cz_max_max = min(acc_cz_max);
433     else
434         acc_cz_max_max = max(acc_cz_max);
435     end
436 
437     % Calculate a_v_abs max
```

```
438      if abs(min(acc_t_max))>max(acc_t_max)
439          acc_v_max_max = min(acc_v_max);
440      else
441          acc_v_max_max = max(acc_v_max);
442      end
443
444      if abs(min(acc_vx_max))>max(acc_vx_max)
445          acc_vx_max_max = min(acc_vx_max);
446      else
447          acc_vx_max_max = max(acc_vx_max);
448      end
449
450      if abs(min(acc_vz_max))>max(acc_vz_max)
451          acc_vz_max_max = min(acc_vz_max);
452      else
453          acc_vz_max_max = max(acc_vz_max);
454      end
455
456      % Calculate omega max
457      if abs(min(omega_max))>max(omega_max)
458          omega_max_max = min(omega_max);
459      else
460          omega_max_max = max(omega_max);
461      end
462
463      % Calculate alpha max
464      if abs(min(alpha_max))>max(alpha_max)
465          alpha_max_max = min(alpha_max);
466      else
467          alpha_max_max = max(alpha_max);
468      end
469
470      % Calculate tang ver vel max
471      if abs(min(v_ver_max))>max(v_ver_max)
472          v_ver_max_max = min(v_ver_max);
473      else
474          v_ver_max_max = max(v_ver_max);
475      end
476
477  %% Rotation axis calculation
478  clear all
479  close all
480  clc
481  load processed_data              % Load calibrated and synchronized data from script above
482
483  g = 9.81;                        %Gravitational acceleration
484  for i = 1:size(subjects,1);
485
486  % Trim trajectory to 1 cycle containing maximum vertex acceleration
487  [a_xv_max_pos, i_max_pos]    = max(sen.(subjects(i,:)).a.vx);
                                                              % Maximum positive a_xv value
488  [a_xv_max_neg, i_max_neg]    = min(sen.(subjects(i,:)).a.vx);
                                                              % Maximum negative a_xv value
489  [pospks,poslocs]     = findpeaks(sen.(subjects(i,:)).a.vx,'MinPeakHeight',0.3*a_xv_max_pos
         ,'MinPeakDistance',500);    % Find other peaks
490  [negpks,neglocs]     = findpeaks(-sen.(subjects(i,:)).a.vx,'MinPeakHeight',0.3*-
         a_xv_max_neg,'MinPeakDistance',500); % Find other peaks
491
492      if abs(a_xv_max_neg)>=a_xv_max_pos
493          loc(1)  = i_max_neg;                                % Index of first minimum
494          xv_max3 = negpks(find(-negpks==a_xv_max_neg)+1);    % Find NEXT minimum
495          loc(2)  = neglocs(find(negpks==xv_max3));           % Find index of NEXT minimum
                 (used later on)
496      else
497          loc(1)  = i_max_pos;                                % Index of first maximum
498          xv_max3 = pospks(find(pospks==a_xv_max_pos)+1);     % Find NEXT maximum
499          loc(2)  = poslocs(find(pospks==xv_max3));           % Find index of NEXT maximum
                 (used later on)
500      end
501
502  clear a_xv_max_neg a_xv_max_pos i_max_neg i_max_pos pospks poslocs negpks neglocs xv_max3
503
```

```
504 extra=100; % to be sure that the round ends are included
505 mot.(subjects(i,:)).s.cx_trim = mot.(subjects(i,:)).s.cx(loc(1)-extra:loc(2)+extra);
506 mot.(subjects(i,:)).s.cz_trim = mot.(subjects(i,:)).s.cz(loc(1)-extra:loc(2)+extra);
507 mot.(subjects(i,:)).s.vx_trim = mot.(subjects(i,:)).s.vx(loc(1)-extra:loc(2)+extra);
508 mot.(subjects(i,:)).s.vz_trim = mot.(subjects(i,:)).s.vz(loc(1)-extra:loc(2)+extra);
509 mot.(subjects(i,:)).s.vy_trim = mot.(subjects(i,:)).s.vy(loc(1)-extra:loc(2)+extra);
510 t_trim.(subjects(i,:)) = t.(subjects(i,:))(loc(1)-extra:loc(2)+extra);
511 sen.(subjects(i,:)).a.vx_trim = sen.(subjects(i,:)).a.vx(loc(1)-extra:loc(2)+extra);
512 sen.(subjects(i,:)).a.vz_trim = sen.(subjects(i,:)).a.vz(loc(1)-extra:loc(2)+extra);
513 sen.(subjects(i,:)).a.vy_trim = sen.(subjects(i,:)).a.vy(loc(1)-extra:loc(2)+extra);
514 sen.(subjects(i,:)).a.cx_trim = sen.(subjects(i,:)).a.cx(loc(1)-extra:loc(2)+extra);
515 sen.(subjects(i,:)).a.cz_trim = sen.(subjects(i,:)).a.cz(loc(1)-extra:loc(2)+extra);
516 sen.(subjects(i,:)).a.tx_trim = sen.(subjects(i,:)).a.tx(loc(1)-extra:loc(2)+extra);
517 sen.(subjects(i,:)).a.tz_trim = sen.(subjects(i,:)).a.tz(loc(1)-extra:loc(2)+extra);
518 sen.(subjects(i,:)).a.c_abs_trim = sen.(subjects(i,:)).a.c_abs(loc(1)-extra:loc(2)+extra)
    ;
519 sen.(subjects(i,:)).a.v_abs_trim = sen.(subjects(i,:)).a.v_abs(loc(1)-extra:loc(2)+extra)
    ;
520 theta_trim.(subjects(i,:)) = theta.(subjects(i,:))(loc(1)-extra:loc(2)+extra);
521 calc.(subjects(i,:)).w.gy_trim = calc.(subjects(i,:)).w.gy(loc(1)-extra:loc(2)+extra);
522 calc.(subjects(i,:)).alpha_trim = calc.(subjects(i,:)).alpha(loc(1)-extra:loc(2)+extra)
    .';
523 clear loc
524
525     % Calculate slop of tangential and perpendicular lines (for every point in the shake
        cycle)
526     for k=1:length(mot.(subjects(i,:)).s.cx_trim)-1
527         slope_cog_tang(k) = (mot.(subjects(i,:)).s.cz_trim(k+1) - mot.(subjects(i,:)).s.
            cz_trim(k)) / (mot.(subjects(i,:)).s.cx_trim(k+1) - mot.(subjects(i,:)).s.
            cx_trim(k)); %calculate slope COG tangentline
528         slope_ver_tang(k) = (mot.(subjects(i,:)).s.vz_trim(k+1) - mot.(subjects(i,:)).s.
            vz_trim(k)) / (mot.(subjects(i,:)).s.vx_trim(k+1) - mot.(subjects(i,:)).s.
            vx_trim(k)); %calculate slope vertex tangentline
529         slope_cog_perp(k) = -1/slope_cog_tang(k); %calculate slope COG perpline
530         slope_ver_perp(k) = -1/slope_ver_tang(k); %calculate slope vertex perpline
531     end
532     fprintf('Calculating rotation centers... \n', subjects(i,:))
533
534     % Calculate intersection point of perpendicular lines for every point
535     % in the shake cycle
536     threshold=1000000; %length of perpendicular lines, must be increased if no
        intersection point could be found
537     for k=1:length(slope_cog_tang)
538
539         x_axis_cog_tang = linspace(mot.(subjects(i,:)).s.cx_trim(k)-threshold,mot.(
            subjects(i,:)).s.cx_trim(k)+threshold);      %calculate an X-axis for COG
            tangentline
540         x_axis_ver_tang = linspace(mot.(subjects(i,:)).s.vx_trim(k)-threshold,mot.(
            subjects(i,:)).s.vx_trim(k)+threshold);      %calculate an X-axis for vertex
            tangentline
541
542         b_cog_tang=(mot.(subjects(i,:)).s.cz_trim(k)-(slope_cog_tang(k)*mot.(subjects(i
            ,:)).s.cx_trim(k)));  %calculate b for COG tangentline (for the line equation
            : y=slope*x+b)
543         b_ver_tang=(mot.(subjects(i,:)).s.vz_trim(k)-(slope_ver_tang(k)*mot.(subjects(i
            ,:)).s.vx_trim(k)));  %calculate b for vertex tangentline
544         b_cog_perp=(mot.(subjects(i,:)).s.cz_trim(k)-(slope_cog_perp(k)*mot.(subjects(i
            ,:)).s.cx_trim(k)));  %calculate b for COG perpline
545         b_ver_perp=(mot.(subjects(i,:)).s.vz_trim(k)-(slope_ver_perp(k)*mot.(subjects(i
            ,:)).s.vx_trim(k)));  %calculate b for vertex perpline
546
547         for p=1:length(x_axis_cog_tang)
548             z_coordinate_cog_tang(p) = slope_cog_tang(k)*x_axis_cog_tang(p)+b_cog_tang;
549             z_coordinate_cog_perp(p) = slope_cog_perp(k)*x_axis_cog_tang(p)+b_cog_perp;
550         end
551
552         for p=1:length(x_axis_ver_tang)
553             z_coordinate_ver_tang(p) = slope_ver_tang(k)*x_axis_ver_tang(p)+b_ver_tang;
554             z_coordinate_ver_perp(p) = slope_ver_perp(k)*x_axis_ver_tang(p)+b_ver_perp;
555         end
556
557         L1=[x_axis_cog_tang ;z_coordinate_cog_perp];    % Perpendicular line COG
```

```
558         L2=[x_axis_ver_tang ;z_coordinate_ver_perp];    % Perpendicular line vertex
559         P=InterX(L1,L2);                                % Intersection point between two
                perp lines = instantaneous center of rotation in world coordinates
560
561             if isempty(P)==1 %check whether an intersection point was found. If P is
                    empty, no intersection was found and NaN is assigned.
562                 fprintf('Error: somewhere at the interval no intersection point was found
                        . Increase threshold!\n')
563                 fprintf('Current threshold: ')
564                 disp(threshold)
565                 pause;
566             else
567                 IAOR.(subjects(i,:)).x(k)   = P(1);
568                 IAOR.(subjects(i,:)).z(k)   = P(2);
569                 ROC.(subjects(i,:))(k)      = sqrt((mot.(subjects(i,:)).s.cx_trim(k)-IAOR
                        .(subjects(i,:)).x(k))^2 + (mot.(subjects(i,:)).s.cz_trim(k)-IAOR.(
                        subjects(i,:)).z(k))^2);
570             end
571     end
572
573     for k=1:length(mot.(subjects(i,:)).s.vx_trim)-1
574
575     % Calculate vectors from o to o' expressed in moving reference frame coordinates
576     r_oox.(subjects(i,:))(k) = (-cos(theta_trim.(subjects(i,:))(k))*(IAOR.(subjects(i,:))
            .x(k)))-(sin(theta_trim.(subjects(i,:))(k))*(IAOR.(subjects(i,:)).z(k)));
577     r_ooz.(subjects(i,:))(k) = (-sin(theta_trim.(subjects(i,:))(k))*(IAOR.(subjects(i,:))
            .x(k)))+(cos(theta_trim.(subjects(i,:))(k))*(IAOR.(subjects(i,:)).z(k)));
578
579
580     % Calculate vectors from o' to COG and Vertex expressed in moving reference frame
            coordinates
581     r_ocx.(subjects(i,:))(k)     = (-cos(theta_trim.(subjects(i,:))(k))*(mot.(subjects(i
            ,:)).s.cx_trim(k)-IAOR.(subjects(i,:)).x(k)))-(sin(theta_trim.(subjects(i,:))(k))
            *(mot.(subjects(i,:)).s.cz_trim(k)-IAOR.(subjects(i,:)).z(k)));
582     r_ocz.(subjects(i,:))(k)     = (-sin(theta_trim.(subjects(i,:))(k))*(mot.(subjects(i
            ,:)).s.cx_trim(k)-IAOR.(subjects(i,:)).x(k)))+(cos(theta_trim.(subjects(i,:))(k))
            *(mot.(subjects(i,:)).s.cz_trim(k)-IAOR.(subjects(i,:)).z(k)));
583     end
584
585     r_ovx.(subjects(i,:)) = r_ocx.(subjects(i,:));
586     r_ovz.(subjects(i,:)) = r_ocz.(subjects(i,:))+ 0.05982; %59.82mm offset between
            sensors COG and VERTEX
587
588
589     % Velocity and acceleration vectors from o' to COG and Vertex expressed in moving
            reference frame coordinates
590     r_ocx.dot.(subjects(i,:))       = gradient(r_ocx.(subjects(i,:)),dt);
591     r_ocz.dot.(subjects(i,:))       = gradient(r_ocz.(subjects(i,:)),dt);
592     r_ovx.dot.(subjects(i,:))       = gradient(r_ovx.(subjects(i,:)),dt);
593     r_ovz.dot.(subjects(i,:))       = gradient(r_ovz.(subjects(i,:)),dt);
594     r_ocx.dot.dot.(subjects(i,:))   = gradient(r_ocx.dot.(subjects(i,:)),dt);
595     r_ocz.dot.dot.(subjects(i,:))   = gradient(r_ocz.dot.(subjects(i,:)),dt);
596     r_ovx.dot.dot.(subjects(i,:))   = gradient(r_ovx.dot.(subjects(i,:)),dt);
597     r_ovz.dot.dot.(subjects(i,:))   = gradient(r_ovz.dot.(subjects(i,:)),dt);
598
599     %Calculate origin velocity and acceleration expressed in B frame
600     r_oox.dot.(subjects(i,:))       = gradient(r_oox.(subjects(i,:)),dt);
601     r_ooz.dot.(subjects(i,:))       = gradient(r_ooz.(subjects(i,:)),dt);
602     r_oox.dot.dot.(subjects(i,:))=sen.(subjects(i,:)).a.cx_trim(1:end-1) -    (calc.(
            subjects(i,:)).alpha_trim(1:end-1).*r_ocz.(subjects(i,:)).')  + ((calc.(subjects(
            i,:)).w.gy_trim(1:end-1).^2).*r_ocx.(subjects(i,:)).')- r_ocx.dot.dot.(subjects(i
            ,:)).' -    ((2*calc.(subjects(i,:)).w.gy_trim(1:end-1)).*r_ocz.dot.(subjects(i,:)
            ).') -g*sin(theta_trim.(subjects(i,:))(1:end-1)).';
603     r_ooz.dot.dot.(subjects(i,:))=sen.(subjects(i,:)).a.cz_trim(1:end-1) +    (calc.(
            subjects(i,:)).alpha_trim(1:end-1).*r_ocx.(subjects(i,:)).')  + ((calc.(subjects(
            i,:)).w.gy_trim(1:end-1).^2).*r_ocz.(subjects(i,:)).')- r_ocz.dot.dot.(subjects(i
            ,:)).' +    ((2*calc.(subjects(i,:)).w.gy_trim(1:end-1)).*r_ocx.dot.(subjects(i,:)
            ).') +g*cos(theta_trim.(subjects(i,:))(1:end-1)).';
604
605     %Calculate vertex and center of gravity acceleration with equations of
606     %motion Moving ICOR model
607     calc.(subjects(i,:)).a.vx = g*sin(theta_trim.(subjects(i,:))(1:end-1)).'+r_oox.dot.
```

```
        dot.(subjects(i,:))+(calc.(subjects(i,:)).alpha_trim(1:end-1).*r_ovz.(subjects(i
        ,:)).')  + (-(calc.(subjects(i,:)).w.gy_trim(1:end-1).^2).*r_ovx.(subjects(i,:))
        .')+ r_ovx.dot.dot.(subjects(i,:)).' +   ((2*calc.(subjects(i,:)).w.gy_trim(1:end
        -1)).*r_ovz.dot.(subjects(i,:)).');
608     calc.(subjects(i,:)).a.vz = -g*cos(theta_trim.(subjects(i,:))(1:end-1)).'+r_ooz.dot.
        dot.(subjects(i,:))-(calc.(subjects(i,:)).alpha_trim(1:end-1).*r_ovx.(subjects(i
        ,:)).')  + (-(calc.(subjects(i,:)).w.gy_trim(1:end-1).^2).*r_ovz.(subjects(i,:))
        .')+ r_ovz.dot.dot.(subjects(i,:)).' -   ((2*calc.(subjects(i,:)).w.gy_trim(1:end
        -1)).*r_ovx.dot.(subjects(i,:)).');
609
610     calc.(subjects(i,:)).a.cx = g*sin(theta_trim.(subjects(i,:))(1:end-1)).'+r_oox.dot.
        dot.(subjects(i,:))+(calc.(subjects(i,:)).alpha_trim(1:end-1).*r_ocz.(subjects(i
        ,:)).')  + (-(calc.(subjects(i,:)).w.gy_trim(1:end-1).^2).*r_ocx.(subjects(i,:))
        .')+ r_ocx.dot.dot.(subjects(i,:)).' +   ((2*calc.(subjects(i,:)).w.gy_trim(1:end
        -1)).*r_ocz.dot.(subjects(i,:)).');
611     calc.(subjects(i,:)).a.cz = -g*cos(theta_trim.(subjects(i,:))(1:end-1)).'+r_ooz.dot.
        dot.(subjects(i,:))-(calc.(subjects(i,:)).alpha_trim(1:end-1).*r_ocx.(subjects(i
        ,:)).')  + (-(calc.(subjects(i,:)).w.gy_trim(1:end-1).^2).*r_ocz.(subjects(i,:))
        .')+ r_ocz.dot.dot.(subjects(i,:)).' -   ((2*calc.(subjects(i,:)).w.gy_trim(1:end
        -1)).*r_ocx.dot.(subjects(i,:)).');
612
613     % Calculate RMSE and residual accelerations
614     for k=1:length(calc.(subjects(i,:)).a.vx)
615         RESIDUAL_VX.(subjects(i,:))(k) = (calc.(subjects(i,:)).a.vx(k) - sen.(subjects(i
            ,:)).a.vx_trim(k));  % Residual acceleration
616         RESIDUAL_VZ.(subjects(i,:))(k) = (calc.(subjects(i,:)).a.vz(k) - sen.(subjects(i
            ,:)).a.vz_trim(k));
617     end
618     RMSE_VX(i,:) = (sqrt(mean((sen.(subjects(i,:)).a.vx_trim(1:end-1) - calc.(subjects(i
        ,:)).a.vx).^2)));   % Root Mean Squared Error
619     RMSE_VZ(i,:) = (sqrt(mean((sen.(subjects(i,:)).a.vz_trim(1:end-1) - calc.(subjects(i
        ,:)).a.vz).^2)));
620     RMSE_CX(i,:) = (sqrt(mean((sen.(subjects(i,:)).a.cx_trim(1:end-1) - calc.(subjects(i
        ,:)).a.cx).^2)));
621     RMSE_CZ(i,:) = (sqrt(mean((sen.(subjects(i,:)).a.cz_trim(1:end-1) - calc.(subjects(i
        ,:)).a.cz).^2)));
622
623 % Calculate values for CAT-I methods:
624 % Vertex
625 r= 0.05982+0.027+0.04; % [m] distance VER to COG + COG to skull base + skull base to C5-
    C6
626 cat1.(subjects(i,:)).a.vx = r*calc.(subjects(i,:)).alpha_trim;
627 cat1.(subjects(i,:)).a.vz = - calc.(subjects(i,:)).w.gy_trim.^2*r;
628 RMSE_CAT1_VX(i,:) = sqrt(mean((sen.(subjects(i,:)).a.vx_trim - cat1.(subjects(i,:)).a.vx)
    .^2));
629 RMSE_CAT1_VZ(i,:) = sqrt(mean((sen.(subjects(i,:)).a.vz_trim - cat1.(subjects(i,:)).a.vz)
    .^2));
630 RESIDUAL_CAT1_VX.(subjects(i,:))=(cat1.(subjects(i,:)).a.vx-sen.(subjects(i,:)).a.vx_trim
    ).';
631 RESIDUAL_CAT1_VZ.(subjects(i,:))=(cat1.(subjects(i,:)).a.vz-sen.(subjects(i,:)).a.vz_trim
    ).';
632 % COG
633 r= 0.027+0.04; % [m] distance COG to skull base + skull base to C5-C6
634 cat1.(subjects(i,:)).a.cx = r*calc.(subjects(i,:)).alpha_trim;
635 cat1.(subjects(i,:)).a.cz = - calc.(subjects(i,:)).w.gy_trim.^2*r;
636 RMSE_CAT1_CX(i,:) = sqrt(mean((sen.(subjects(i,:)).a.cx_trim - cat1.(subjects(i,:)).a.cx)
    .^2));
637 RMSE_CAT1_CZ(i,:) = sqrt(mean((sen.(subjects(i,:)).a.cz_trim - cat1.(subjects(i,:)).a.cz)
    .^2));
638
639 % Calculate values for CAT-II methods:
640 % Vertex
641 cat2.(subjects(i,:)).a.vx = sen.(subjects(i,:)).a.tx_trim;
642 RMSE_CAT2_VX(i,:) = sqrt(mean((sen.(subjects(i,:)).a.vx_trim - cat2.(subjects(i,:)).a.vx)
    .^2));
643 RESIDUAL_CAT2_VX.(subjects(i,:))=(cat2.(subjects(i,:)).a.vx-sen.(subjects(i,:)).a.vx_trim
    ).';
644 % COG
645 cat2.(subjects(i,:)).a.cx = sen.(subjects(i,:)).a.tx_trim;
646 RMSE_CAT2_CX(i,:) = sqrt(mean((sen.(subjects(i,:)).a.cx_trim - cat2.(subjects(i,:)).a.cx)
    .^2));
647
```

```
% Calculate values for CAT-IIIA methods:
% Vertex
r= 0.05982+0.027+0.055; % [m] distance VER to COG + COG to skull base + skull base to neck base
cat3a.(subjects(i,:)).a.vx = (cos(theta_trim.(subjects(i,:))).'.*sen.(subjects(i,:)).a.tx_trim)-(sin(theta_trim.(subjects(i,:))).'.*sen.(subjects(i,:)).a.tz_trim)+ r*calc.(subjects(i,:)).alpha_trim;
cat3a.(subjects(i,:)).a.vz = (sin(theta_trim.(subjects(i,:))).'.*sen.(subjects(i,:)).a.tx_trim)+(cos(theta_trim.(subjects(i,:))).'.*sen.(subjects(i,:)).a.tz_trim)- calc.(subjects(i,:)).w.gy_trim.^2*r;
RMSE_CAT3A_VX(i,:) = sqrt(mean((sen.(subjects(i,:)).a.vx_trim - cat3a.(subjects(i,:)).a.vx).^2));
RMSE_CAT3A_VZ(i,:) = sqrt(mean((sen.(subjects(i,:)).a.vz_trim - cat3a.(subjects(i,:)).a.vz).^2));
RESIDUAL_CAT3A_VX.(subjects(i,:))=(cat3a.(subjects(i,:)).a.vx-sen.(subjects(i,:)).a.vx_trim).';
RESIDUAL_CAT3A_VZ.(subjects(i,:))=(cat3a.(subjects(i,:)).a.vz-sen.(subjects(i,:)).a.vz_trim).';
% COG
r= 0.027+0.055; % [m] distance COG to skull base + skull base to neck base
cat3a.(subjects(i,:)).a.cx = (cos(theta_trim.(subjects(i,:))).'.*sen.(subjects(i,:)).a.tx_trim)-(sin(theta_trim.(subjects(i,:))).'.*sen.(subjects(i,:)).a.tz_trim)+ r*calc.(subjects(i,:)).alpha_trim;
cat3a.(subjects(i,:)).a.cz = (sin(theta_trim.(subjects(i,:))).'.*sen.(subjects(i,:)).a.tx_trim)+(cos(theta_trim.(subjects(i,:))).'.*sen.(subjects(i,:)).a.tz_trim)- calc.(subjects(i,:)).w.gy_trim.^2*r;
RMSE_CAT3A_CX(i,:) = sqrt(mean((sen.(subjects(i,:)).a.cx_trim - cat3a.(subjects(i,:)).a.cx).^2));
RMSE_CAT3A_CZ(i,:) = sqrt(mean((sen.(subjects(i,:)).a.cz_trim - cat3a.(subjects(i,:)).a.cz).^2));

% Calculate values for CAT-IIIA methods:
% Vertex
r= 0.05982+0.027; % [m] distance VER to COG + COG to skull base
cat3b.(subjects(i,:)).a.vx = (cos(theta_trim.(subjects(i,:))).'.*sen.(subjects(i,:)).a.tx_trim)-(sin(theta_trim.(subjects(i,:))).'.*sen.(subjects(i,:)).a.tz_trim)+ r*calc.(subjects(i,:)).alpha_trim;
cat3b.(subjects(i,:)).a.vz = (sin(theta_trim.(subjects(i,:))).'.*sen.(subjects(i,:)).a.tx_trim)+(cos(theta_trim.(subjects(i,:))).'.*sen.(subjects(i,:)).a.tz_trim)- calc.(subjects(i,:)).w.gy_trim.^2*r;
RMSE_CAT3B_VX(i,:) = sqrt(mean((sen.(subjects(i,:)).a.vx_trim - cat3b.(subjects(i,:)).a.vx).^2));
RMSE_CAT3B_VZ(i,:) = sqrt(mean((sen.(subjects(i,:)).a.vz_trim - cat3b.(subjects(i,:)).a.vz).^2));
RESIDUAL_CAT3B_VX.(subjects(i,:))=(cat3b.(subjects(i,:)).a.vx-sen.(subjects(i,:)).a.vx_trim).';
RESIDUAL_CAT3B_VZ.(subjects(i,:))=(cat3b.(subjects(i,:)).a.vz-sen.(subjects(i,:)).a.vz_trim).';
% COG
r= 0.027; % [m] distance COG to skull base
cat3b.(subjects(i,:)).a.cx = (cos(theta_trim.(subjects(i,:))).'.*sen.(subjects(i,:)).a.tx_trim)-(sin(theta_trim.(subjects(i,:))).'.*sen.(subjects(i,:)).a.tz_trim)+ r*calc.(subjects(i,:)).alpha_trim;
cat3b.(subjects(i,:)).a.cz = (sin(theta_trim.(subjects(i,:))).'.*sen.(subjects(i,:)).a.tx_trim)+(cos(theta_trim.(subjects(i,:))).'.*sen.(subjects(i,:)).a.tz_trim)- calc.(subjects(i,:)).w.gy_trim.^2*r;
RMSE_CAT3B_CX(i,:) = sqrt(mean((sen.(subjects(i,:)).a.cx_trim - cat3b.(subjects(i,:)).a.cx).^2));
RMSE_CAT3B_CZ(i,:) = sqrt(mean((sen.(subjects(i,:)).a.cz_trim - cat3b.(subjects(i,:)).a.cz).^2));

clear slope_cog_perp slope_cog_tang slope_ver_perp slope_ver_tang x_axis_cog_tang x_axis_ver_tang b_cog_tang b_ver_tang b_cog_perp b_ver_perp z_coordinate_cog_tang z_coordinate_cog_perp z_coordinate_ver_tang z_coordinate_ver_perp L1 L2 P
end
```

# Appendix VII

Statistics

A multivariate analysis of variance (MANOVA) was conducted to test whether differences were present in the dependent variables (torso acceleration, head center-of-gravity (COG) acceleration, head vertex acceleration, head angular velocity, head angular acceleration, head vertex velocity and shake frequency) between the groups (men and women).

The following assumptions must be met for the MANOVA to be valid:

- **Level of the variables**: independent variable must be categorical, dependent variables must be continuous or interval (assumption was met; gender was categorical, shaking variables were continuous)
- **Data approximately normally distributed** (Checked with Shapiro-Wilk test and Q-Q Plots)
- **Homogeneity of variances and covariances** (Checked with Box's test and Levene's test)

## Testing MANOVA assumptions

### Normal distribution

According to the Shapiro-Wilk test (Table A7.1), often used for small samples, all shaking variables for women were normally distributed ($p>0.05$). For men; head COG acceleration, head angular velocity, head angular acceleration, head vertex velocity were normally distributed as well ($p>0.05$). However, torso acceleration, head vertex acceleration and shake frequency were not normally distributed for men ($p\leq0.05$).

The Q-Q plots for torso acceleration, head vertex acceleration and shake frequency for men (Figure A7.1-A7.3 respectively) indicated that the data reasonably agreed with a normal distribution (straight line). Therefore, it is assumed that despite the failing Shapiro-Wilk test results, data were approximately normally distributed.

*Table A7.1 - Tests of normality*

| | | Kolmogorov-Smirnov[a] | | | Shapiro-Wilk | | |
|---|---|---|---|---|---|---|---|
| | Gender | Statistic | df | Sig. | Statistic | df | Sig. |
| a_tor | Male | .158 | 21 | .182 | .861 | 21 | .007 |
| | Female | .293 | 8 | .041 | .905 | 8 | .318 |
| a_cog | Male | .172 | 21 | .104 | .914 | 21 | .065 |
| | Female | .195 | 8 | .200* | .933 | 8 | .546 |
| a_ver | Male | .176 | 21 | .088 | .876 | 21 | .012 |
| | Female | .178 | 8 | .200* | .962 | 8 | .829 |
| Angular velocity | Male | .106 | 21 | .200* | .967 | 21 | .668 |
| | Female | .227 | 8 | .200* | .870 | 8 | .151 |
| Angular acceleration | Male | .124 | 21 | .200* | .939 | 21 | .206 |
| | Female | .177 | 8 | .200* | .962 | 8 | .831 |
| v_ver | Male | .097 | 21 | .200* | .991 | 21 | .998 |
| | Female | .169 | 8 | .200* | .967 | 8 | .876 |
| Shake frequency | Male | .208 | 21 | .018 | .898 | 21 | .031 |
| | Female | .176 | 8 | .200* | .949 | 8 | .703 |

*. This is a lower bound of the true significance.
a. Lilliefors Significance Correction

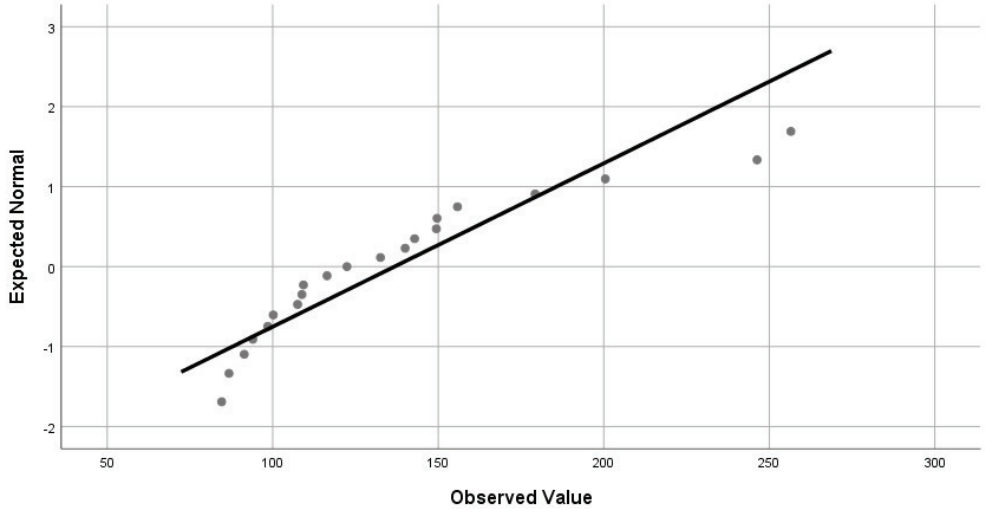


*Figure A7.1 - Normal Q-Q plot of torso acceleration for men*

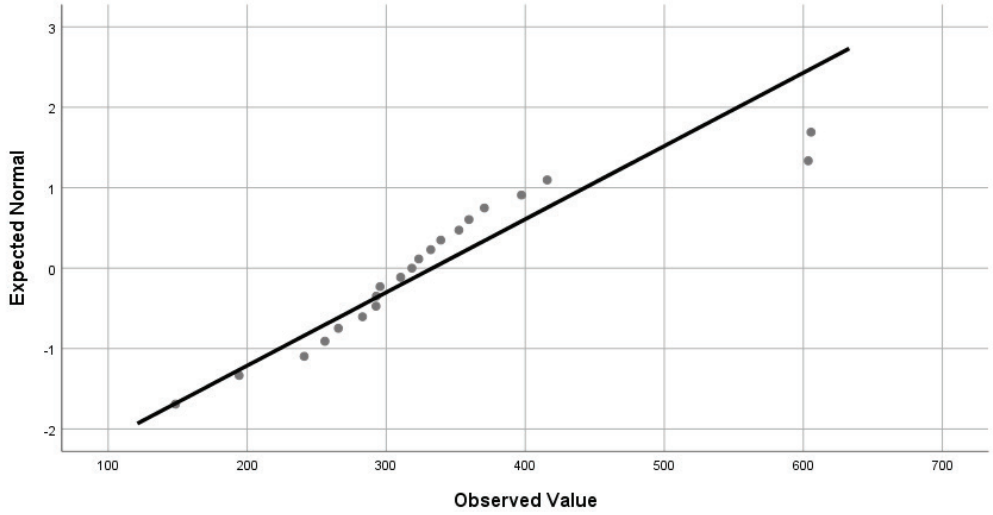


*Figure A7.2 - Normal Q-Q plot of head vertex acceleration for men*

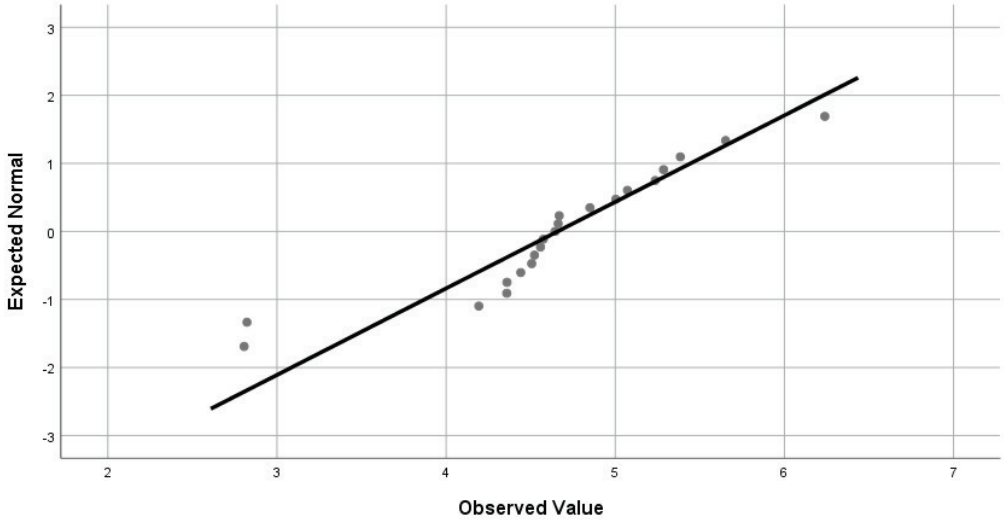


*Figure A7.3 - Normal Q-Q plot of shaking frequency for men*

## Homogeneity of variances and covariances

The assumption of homogeneity of variance and covariance was not violated. The observed covariance matrices of the dependent variables were equal across the groups (p>0.05) (Table A7.2). The error variance of the dependent variables were equal across the groups (p>0.05) (Table A7.3).

*Table A7.2 - Box's test of equality of covariance matrices*

| | |
|---|---|
| Box's M | 58.493 |
| F | 1.197 |
| df1 | 28 |
| df2 | 637.016 |
| Sig. | .224 |

Tests the null hypothesis that the observed covariance matrices of the dependent variables are equal across groups.

*Table A7.3 - Levene's test of equality of error variances*

| | | Levene Statistic | df1 | df2 | Sig. |
|---|---|---|---|---|---|
| a_tor | Based on Mean | 3.342 | 1 | 27 | .079 |
| | Based on Median | 2.631 | 1 | 27 | .116 |
| | Based on Median and with adjusted df | 2.631 | 1 | 23.087 | .118 |
| | Based on trimmed mean | 3.118 | 1 | 27 | .089 |
| a_cog | Based on Mean | .361 | 1 | 27 | .553 |
| | Based on Median | .373 | 1 | 27 | .547 |
| | Based on Median and with adjusted df | .373 | 1 | 24.042 | .547 |
| | Based on trimmed mean | .374 | 1 | 27 | .546 |
| a_ver | Based on Mean | .217 | 1 | 27 | .645 |
| | Based on Median | .153 | 1 | 27 | .699 |
| | Based on Median and with adjusted df | .153 | 1 | 22.295 | .699 |
| | Based on trimmed mean | .188 | 1 | 27 | .668 |
| Angular velocity | Based on Mean | 1.856 | 1 | 27 | .184 |
| | Based on Median | 2.098 | 1 | 27 | .159 |
| | Based on Median and with adjusted df | 2.098 | 1 | 25.808 | .159 |
| | Based on trimmed mean | 1.943 | 1 | 27 | .175 |
| Angular acceleration | Based on Mean | 1.398 | 1 | 27 | .247 |
| | Based on Median | 1.225 | 1 | 27 | .278 |
| | Based on Median and with adjusted df | 1.225 | 1 | 24.496 | .279 |
| | Based on trimmed mean | 1.275 | 1 | 27 | .269 |
| v_ver | Based on Mean | .454 | 1 | 27 | .506 |
| | Based on Median | .441 | 1 | 27 | .512 |
| | Based on Median and with adjusted df | .441 | 1 | 26.792 | .512 |
| | Based on trimmed mean | .454 | 1 | 27 | .506 |
| Shake frequency | Based on Mean | .289 | 1 | 27 | .595 |
| | Based on Median | .320 | 1 | 27 | .576 |
| | Based on Median and with adjusted df | .320 | 1 | 24.299 | .577 |
| | Based on trimmed mean | .286 | 1 | 27 | .597 |

Tests the null hypothesis that the error variance of the dependent variable is equal across groups.

# MANOVA results

## Multivariate test results

The multivariate test (Table A7.4) indicated a significant (p≤0.05) difference between the groups on the **total combination** of the dependent variables (Wilk's Lambda = 0.28, F(7,21)=7.66, p=0.00).

## Univariate effects

The results of the multivariate test were significant, therefore the results of the univariate test can be interpreted to see for which of the dependent variables there is a difference between the groups. Post-hoc analysis was not required because only two groups were compared. Therefore, results of the between-subjects effects test may be interpreted directly. A significant difference was present between the groups for all shaking variables (p≤0.05) (Table A7.5). See Table A7.6 for descriptive statistics.

*Table A7.4 - Multivariate tests*

| Effect | | Value | F | Hypothesis df | Error df | Sig. |
|---|---|---|---|---|---|---|
| Intercept | Pillai's Trace | .996 | 715.346[a] | 7.000 | 21.000 | .000 |
| | Wilks' Lambda | .004 | 715.346[a] | 7.000 | 21.000 | .000 |
| | Hotelling's Trace | 238.449 | 715.346[a] | 7.000 | 21.000 | .000 |
| | Roy's Largest Root | 238.449 | 715.346[a] | 7.000 | 21.000 | .000 |
| Gender | Pillai's Trace | .718 | 7.657[a] | 7.000 | 21.000 | .000 |
| | Wilks' Lambda | .282 | 7.657[a] | 7.000 | 21.000 | .000 |
| | Hotelling's Trace | 2.552 | 7.657[a] | 7.000 | 21.000 | .000 |
| | Roy's Largest Root | 2.552 | 7.657[a] | 7.000 | 21.000 | .000 |

a. Exact statistic

*Table A7.5 - Tests of between-subjects effects*

| Source | Dependent Variable | Type III Sum of Squares | df | Mean Square | F | Sig. |
|---|---|---|---|---|---|---|
| Corrected Model | a_tor | 14244.341[a] | 1 | 14244.341 | 7.450 | .011 |
| | a_cog | 14701.597[b] | 1 | 14701.597 | 8.015 | .009 |
| | a_ver | 82347.099[c] | 1 | 82347.099 | 7.990 | .009 |
| | Angular velocity | 1121.222[d] | 1 | 1121.222 | 13.932 | .001 |
| | Angular acceleration | 9858891.365[e] | 1 | 9858891.365 | 13.398 | .001 |
| | v_ver | 9.005[f] | 1 | 9.005 | 7.052 | .013 |
| | Shake frequency | 2.548[g] | 1 | 2.548 | 4.758 | .038 |
| Intercept | a_tor | 290651.570 | 1 | 290651.570 | 152.025 | .000 |
| | a_cog | 441501.881 | 1 | 441501.881 | 240.686 | .000 |
| | a_ver | 1734277.768 | 1 | 1734277.768 | 168.269 | .000 |
| | Angular velocity | 36785.082 | 1 | 36785.082 | 457.087 | .000 |
| | Angular acceleration | 170153529.000 | 1 | 170153529.000 | 231.227 | .000 |
| | v_ver | 378.621 | 1 | 378.621 | 296.488 | .000 |
| | Shake frequency | 433.928 | 1 | 433.928 | 810.325 | .000 |
| Gender | a_tor | 14244.341 | 1 | 14244.341 | 7.450 | .011 |
| | a_cog | 14701.597 | 1 | 14701.597 | 8.015 | .009 |
| | a_ver | 82347.099 | 1 | 82347.099 | 7.990 | .009 |
| | Angular velocity | 1121.222 | 1 | 1121.222 | 13.932 | .001 |
| | Angular acceleration | 9858891.365 | 1 | 9858891.365 | 13.398 | .001 |
| | v_ver | 9.005 | 1 | 9.005 | 7.052 | .013 |
| | Shake frequency | 2.548 | 1 | 2.548 | 4.758 | .038 |
| Error | a_tor | 51620.419 | 27 | 1911.867 | | |
| | a_cog | 49527.304 | 27 | 1834.345 | | |

*Table A7.6 (continued) - Tests of between-subjects effects*

| | | | | | | |
|---|---|---|---|---|---|---|
| | a_ver | 278277.003 | 27 | 10306.556 | | |
| | Angular velocity | 2172.886 | 27 | 80.477 | | |
| | Angular acceleration | 19868565.640 | 27 | 735872.801 | | |
| | v_ver | 34.480 | 27 | 1.277 | | |
| | Shake frequency | 14.458 | 27 | .535 | | |
| Total | a_tor | 505389.432 | 29 | | | |
| | a_cog | 710856.818 | 29 | | | |
| | a_ver | 2975780.630 | 29 | | | |
| | Angular velocity | 56817.999 | 29 | | | |
| | Angular acceleration | 291107371.295 | 29 | | | |
| | v_ver | 585.108 | 29 | | | |
| | Shake frequency | 598.011 | 29 | | | |
| Corrected Total | a_tor | 65864.760 | 28 | | | |
| | a_cog | 64228.902 | 28 | | | |
| | a_ver | 360624.103 | 28 | | | |
| | Angular velocity | 3294.108 | 28 | | | |
| | Angular acceleration | 29727457.005 | 28 | | | |
| | v_ver | 43.485 | 28 | | | |
| | Shake frequency | 17.006 | 28 | | | |

a. R Squared = .216 (Adjusted R Squared = .187)
b. R Squared = .229 (Adjusted R Squared = .200)
c. R Squared = .228 (Adjusted R Squared = .200)
d. R Squared = .340 (Adjusted R Squared = .316)
e. R Squared = .332 (Adjusted R Squared = .307)
f. R Squared = .207 (Adjusted R Squared = .178)
g. R Squared = .150 (Adjusted R Squared = .118)

*Table A7.6 - Descriptive statistics*

| | Gender | Mean | Std. Deviation | N |
|---|---|---|---|---|
| a_tor | Male | 136.79 | 48.933 | 21 |
| | Female | 87.20 | 23.087 | 8 |
| | Total | 123.11 | 48.501 | 29 |
| a_cog | Male | 163.22 | 46.143 | 21 |
| | Female | 112.84 | 31.496 | 8 |
| | Total | 149.32 | 47.895 | 29 |
| a_ver | Male | 333.19 | 109.828 | 21 |
| | Female | 213.96 | 72.736 | 8 |
| | Total | 300.30 | 113.488 | 29 |
| Angular velocity | Male | 46.80 | 9.760 | 21 |
| | Female | 32.89 | 6.183 | 8 |
| | Total | 42.96 | 10.847 | 29 |
| Angular acceleration | Male | 3362.06 | 933.444 | 21 |
| | Female | 2057.51 | 590.666 | 8 |
| | Total | 3002.18 | 1030.386 | 29 |
| v_ver | Male | 4.666 | 1.1718 | 21 |
| | Female | 3.419 | 1.0011 | 8 |
| | Total | 4.322 | 1.2462 | 29 |

| | | | | |
|---|---|---|---|---|
| Shake frequency | Male | 4.659 | .7865 | 21 |
| | Female | 3.996 | .5459 | 8 |
| | Total | 4.476 | .7793 | 29 |

## SPSS syntax

```
* Encoding: UTF-8.

 * Correlations:

CORRELATIONS
  /VARIABLES=a_tor a_cog a_ver Omega Alpha v_ver Freq_shake Age Height Weight
  /PRINT=TWOTAIL NOSIG
  /MISSING=PAIRWISE.


 * Normal distribution check:

EXAMINE VARIABLES=a_tor a_cog a_ver Omega Alpha v_ver Freq_shake BY Gender
  /PLOT HISTOGRAM NPPLOT
  /STATISTICS DESCRIPTIVES
  /CINTERVAL 95
  /MISSING LISTWISE
  /NOTOTAL.


 * MANOVA and descriptive statistics:

GLM a_tor a_cog a_ver Omega Alpha v_ver Freq_shake BY Gender
  /METHOD=SSTYPE(3)
  /INTERCEPT=INCLUDE
  /PRINT=DESCRIPTIVE ETASQ HOMOGENEITY
  /CRITERIA=ALPHA(.05)
  /DESIGN= Gender.
```

# Appendix VIII

Full overview of the experimental results

Full overview of shaking variables for each participant (Table A8.1). Minus sign indicates direction. Mean and SD were calculated with absolute values of the shaking variables.

*Table A8.1 - Shaking variables for each participant*

| *Subject* | *a_tor_max (m/s^2)* | *a_cog_max (m/s^2)* | *a_ver_max (m/s^2)* | *Omega_max (rad/s)* | *Alpha_max (rad/s^2)* | *v_ver_max (m/s)* | *f_shake (Hz)* |
|---|---|---|---|---|---|---|---|
| SUBJ01 | 109 | 119 | 241 | -36 | 2370 | -3.4 | 5.2 |
| SUBJ02 | 98 | 140 | 256 | -47 | 2680 | 6.3 | 2.8 |
| SUBJ03 | 106 | 141 | 296 | -33 | 2378 | 3.9 | 3.3 |
| SUBJ04 | 257 | 268 | 606 | -66 | 6010 | 5.7 | 4.5 |
| SUBJ05 | 156 | 132 | 293 | -46 | 3226 | 4.1 | 4.4 |
| SUBJ06 | 150 | 149 | 359 | -51 | 3555 | 5.1 | 4.7 |
| SUBJ07 | 246 | 276 | 604 | -53 | 4679 | 5.6 | 5.1 |
| SUBJ08 | 132 | 144 | 316 | -42 | 3104 | 4.1 | 4.4 |
| SUBJ09 | 85 | 111 | 230 | -32 | 1925 | -3.6 | 3.4 |
| SUBJ10 | 140 | 180 | 397 | -47 | 3884 | 4.5 | 4.9 |
| SUBJ11 | 122 | 131 | 283 | -36 | 2698 | -3.6 | 4.6 |
| SUBJ12 | 85 | 92 | 148 | -32 | 1913 | 2.4 | 6.2 |
| SUBJ13 | 57 | 68 | 107 | -26 | 1271 | 1.6 | 5.0 |
| SUBJ14 | 68 | 94 | 153 | 26 | 1441 | 2.9 | 4.1 |
| SUBJ15 | 143 | 169 | 352 | -40 | 3161 | -4.6 | 4.4 |
| SUBJ16 | 100 | 146 | 266 | 36 | 2607 | -3.8 | 4.4 |
| SUBJ17 | 87 | 102 | 194 | -31 | 2268 | -2.9 | 5.4 |
| SUBJ18 | 200 | 174 | 416 | -57 | 4183 | 5.2 | 4.5 |
| SUBJ19 | 109 | 115 | 293 | -39 | 2997 | 3.4 | 5.0 |
| SUBJ20 | 179 | 203 | 323 | 44 | 3149 | -4.3 | 4.8 |
| SUBJ21 | 133 | 167 | 296 | 45 | 3147 | -4.9 | 4.6 |
| SUBJ22 | 83 | 158 | 255 | 42 | 2491 | -5.0 | 4.0 |
| SUBJ23 | 84 | 97 | 173 | -31 | 1870 | 3.1 | 3.7 |
| SUBJ24 | 83 | 91 | 180 | -31 | 1980 | 3.1 | 4.1 |
| SUBJ25 | 108 | 185 | 371 | 60 | 4078 | -6.3 | 4.2 |
| SUBJ26 | 149 | 158 | 332 | -60 | 3809 | 4.5 | 5.7 |
| SUBJ27 | 116 | 179 | 339 | 50 | 3239 | -5.3 | 4.7 |
| SUBJ28 | 91 | 167 | 318 | -49 | 2574 | 7.0 | 2.8 |
| SUBJ29 | 94 | 173 | 310 | 54 | 3641 | -5.0 | 4.6 |
| **Maximum** | 257 | 276 | 606 | -66 | 6010 | 7.0 | 6.2 |
| **Mean** | 130 | 155 | 302 | 43 | 3033 | 4.5 | 4.5 |
| **SD** | 51 | 51 | 108 | 10 | 995 | 1.3 | 0.8 |

# Appendix IX

Excluded experimental data

Overview of shaking variables for excluded participants (Table A9.1). Minus sign indicates direction. Mean and SD were calculated with absolute values of the shaking variables.

*Table A9.1 - Shaking variables for each participant*

| *Subject* | *a_tor_max (m/s^2)* | *a_cog_max (m/s^2)* | *a_ver_max (m/s^2)* | *Omega_max (rad/s)* | *Alpha_max (rad/s^2)* | *v_ver_max (m/s)* | *f_shake (Hz)* |
|---|---|---|---|---|---|---|---|
| SUBJ30 | 237 | 276 | 336 | -50 | -4144 | 6.3 | 3.7 |
| SUBJ31 | 186 | 202 | 366 | 49 | -3627 | 5.2 | 5.7 |
| SUBJ32 | 142 | 120 | 218 | -40 | -2271 | -4.5 | 4.6 |
| SUBJ33 | 170 | 171 | 334 | 49 | -2271 | 6.3 | 5.7 |
| **Maximum** | 237 | 276 | 366 | 50 | -4144 | 6.3 | 5.7 |
| **Mean** | 184 | 192 | 314 | 47 | 3439 | 5.5 | 4.5 |